Department of Precision and Microsystems Engineering

Control of Voicecoil transducers

R. Valk

Report no : MSD 2013.030
Coach : Prof.ir. Robert-H. Munnig Schmidt
Professor : Prof.ir. Robert-H. Munnig Schmidt
Specialisation : Mechatronic System Design
Type of report : Master of Science Thesis
Date : 12 November 2013

Control of Voicecoil transducers

Design and implementation of a Motional Feedback Loudspeaker Woofer

R. Valk

Master of Science Thesis

TU Delft Delft University of Technology

Control of Voicecoil transducers

Design and implementation of a Motional Feedback Loudspeaker Woofer

Master of Science Thesis

For the degree of Master of Science in Mechanical Engineering at Delft University of Technology

R. Valk

November 13, 2013

Faculty of Mechanical, Maritime and Materials Engineering (3mE) · Delft University of Technology

The work in this thesis was supported by the department Precision Microsystems Engineering.
Their cooperation is hereby gratefully acknowledged.

Abstract

This master thesis describes the dynamical behaviour of a loudspeaker woofer and the modelling of it. By the use of the knowledge gained from the model, a feedback controller is implemented in order to enhance the woofer's performance in terms of acoustic total harmonic distortion (THD) and low frequency bandwidth. The first objective of the research is to build a woofer set-up that suppresses the THD below 1% during operation. The second objective is to evaluate diaphragm break-up and compensate for this break-up by the use of feedback.

The woofer is equipped with an accelerometer sensor. By the use of feedback, the motion of the voice-coil of the loudspeaker is controlled. This enhanced motion results into an acoustic enhancement.

Since the motion of only a single point on the woofer diaphragm is measured and used for feedback, only the local distortion is reduced. Even when feedback is applied, the surround of the woofer is radiating acoustic distortion. Initially a woofer is used that has some very specific characteristics in terms of acoustic radiation. The contribution of distortion by the surround is large with the chosen woofer. Therefore, the increase in performance measured on the accelerometer is not identical to the increase in performance measured by the microphone. Where the accelerometer is mounted, the motion of the diaphragm is improved, but the acoustic distortion radiated by the surround is not reduced.

After analysing the first woofer, the knowledge gained from the experiments is used to determine a better candidate for the experiments. The experiments are repeated on a second set-up.

Two important observations have led to the final result. One observation is that the surround of the woofer is a large contributor of the acoustic radiation. Choosing a woofer that is very uniform in terms of the distortion profile across the diaphragm, is advised. In that situation, when the motion of the location where the sensor is mounted is improved, the same holds for the surround of the woofer. Secondly, it is observed that when using a piezoelectric sensor, the sensor output is not only determined by the acceleration. Stress leading to deformation of the sensor is measured too. When the contribution of measured deformation becomes dominant over the measured acceleration, the magnitude of the signal is that of the deformation instead

of the acceleration. For low frequencies, this leads to a limitation in terms of potential loop gain.

To some extend, both problems have been solved by the use of a different type of sensor mount and by a careful selection of the woofer. The second woofer used, has an acoustic distortion profile that is nearly identical across the membrane. This observation indicates that for the operating bandwidth of the woofer, the motion of the diaphragm is a close match to that of a rigid piston. Increasing the performance in terms of the motion of the centre, therefore leads to an increase in performance throughout the entire diaphragm. In order to solve the problem of the measured deformation of the sensor, a different type of sensor mount is designed. This sensor mount reduces the deformation of the sensor. This leads to a steeper roll-off slope in the sub-resonant frequency band of the woofer. This steeper slope makes it possible to design a controller, that leads to higher distortion suppression.

The achieved reduction of harmonic distortion measured on the accelerometer sensor is up to 22 dB, a factor 12,5. The acoustic reduction of harmonic distortion measured with a microphone is up to 22 dB too. In practice, the frequency band of this high suppression is narrow. The frequency band in which the suppression is over 17 dB, a factor 7, is between 40 Hz and 150 Hz

When the woofer excursion becomes large, the THD without feedback can be over 12,5%. Suppressing the distortion by a factor 12,5 therefore does not lead to the target THD of under 1%. The diaphragm break-up is evaluated, but a controller that suppresses this motion is not implemented. A controller would only compensate for the break-up effect on the diaphragm location where the sensor is mounted. The actual break-up in the diaphragm would remain.

Table of Contents

Preface

This research is inspired by a product developed by Philips. In 1970, Philips developed the MFB series of loudspeakers in which a woofer is equipped with a piezoelectric accelerometer. This accelerometer is used as a sensor to measure the acceleration of the centre of a woofer. That sensor signal is used for feedback control that makes the loudspeaker perform better by means of Total Harmonics Distortion (THD) in the first octaves and extend the low frequency bandwidth.

After reading on that series of loudspeakers, interest grew large on how that control might be enhanced by the use of modern digital electronics.

The Philips MFB series implemented feedback that reduced the harmonic distortion up to 10 dB, a factor 3,3. The Philips research facility [33], later on improved the motional feedback control loop and reported significant improvements over the control loop that was implemented in the regular production units. This enhanced control loop however, was never implemented in a commercially available product.

The enhanced control loop is different from the original circuitry in terms of the method used in order to achieve a high loop-gain. It uses two signals that are added to the sensor output. These two signals, depending on the frequency content of the input, can be dominant or sub-dominant over the sensor output. This method thereby creates a low frequency and high frequency masking effect. The frequency band in which the sensor output is dominant over the two masking signals is the control bandwidth of the woofer. This different approach to loop-shaping results in a loop gain, that is higher than the loop gain that was achieved before. In appendix A-23, more information about this improved control loop is available.

With the implementation of modern Digital Signal Processors (DSP), the new method developed by Philips is not required in order to obtain a high loop gain. Due to the flexibility a DSP introduces, regular loop-shaping can be applied, as is done in the initial MFB series. Since the limitations in terms of analogue circuit design are reduced by the DSP flexibility, the remainder of limitations are the dynamics of the loudspeaker woofer itself. Both achieving a high loop gain and extending the control bandwidth, are the objectives of this research.

The research led to satisfactory results and was performed with great pleasure. Performing research on a topic that is close to the heart, eased the perceived workload.

Acknowledgements

I would like to thank my supervisor prof.ir. R.H. Munnig Schmidt for his assistance during the process of this research. Having a supervisor with similar interests and enthusiasm, was a great stimulus and help in working on the project.

I would like to thank Philips for giving acces to the NatLab report on the application of MFB loudspeakers.

I would like to thank the following companies for donating equipment in order to help me out on this project; Analog Devices, Tymphany, SEAS and RMS Acoustics & Mechatronics.

Delft, University of Technology R. Valk
November 13, 2013

List of Symbols and Abbreviations

Symbol	Description
P_{a}	Acoustic power
v_{d}	Diaphragm speed
A_{d}	Surface area of diaphragm
R_{a}	Real part of acoustic radiation impedance
ρ	Air density
ω	Acoustic frequency
c	Speed of sound
I	Current flow through voice coil
F_{L}	Lorentz actuator force
ℓ	Length of voice coil wire
B	Flux density through the voice coil
F_{s}	Spring force
x_{d}	Excursion of the diaphragm
f_{s}	Eigen-frequency of mass-spring-damper system
k_{s}	Spring constant of system
M_{d}	Moving mass of woofer
a_{d}	Acceleration of the diaphragm
c_{s}	Damping constant of system
Q	Peaking factor of mass-spring-damper system
V_{M}	Matlab magnitude value
g_{a}	Voltage to current gain of current amplifier
r	Audio reference signal
y	System output value
e	Error between reference value and output value
$OL_{ye}(s)$	Open loop transfer function
$CL_{yr}(s)$	Closed loop transfer function
g_m	Gain margin
φ_m	Phase margin
m_m	Modulus margin

Abbreviation	Description
THD	Total Harmonic Distortion
DSP	Digital Signal Processor
MFB	Motional Feedback
SPL	Sound Pressure Level
MDF	Medium Density Fiber
DAQ	Data Acquisition system
ADC	Analogue to digital converter
DAC	Digital to analogue converter

"Those who have not heard, cannot imagine the joy of really hearing"
— *Greg Calbi*

Chapter 1

Introduction

1-1 The loudspeaker

Loudspeakers are devices that use electrical power and turn that power into motion of a diaphragm. This motion causes pressure changes in the air that are perceived as sound. The transfer between these two quantities, electrical power and sound, is one that is very complex. Within this statement lies the very existence of manufactures of loudspeakers. Every individual manufacturer of loudspeakers or acoustic equipment, has a different method on trying to approach a perfect transfer. One of the problems in the reproduction of the recorded wave front, is the acoustic property of the environment. Some frequencies of the propagated wave front remain identical in magnitude, while others are boosted or delayed by standing waves and other acoustical influences. Toole [30] performed research on this subject and concluded that the listening room, loudspeaker position and recording highly influence the perceived sound. For example, Figure 1-1 shows the results from a series of measurements performed on different locations in a listening room. The figure indicates the large deviations from the average response, based on the location of the measurement. The location of the loudspeakers, the location of the microphone and the shape and volume of the room, all contribute to the measured sound. This issue, however, is not the focus of this research. This research focusses on the mechanical- and control-aspect of the chain of the earlier mentioned transformation from electrical power to sound.

1-2 Voice-coil transducer dynamics

A typical loudspeaker woofer consists of a diaphragm and a Lorentz actuator. The diaphragm is suspended by a centring spider. A flexible surround is used to connect the moving edges of the diaphragm to the static frame of the woofer. This creates a barrier between the pressure on the front side and back side of the diaphragm. The spider and surround ensure that the motion of the diaphragm is kept within one axis. Next to that, the spider is often used as a carrier for the wires that connect the moving voice-coil to the static frame of the woofer. As

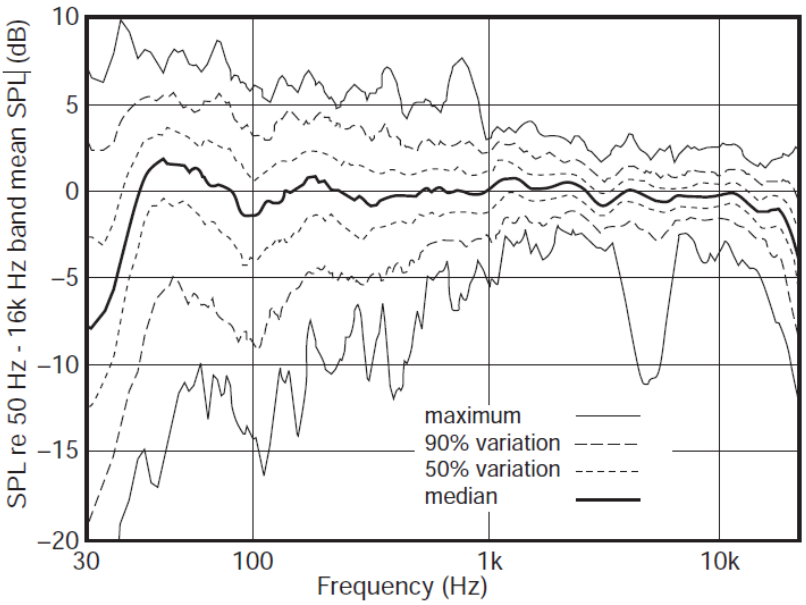

Figure 1-1: Acoustic measurements in a room with loudspeakers, on different locations. Deviations in the order of 20 dB are measured. [30]

with all moving systems, the mass of the moving diaphragm and all other physical properties of the moving parts create a dynamic system. Al-Ali [1] performed an analysis on the dynamics of the actuator and the moving mass. Both in the mechanical domain and electrical domain, the motion of the voice-coil and diaphragm are described with high-order transfer functions.

The surround, which connects the moving diaphragm to the static frame of the driver, can be modelled as a non-linear spring and damper. The spider can be modelled as a similar component as the surround. The Lorentz actuator has a dynamic behaviour with non-linearities and frequency dependence too. This, in combination with the mass, shape and stiffness of the diaphragm, creates a combined behaviour of the transducer, that is non-linear.

1-3 Thiele/Small parameters

The most dominant parameters that describe the low frequency behaviour of a woofer, are measured by the manufacturer of a loudspeaker driver. Due to the success of two pioneers in this line of analysis, these parameters are known as the Thiele/Small parameters. The advantage of using these parameters is that they are universally used and fairly accurately describe the low frequency behaviour of a loudspeaker driver. These parameters however, can only describe the linear behaviour of a woofer within a narrow frequency band.

1-4 Feedback Control

The Thiele/Small parameters describe the linear low frequency behaviour of a loudspeaker driver, while in practice the linear range of this system model is limited. In order to reduce

the influence of non-linear components, feedback control or feedforward control can be applied to the system. By suppressing the non-linear motion, the remaining motion is a closer match to the reference audio signal.

Schurer [27] developed a method to suppress non-linear disturbances by designing a non-linear model of the motor dynamics. By implementing the inverse of the non-linear model in a DSP, the distortion was reduced by up to 12 dB, a factor 4. If a perfect non-linear model was developed, this method would be interesting to use. However, due to ageing of components or a change in temperature, the non-linear model no longer is a match to the actual motion of the membrane.

Therefore, in this research, feedback control is used instead of feedforward control.

The mismatch between a desired response and the measured actual response can be described as a disturbance or error. Disturbances on electrodynamic systems can be reduced by applying a well designed feedback control loop. A control loop measures the motion of the loudspeaker and compares that to the reference. The error between the two values can be used to compensate for the disturbance. This classic single input single output control system is one of the most common types of control.

There are many fields of application of feedback control. The method of improving the performance of a loudspeaker driver has been implemented by Philips in the 1970s and 1980s. That system uses a woofer with a piezoelectric accelerometer as a sensor. The sensor data is fed back to an analogue circuit, that compares it to the reference signal and implements control by multiplying the error by a linear transfer function. In practice, the transfer function is a circuit with a non-flat magnitude and phase over frequency that changes the open loop transfer function, as shown in Figure 1-2.

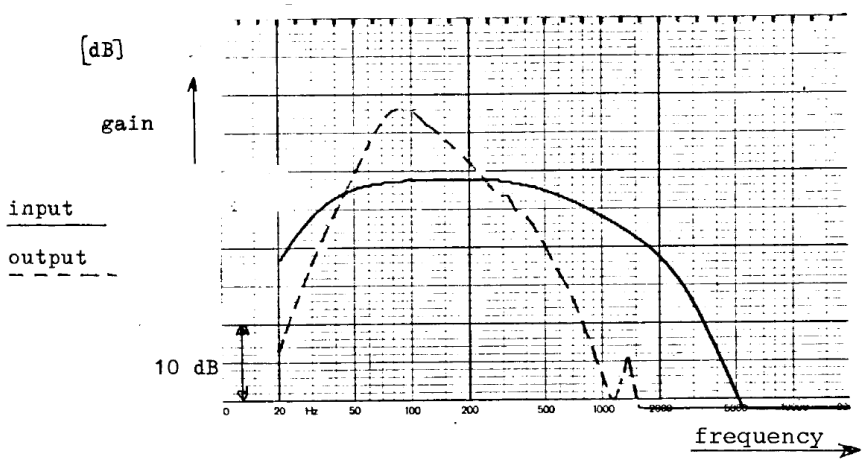

Figure 1-2: Open loop figure of controller dynamics, with a peak of 10 dB around 80 Hz, courtesy of Philips

Besides the research team of Philips, other engineers have been exploring the possibilities of using feedback in a loudspeaker design too. Al-Ali [1] performed both the analysis of the dynamics of the loudspeaker and the application of feedback control, in order to obtain higher performances of the system used. The research uses the Total Harmonics Distortion (THD) as a performance measure of the woofer. Applying the control loop increased the performance

in the low frequency regions by a maximum of 6 dB, a factor 2. Al-Ali advises to perform additional research on the modelling and control of the woofer. Other engineers focused on the identification methods. Wei [35] focused on the Volterra filter for parametric loudspeaker system identification. Results show that this method can effectively and accurately predict the sound pressures and THD within the bandwidth of the identification signal. Loutridis performed a comparison between loudspeaker system identification methods. Yali [15, 20] too, evaluated alternative identification methods and found that the empirical mode decomposition (EMD) method performs well in the identification of loudspeaker dynamics. The concept of performing feedback on loudspeaker woofers is applied by Breden [3], Chiu [5] and Dzisiewski-Smith [8]. Breden used velocity feedback of a dual voice-coil subwoofer to extend the low frequency capabilities of the woofer. He does not mention an increase in THD performance. Chiu has successfully performed a feedback loop by the use of a microphone. He achieved a maximal reduction in THD of 10 dB, a factor 3,3. Chiu advises to perform more research on the control of the frequencies at which the diaphragm break-up starts, since that limited his control performance. It is clear that this topic is explored widely.

1-5 Diaphragm breakup

Since the diaphragm of a loudspeaker driver is made out of a physical material, it has a dynamic behaviour when excited. At certain frequencies, the diaphragm no longer moves as a rigid piston, but shows break-up modes within the surface. These frequencies are considered to fall outside of the practical bandwidth of a loudspeaker driver or, in some cases, are ignored. Designers of loudspeakers try to stay away from this phenomenon in order to make sure that this movement is not interfering with the acoustics. In typical feedback systems of acoustic transducers, the non-rigid deformation of the diaphragm is not monitored by a separate sensor.

Research is performed on the mapping of non-linearities of the loudspeaker. Zhang [29] performed analysis on the diaphragm break-up and measured the acoustic influence of the non-linear behaviour of the transducer. The non-linearity is acknowledged, but the control design is not described. Suykens [31] performed a linearisation of a typical non-linear transducer model. The results show that under strict assumptions, the linearisation holds. Gelat [12] analysed a method of describing the break-up of a woofer diaphragm. The dynamic stiffness method showed to have high resemblance to actual measurements. In that research, a feedback control loop is not of interest. Ravaud [26] analysed the non-linearities of a loudspeaker-like structure. The focus of Ravaud is on the time-varying influence of the dynamics. Even though diaphragm break-up is not the focus, it clearly shows the influence on the dynamics of the transducer.

As described above, many of the researches do not apply feedback control. A lot of insight on the motion and non-linear behaviour of the woofer is available, but the application of that knowledge in terms of designing a feedback loop is limited. Then again, the research that is available on applied feedback, focuses on the electronics and achieves only a limited increase in performance in terms of THD.

1-6 Research objective

This research is about evaluating the limitations of applying feedback on a loudspeaker woofer. The potential of applying feedback has been proven before. With the information available in literature, there should be no problem in achieving a THD-reduction of 10 dB within the control bandwidth of 40 Hz to 200 Hz.

One of the objectives is to get a reduction in THD of the woofer, so that it is below 1% during operation. Another objective is to extend the control bandwidth beyond the frequency at which diaphragm break-up occurs.

Mechanical and electrical limitations are evaluated and attempted to overcome. With every limitation evaluated and possibly solved, only the fundamental mechanical limitations remain.

As an example of the problems occurring, Figure 1-3 shows a time domain measurement of a sensor signal that is mounted on the voice-coil of a woofer. Ideally, the sensor would show a 20 Hz sinusoidal shape on the output. However, due to non-linearities, distortion is observed in the form of harmonics of the fundamental frequency at 40 Hz and 80 Hz. Since the reference value in this situation is merely the fundamental frequency, all deviations from that signal are considered to be disturbances. The design and implementation of a feedback controller has the goal of reducing these disturbances, while maintaining the fundamental frequency.

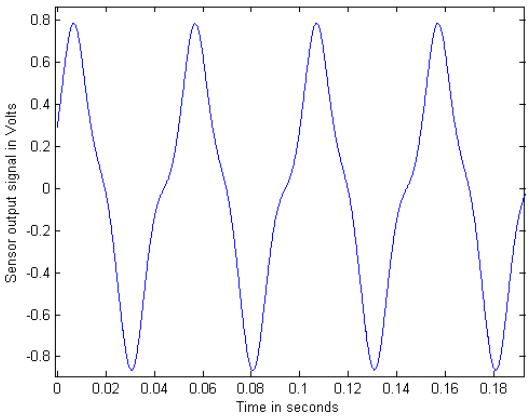

Figure 1-3: Signal output from an accelerometer mounted on the actuator of a loudspeaker woofer. The deviations from the 20 Hz sine wave are clearly visible.

Chapter 2

Loudspeaker dynamics

2-1 Overview

In Figure 2-1, a model of a loudspeaker woofer shows the components that determine the most dominant dynamical behaviour. The moving part of the woofer that causes the difference in air pressure, is the diaphragm or cone, due to resemblance of the commonly used shape of it. The diaphragm is forced to move by a Lorentz actuator, connected to the centre of the diaphragm. In order to keep the actuator free from dust, in many woofers a dust cover is used to seal the actuator from the environment. To keep the motion of the diaphragm in a straight path and to seal the internal volume of the loudspeaker enclosure from the environment, a suspension is required. The suspension consists of a surround, on the outer ring of the cone, that seals the volume and suspends the outer part of the diaphragm. A spider is used to keep the diaphragm aligned in the air gap of the Lorentz actuator. The frame is the static part of the woofer that is connected to the loudspeaker enclosure.

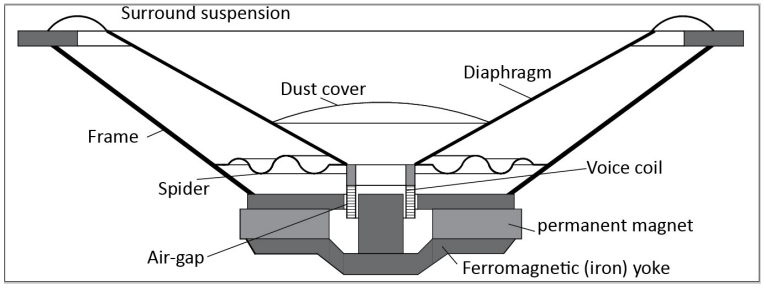

Figure 2-1: Model of a loudspeaker, with the cone shaped diaphragm, spider, dust cap and surround, courtesy of RMS Acoustic & Mechatronics

2-2 Forces that act upon the diaphragm

In order to evaluate the motion of the diaphragm, the forces that act upon the diaphragm are evaluated.

2-2-1 Lorentz actuator

A Lorentz actuator transforms electric current into a force. This type of actuation is not the only type available in loudspeakers, but for low frequency acoustic power, it is required to move a large quantity of air. Equation (2-1) shows the acoustic power, P_{a}, expressed by the speed of the diaphragm, v_{d}, diaphragm surface area, A_{d}, and real part of the acoustic radiation impedance, R_{a}.

$$P_{\mathrm{a}} = (v_{\mathrm{d}} \cdot A_{\mathrm{d}})^2 \cdot R_{\mathrm{a}} \tag{2-1}$$

Equation (2-2) shows, for low frequencies, the real part of the acoustic impedance, R_{a}, expressed in the air density, ρ, the acoustic frequency, ω, and speed of sound in air, c.

$$R_{\mathrm{a}} = \frac{\rho \cdot \omega^2}{2 \cdot \pi \cdot c} \tag{2-2}$$

Equation (2-1) and (2-2) show that for low frequencies, the diaphragm velocity and excursion need to be large. Lorentz actuators are capable of large excursions. Therefore, the Lorentz actuator is used in most woofers and subwoofers.

The actuator consists of two elements; the voice coil, a wire wound around the voice-coil carrier that is attached to the diaphragm, and a magnet that causes a magnetic flux through the voice coil. The current, I, in the wires in the voice-coil results in a force, F_{L}, by equation (2-3), where B is the flux density through the voice coil, ℓ, is the length of wire inside the magnetic field and I is the current in the wire.

$$F_{\mathrm{L}} = B \cdot \ell \cdot I \tag{2-3}$$

For now, B and ℓ are considered to be constants.

2-2-2 Suspension

The spider, air volume in the enclosure and the surround, can be combined in the physical model as a pair of non-linear springs and dampers in parallel. The stiffness is low at very small excursions, while increasing exponentially for larger excursions. This behaviour can be described by a third order polynomial. Equation (2-4) indicates that the spring force, F_{s}, is not linear to the excursion, x_{d}, of the diaphragm. Since the excursion at low frequencies is large, the effect of this non-linearity is large at these frequencies. For the damping, a similar non-linear effect is noticed.

$$F_{\mathrm{s}} = k_1 \cdot x_{\mathrm{d}} + k_2 \cdot x_{\mathrm{d}}^2 + k_3 \cdot x_{\mathrm{d}}^3 \tag{2-4}$$

The combination of Equation (2-1) and Equation (2-2) show that for low frequencies, the speed of the diaphragm, v_{d}, must be increased in order to maintain acoustic power, P_{a}. Substituting the diaphragm speed by the excursion, x_{d}, leads to Equation (2-5) that shows the quadratic relationship between the frequency, ω, and excursion.

$$P_{\mathrm{a}} = (x_{\mathrm{d}} \cdot \omega^2 \cdot A_{\mathrm{d}})^2 \cdot \frac{\rho}{2 \cdot \pi \cdot c} \tag{2-5}$$

Equation (2-4) indicates that for higher values of excursion of the diaphragm, the contribution of non-linear behaviour increases. Therefore, for low frequency acoustic power, where the excursions need to be large, the non-linearities from the suspension are more dominant than in the higher frequencies.

2-3 Mass-Spring-Damper system

The combination of forces described in Section 2-2, lead to a mass-spring-damper mechanical behaviour, as shown in Figure 2-2. This is the most dominant mechanical behaviour of a loudspeaker woofer in a sealed enclosure. This behaviour describes the linearised model from a force to an acceleration of the mass. Since the force from the actuator is proportional to the current through the voice-coil, the model holds for a current input, I, too. Equation (2-6) describes the eigen-frequency, f_s, of the woofer motion, expressed in Hz, for a combined stiffness, k, and mass, M_{d}.

$$f_s = \frac{1}{2 \cdot \pi} \cdot \sqrt{k/M_{\mathrm{d}}} \tag{2-6}$$

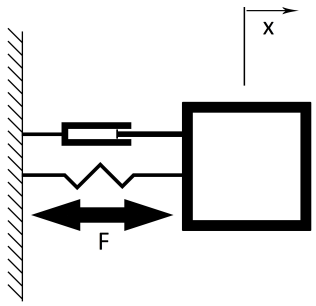

Figure 2-2: Mass spring damper system actuated by a force from the Lorentz actuator.

2-4 Woofer selection

The first woofer evaluated is the Peerless SLS-P830946, a 6.5 inch diameter woofer of which the specifications are detailed in Appendix A-11. Figure 2-3 shows many characteristics that are typical for loudspeaker woofers. However, there is one distinct frequency band in which the driver has very low Sound Pressure Level (SPL) output. Between 600 Hz and 800 Hz,

there is a 20 dB dip of SPL output. It is expected that within that frequency band, the first diaphragm break-up mode, where the outer part of the diaphragm is no longer following the motion of the centre part, is causing this reduced output.

The objective of this research is not only to suppress non-linear influences on the acoustic output, but to compensate for diaphragm break-up too. Because the woofer SPL figure shows all the signs of problematic diaphragm break-up, the woofer is chosen to be the test subject of this research.

The parameters, provided by the manufacturer of the woofer, are noted in Table 2-1. In order to make an accurate linear model of the woofer that is used for further research, the dynamic linear behaviour of the woofer must be measured in an identification process.

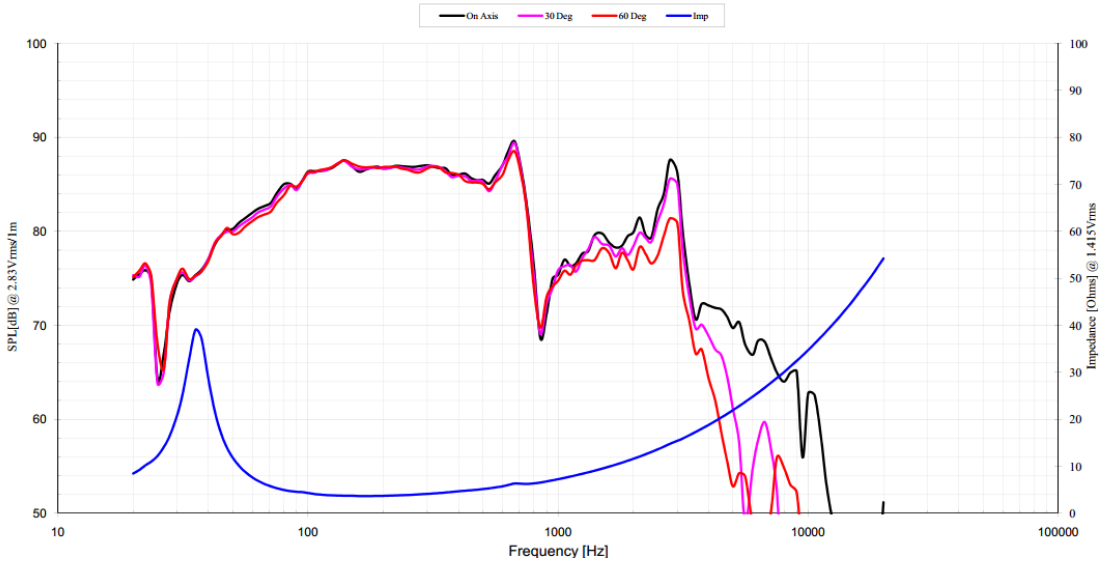

Figure 2-3: SPL expressed in decibels with varying frequency excitation, as provided by the manufacturer, Peerless. Additional specifications are noted in Appendix A-11

Table 2-1: Peerless SLS-P830946 parameters

Unit	Symbol	Value
DC resistance	R	2,7 Ohm
Inductance	L	0,65 mH
Moving mass	M	30,5 gr.
Motor force factor	B $\cdot \ell$	7,6
Compliance	1/k	467 μm/N
Mechanical Q factor	Qms	2,81
Electrical Q factor	Qes	0,80
Total Q factor	Qts	0,62
Resonant frequency	Fs	42 Hz
Ratio fs/Qts	Fs/Qts	119
Energy bandwidth product	(1/Qes) $\cdot$ Fs	110
Motor Efficiency factor	β	21,18
Sensitivity	dB at 1 W/1m	82 dB
Effective piston area	Sd	123,5 cm^2

Chapter 3

System model identification

In order to obtain an accurate linear model, the parameters of the manufacturer are merely used as a guideline. There can be deviations on the parameters and these parameters only provide accurate information up to the first resonance frequency. A measurement is required to match the model to the real system. This measurement can be performed by measuring the movement of the diaphragm under various input signals. The process of obtaining a linear model is required in order to design a controller later on in Chapter 4.

3-1 Test set-up initial testing

In order to get a good grasp of the dynamical behaviour of the loudspeaker, a test set-up is built. The woofer is mounted inside an enclosure, made out of 12 mm Medium Density Fiber (MDF) board. This enclosure's inner dimensions are 220 by 220 by 220 mm. The inside of the enclosure is fitted with sheets of damping material on the surface area. This damping material is used in order to dampen the acoustic enclosure dynamics, which are expected to have a resonance in the 1.300 Hz to 1.500 Hz region. It is advised to dampen these dynamics so that the influence on the woofer dynamics is limited.

The woofer is driven by a current feedback amplifier. Since it is known that the force of the Lorentz actuator is linearly coupled to the electric current, as described in Equation (2-3), driving an ideal current amplifier leads to a scaled force on the centre of the woofer diaphragm. When the input to a mass-spring-damper system, as shown in Figure 2-2, is a force, there is a resonating peak at the eigen frequency, according to Equation (2-6). This resonating peak can be used to have a high loop-gain around the eigen frequency. The other advantage of using a current feedback amplifier, is that when the electric resistance of the woofer or cables change, this does not influence the open-loop characteristics. For a voltage feedback amplifier, a change in electric resistance of the load changes the magnitude of the open-loop.

The current feedback amplifier used is a Kepco BOP 36-6ML, as described in Appendix A-13. This amplifier can drive an inductive load, like that of a woofer, to 6 kHz. The bandwidth of the usable amplification is well beyond the acoustic bandwidth of a typical woofer of 500 Hz.

The exact specifications of the amplifier, driving inductive loads, are not described in detail. Any dynamics introduced by the amplifier are captured in the system identification process.

3-2 Laser measurement on the movement of the woofer

As described in Section 2-4, the woofer is expected to have diaphragm break-up between 600 Hz and 800 Hz. In order to evaluate the behaviour between 600 Hz and 800 Hz, a measurement is performed. This measurement is performed with a laser tracking multiple spots of the moving diaphragm. The laser set-up used is a Polytec PSV-400 Scanning Head vibrometer, as described in Appendix A-16. This device measures the difference in wavelength between an outgoing and reflecting laser beam. Tracking the difference in wavelength can be calculated into a speed of the measured surface.

The signal of interest is the acceleration of the diaphragm. From Section 2-2-1 and Equation (3-1), it is known that the radiated power of a low frequency signal is proportional to the speed of the diaphragm and the angular frequency.

$$P_{\mathrm{a}} = (v_{\mathrm{d}} \cdot A_{\mathrm{d}})^2 \cdot \frac{\rho \cdot \omega^2}{2 \cdot \pi \cdot c} \tag{3-1}$$

For a sinusoidal motion of the diaphragm, Equation (3-1) can be rewritten to Equation (3-3) by substituting the speed of the diaphragm, v_{d}, for the acceleration of the diaphragm, a_{d}, as described in Equation (3-2).

$$a_{\mathrm{d}} = v_{\mathrm{d}} \cdot \omega \tag{3-2}$$

$$P_{\mathrm{air}} = (a_{\mathrm{d}} \cdot A_{\mathrm{d}})^2 \cdot \frac{\rho}{2 \cdot \pi \cdot c} \tag{3-3}$$

Figure 3-1 shows the woofer in the enclosure, with thin pieces of reflective tape attached to the diaphragm. The laser head shown in Figure 3-2 can track the individual spots in order to measure the local movement of the woofer. The measurement is performed by exciting the woofer with different frequencies and magnitudes and tracking the resulting motion of the reflective tape on the woofer. The signal used to excite the woofer is generated by the laser vibrometer software and send to the current amplifier. The amplifier outputs a current proportional to the voltage level on the input.

The low frequency behaviour of the woofer is that of a typical second order high pass with a peak at the resonance frequency and corresponding phase change from +180 degrees to 0 degrees. The amount of damping corresponds to the height of the resonance peak and the slope of the transition between +180 degrees and 0 degrees phase. Equation (3-4) describes the peaking factor, Q, that is the magnitude of the peak at the eigen frequency divided by the magnitude beyond the eigen frequency. The value of Q is calculated from the stiffness of the system, k_{s}, the moving mass of the diaphragm, M_{d}, and the damping of the system, c_{s}.

$$Q = \frac{\sqrt{k_{\mathrm{s}} \cdot M_{\mathrm{d}}}}{c} \tag{3-4}$$

Figure 3-1: Woofer under test circumstances, with reflective tape to enhance laser reflectivity

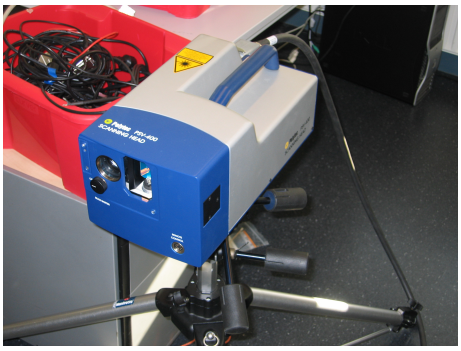

Figure 3-2: Laser scanner used to track the movement of the spots on the woofer

The peak value at the resonance frequency is one of the advantages of using a current feedback amplifier. This peak is later on used to achieve high open-loop gain around the eigen frequency. A voltage feedback amplifier leads to a lower value for Q at the eigen frequency.

The measurement with the laser set-up confirms the 600 Hz to 800 Hz diaphragm break-up dynamics that lead to the reduction of SPL in the specification sheet of the manufacturer. Figure 3-3 shows that between 600 Hz and 800 Hz, the centre of the diaphragm and the surround no longer move synchronised. Around 800 Hz, the motion of the surround area of the diaphragm is 180 degrees out of phase to the motion of the centre of the diaphragm. This implies an opposite motion of the centre of the diaphragm and the outer part of the diaphragm. Since the acoustic radiation of the two surface areas is inverted, the sum of the acoustic radiation at 800 Hz is very low. This observation was expected from the SPL peak and dip shown in Figure 2-3. Additional measurements indicate that the break-up at 800 Hz is axisymmetric.

Figure 3-4 and Figure 3-5 show a visualisation of a typical first diaphragm break-up at which the diaphragm no longer moves as a piston, but when there is movement within the surface area.

When increasing the frequency, at around 3 kHz, a similar behaviour can be noticed. Moving further up the frequency band indicates higher order diaphragm break-ups, possibly with non-axisymmetric shapes. The frequencies of diaphragm break-up modes are beyond the usable acoustic bandwidth of the woofer and control bandwidth of the controller. There is no advantage in controlling the centre of the diaphragm, where the Lorentz actuator is mounted, if the rest of the diaphragm is still deforming.

The measurement confirms that there are more dynamics involved than just the linear second order mass-spring-damper system behaviour, that is described by the Thiele/Small parameters noted in Table 2-1.

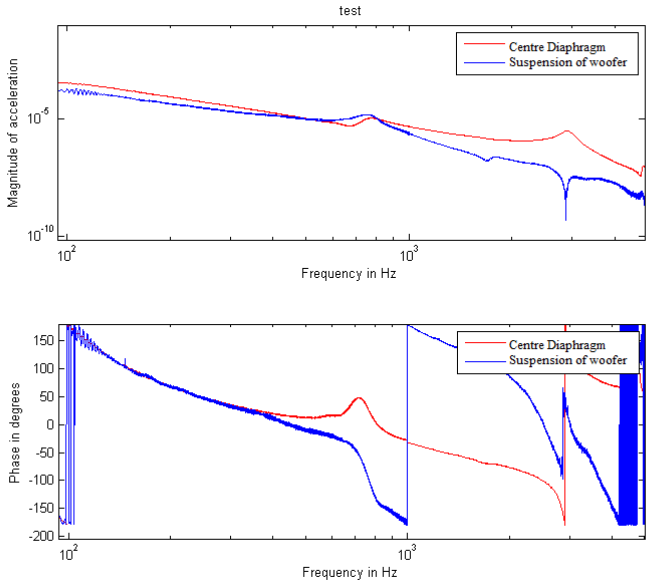

Figure 3-3: Laser measurement showing the magnitude and phase of the acceleration of the centre and surround of the diaphragm

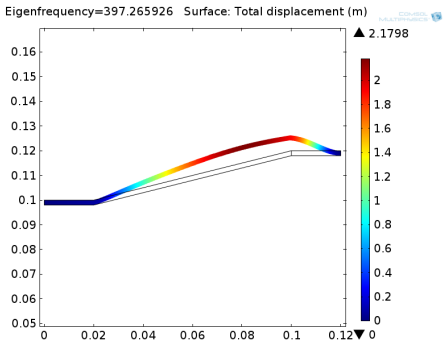

Figure 3-4: 2D visualisation of a typical first diaphragm break-up mode

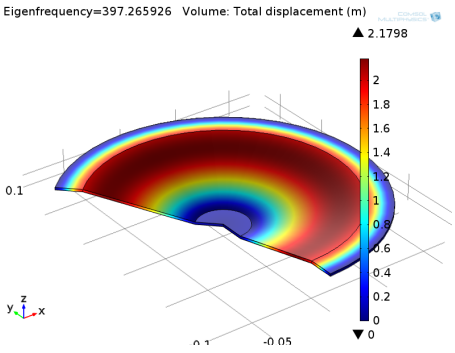

Figure 3-5: 3D visualisation of a typical first diaphragm break-up mode

3-3 Sensor selection

Even though the laser measurement is a useful tool to measure the dynamic behaviour of the woofer, it is not designed to provide real-time control.

In order to implement real-time feedback control, real-time data must be available to the controller. There are multiple types of sensors available for this purpose. Three sensor types that can provide the resolution and speed are evaluated for the use of real-time feedback.

3-3-1 Microphone

A microphone capsule that can be used for feedback, is the Panasonic WM-61A. That microphone capsule has a wide bandwidth, but the behaviour at low frequencies is not provided by the manufacturer. According to the specification sheet in Appendix A-15, the low frequency usable band is 20 Hz. Typically, manufacturers put bandwidth limitations at the frequency of the -3 dB frequency. A microphone, by it's nature, has the property of capturing not only pressure waves nearby, but pressure waves from the environment too. This means that an acoustic disturbance surrounding the microphone is influencing the observed motion of the loudspeaker.

Mounting a microphone inside the woofer enclosure is an option too. In that case, a high pressure level microphone must be used.

3-3-2 Laser

A close range laser distance sensor can be used for tracking the position and, by double derivation, the acceleration. Micro Epsilon, a manufacturer of laser displacement and positioning sensors has a sensor that is capable of capturing a measurement every 0.00001 second. The LD1630, as described in Appendix A-10, with an analogue output, has a stated usable bandwidth between 0 Hz and 100 kHz and a measurement range of up to 50 mm.

3-3-3 Accelerometer

An accelerometer is a sensor that measures the accelerations of the body in one or multiple degrees of freedom. The Lorentz actuator can only exert force in one degree of freedom so only one axis of acceleration measurement is required. A sensor of interest is the Measurement Specialities ACH-01. This is an analogue sensor with a bandwidth from 2 Hz to 20 kHz, as described in Appendix A-19. This sensor has been successfully implemented in MFB set-ups by other engineers.

3-3-4 Sensor choice

Analysing the previously mentioned options, leads to the choice of using an accelerometer.

Using a microphone in front of the woofer diaphragm is expected to lead to an undesired additional time delay and is sensitive to environmental acoustic changes. If the microphone

is used at a distance of 1 cm from the centre of the diaphragm, an acoustic signal of 1 kHz would, by the corresponding delay, introduce an added phase of 14 degrees. Mounting a microphone in front of the woofer therefore is not the chosen option. Mounting a high level microphone inside of the enclosure is an option, but the low frequency roll-off is higher than desired for control purposes.

Only a couple of laser sensors can be used in the wide frequency range and range of excursion of the woofer. Therefore, the sensors that have the required specifications are expensive compared to the other types of sensors. However, the real difficulty with using a positioning sensor is that the sensor output must be differentiated twice before the acceleration is obtained. This introduces additional noise to the measurement.

The accelerometer of choice is the Measurement Specialities ACH-01, shown in Figure 3-8 and described in Appendix A-19. The typical application gain stage, shown in Figure 3-6, is implemented in order the match the performance of the sensor, stated by the manufacturer.

In order to attach the sensor to the moving part of the woofer, the dust cap is removed. An aluminium mounting disc is made on the lathe and is glued on the voice coil carrier. The mounting disc and sensor introduce extra weight to the diaphragm, but that changes the dynamics within acceptable boundaries above the resonance frequency of the system. The added mass lowers the efficiency of the woofer. The sensor and aluminium disc weigh just under 12 grams in total. With an original moving mass of 30,5 grams, the moving mass of the woofer is increased by 40%. The efficiency of the woofer is reduced by 40%. This introduces no problems since the power amplifier can deliver enough power to compensate for the additional mass. The resonance frequency of the woofer is decreased by 18%. The woofer that was not equipped with the additional mass has a resonance frequency of 57 Hz. The resonance frequency with the additional weight will reduce to 47 Hz.

The mounting disc has a dynamic behaviour too, that is not desired to influence the measurement in the operating area of interest. Figure 3-7 shows that the first influence of the mounting disc is at 6.200 Hz, well beyond the predicted crossover frequency of the controller.

The additional mass and the effect on the dynamic behaviour of the woofer, outweigh the disadvantage of the two alternative types of sensors.

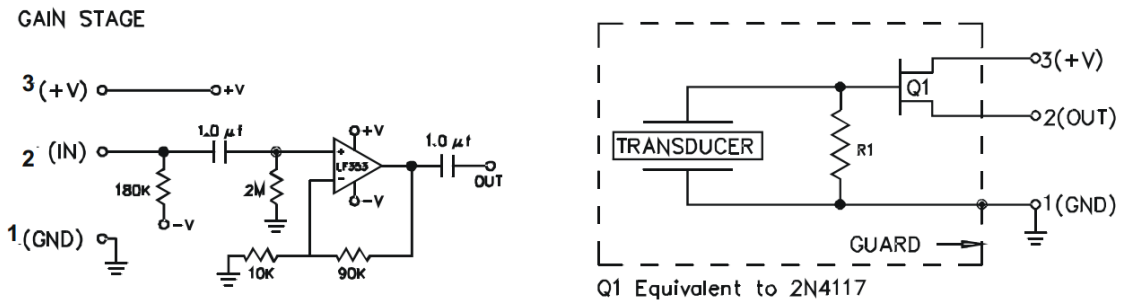

Figure 3-6: Accelerometer gain stage, as in the specification sheet, A-19

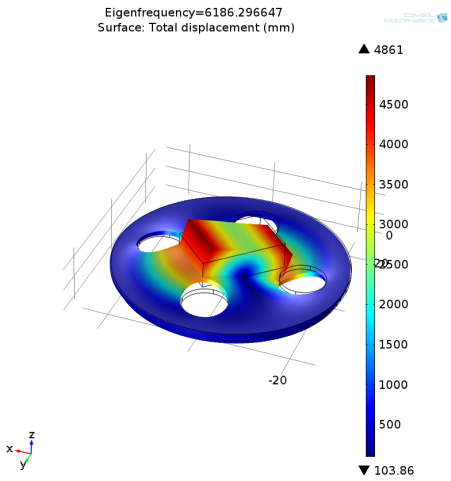

Figure 3-7: Mounting disc with the first resonance at 6.200 Hz

Figure 3-8: Measurement Specialities ACH-01 Accelerometer

3-4 Data accelerometer output

A Data Acquisition system (DAQ) is used in order to measure the accelerometer output signal and drive the power amplifier. The National Instruments USB 6211, as described in detail in Appendix A-17, has two analogue outputs that can be programmed by the use of Mathworks Matlab 2013. Two of the sixteen analogue inputs are used to capture both the identification signal and the output from the accelerometer.

Figure 3-3 shows a system with higher order dynamics, well outside of the expected control bandwidth. The goal of the system identification is to obtain an accurate linear model of the dynamics of the movement of the centre of the woofer diaphragm.

In order to construct the linear model, a logarithmic sine sweep is used to drive the woofer. The sweep excites the woofer from 30 Hz to 6.000 Hz with a fixed peak magnitude, that excites most dynamics of the system. The power amplifier output is a current, scaled to the input voltage. The signal generated in Matlab therefore is a scaled representation of the force generated by the Lorentz actuator. Equation (3-5) indicates the ratio between the values used in Matlab, V_{M}, the gain of the power amplifier, g_{a}, and the motor force factor of the woofer, $B \cdot \ell$, to the resulting motor force, F_{L}. The ratio between the value in Matlab to a force in Newton is $V_{\mathrm{M}} \cdot 4.56$.

$$F_{\mathrm{L}} = V_{\mathrm{M}} \cdot g_{\mathrm{a}} \cdot B \cdot \ell \tag{3-5}$$

$$F_{\mathrm{L}} = V_{\mathrm{M}} \cdot 4.56 \tag{3-6}$$

The DAQ samples the analogue inputs at a rate of 100.000 samples per second. Both the generated sine sweep signal and the sensor output are recorded in order to keep the data synchronised.

With the captured data set from the sensor, an initial impression of the dynamics is acquired by computing an Empirical Transfer Function Estimate (ETFE).

The Nyquist frequency, when sampling at 100 kHz, is 50.000 Hz, half of the sample frequency. Since the highest frequency of excitation is 6.000 Hz, re-sampling by a factor ten removes the estimated output at frequencies which are not excited and limits the ETFE to 5.000 Hz.

An ETFE of the dataset is shown in Figure 3-9. Analysing the ETFE plot shows a series of distinct characteristics which can be related to a combination of mechanical phenomena.

1. 180 degrees phase up to 20 Hz
2. peaking high pass dynamic behaviour at 45 Hz.
3. 0 degrees phase between 70 Hz and 500 Hz.
4. relatively small magnitude change between 70 Hz and 500 Hz.
5. dynamic coupling and decoupling behaviour in the magnitude plot from 600 Hz to 800 Hz.
6. dynamic coupling and decoupling behaviour in the magnitude plot around 1.300 Hz.
7. steep drop in phase at the 3.000 Hz diaphragm resonance

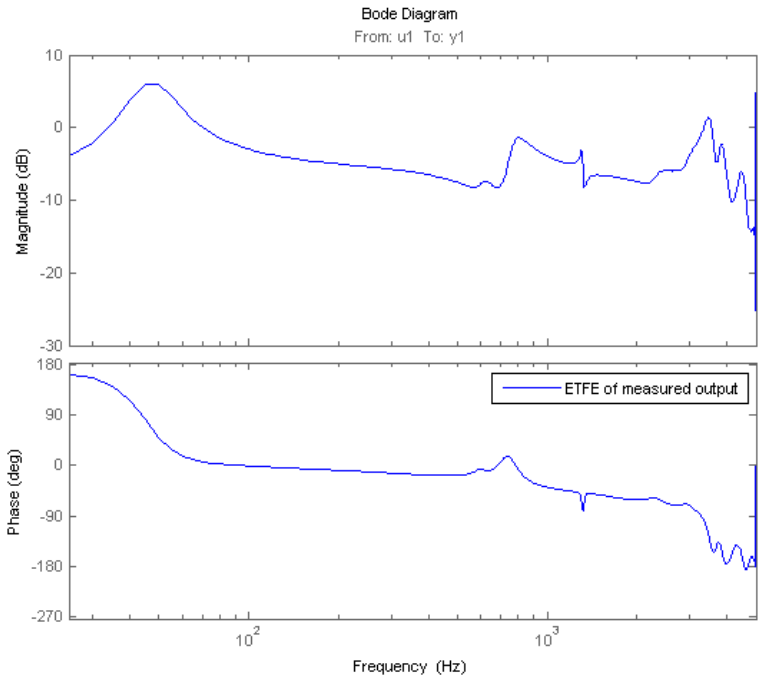

Figure 3-9: ETFE of measurement data

The dynamics described above can be converted to series of linear transfer functions that have a similar behaviour. Figure 3-10 shows the overlay of both the bode plot of the fitted model and the ETFE of the measured data.

There are differences between the acquired ETFE and the fitted model. The low frequency magnitude and phase are different. This is caused by the fact that the distinct peak at the first eigen frequency is only excited for a very small amount of time. Additional measurements that focus on the low frequency behaviour, show a better match in both magnitude and phase around the first eigen frequency of 45 Hz.

There is a mismatch between the model and the data at 600 Hz and from 3.000 Hz. The design of the model is performed based on first principle models that not describe the motion at frequencies over 3.000 Hz. The expected operational bandwidth of the woofer is 40 Hz to 300 Hz. For the purpose of control, an estimation of the magnitude and phase outside of the control bandwidth is of interest, only in order to determine stability

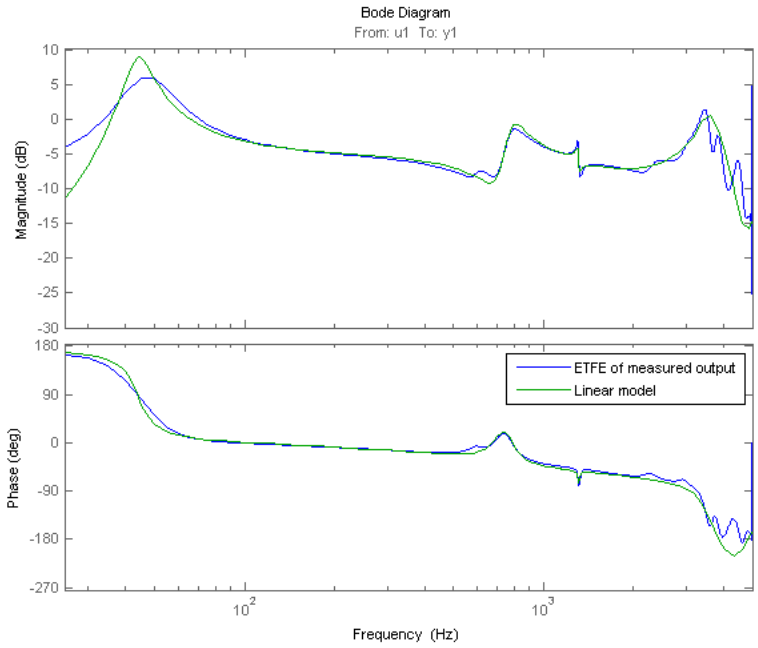

Figure 3-10: ETFE measurement data and the fitted model

Chapter 4

Controller design

4-1 Linear feedback control

In order to apply feedback, a controller is designed. The dynamics of this controller, in combination with the dynamics of the loudspeaker system, determine the overall system performance.

4-1-1 Controller topology

For this controller, a topology is chosen in the form of Figure 4-1. In this topology, r is the reference. In practice, r is the audio signal to be tracked by the woofer. The C-block is the implemented controller. This block, when implemented, consists of a discretized transfer function. The P-block is the Plant or system, identified in the system identification process. In practice, this block is the transfer from the signal send to the amplifier to the measured acceleration by the sensor. The output of the system, y, is compared to the reference, r. The difference between the reference and the measured output is the output error, e.

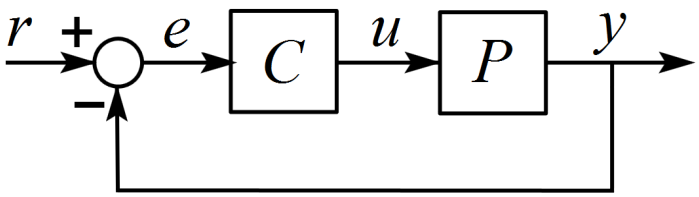

Figure 4-1: Feedback topology

The transfer function from the feedback error, e, to the output, y, is the Open Loop Transfer Function. This transfer function consists of the multiplication of the transfer function of the controller with the transfer function of the linear system model. From the open loop transfer function, a lot of information regarding the closed loop performance can be acquired.

4-1-2 Stability Consideration

When designing the controller, the stability of the system is one of the limitations of the system that needs to be taken into account. Since the frequency response of both the controller and the plant are known, or to be designed, the closed loop system can be evaluated for stability.

A classic way of determining stability of a system, is to evaluate the polynomial of the close loop transfer function. When the poles of the polynomial all are in the left half of the complex plane, the closed loop is stable.

The Nyquist plot is a graphical tool that enables to predict the degree of stability of a closed loop system from the open loop response. Analysing stability from the open loop is useful when instability, after closing the loop, can cause damage to the plant. In that case measuring only the open loop frequency response is sufficient to predict the closed loop behaviour.

Equation (4-1) is the notation of the open loop transfer function, $OL_{ye}(s)$. It is the multiplication of the controller transfer function by the linear model of the plant.

$$OL_{ye}(s) = P(s) \cdot C(s) \tag{4-1}$$

When the loop is closed, the transfer function from the input, r, to the output, y, is described by equation (4-2). The transfer function of the closed loop is determined by the open loop characteristics.

$$CL_{yr}(s) = \frac{P(s) \cdot C(s)}{1 + P(s) \cdot C(s)} \tag{4-2}$$

Maintained oscillation is acquired when the output of the open loop, y, is inverted to the input of the open loop, e. In that situation, the output is inverted again by subtraction and becomes the new input, e, that is identical to the previous input. This situation therefore occurs when the open loop transfer function, $OL_{ye}(s)$, at the given input frequency, is -1.

The characteristics of the open loop transfer function can be plotted in a Nyquist plot. Both the magnitude and the phase of $OL_{ye}(s)$, are captured in the Nyquist plot. The critical point of maintained oscillation is used as a guideline to check whether the system is stable or unstable. The Nyquist stability theorem says that an open loop transfer function does not have have poles in the right half complex plane, when the Nyquist plot does not encircle the critical -1 point. In that situation the roots of the polynomial of the closed loop transfer function are all in the left half complex plane and the system is stable.

The distance from the Nyquist curve to the critical -1 point is expressed by the gain margin, phase margin and modulus margin and describe the degree of stability. Gain margin, g_m, is the gain that can be added before the -1 point is encircled. The phase margin, φ_m, is the phase that can be added before the curve is encircling the -1 point. The modulus margin, m_m, is the shortest distance between from the Nyquist curve to the critical -1 point.

4-1-3 Practical limitations

The practical implementation of the feedback loop is limited by the set-up. These limitations need to be taken into account.

1. The loudspeaker cannot track a static acceleration.
2. The loudspeaker has a limited amount of excursion.
3. The amplifier has a current-, bandwidth- and voltage-limitation.
4. Signals must be sufficiently large in order to obtain an acceptable bit-depth.
5. The digital sample-rate and latency of DSPs are limited.

4-2 Controller objective

The controller must be designed such, that within the acoustic bandwidth of the woofer, the performance is enhanced. The woofer dimensions and characteristics indicate an acoustic operating bandwidth between 40 Hz and 400 Hz. Below 40 Hz, a reasonable acoustic power output requires large excursions from a woofer of this size, as described in Section 2-2-1. Due to the limited excursion of 8 mm, it is decided not to track the lowest frequencies of the audio spectrum. Beyond 400 Hz, the woofer no longer radiates acoustic power as spherical as in the lower frequencies due to the ratio between the size of the diaphragm and the wavelength of the pressure waves.

The objective of the final controller is to obtain an output disturbance rejection that suppresses the THD below 1%. The other objective is to compensate for the diaphragm break-up. In order to reach the objectives, the open loop must have a peak magnitude of over 20 dB, a control bandwidth extended to the diaphragm break-up and reasonable stability margins.

Stability margins are considered to be reasonable under the following conditions.

1. The phase margin, φ_m, is more than 20 degrees
2. The gain margin, g_m, is more than 3 dB

4-3 Controller design

The controller is designed, keeping in mind the limitations of the loudspeaker, the hardware and the frequency bandwidth in which the model of the loudspeaker is accurate. Between 30 Hz and 3.000 Hz, the model is a match to the linearization of the system within 2 dB deviation.

Analysing the practical- and stability-limitations, leads to two required unity-gain crossover frequencies. One crossover frequency is at a low frequency and one at a high frequency. The frequency band in between the two crossover frequencies, except for the frequencies close to these frequencies, is where the controller is suppressing disturbances.

The low frequency crossover frequency is close to 30 Hz. When the slope of the open loop transfer function at the low frequency crossover frequency is close to 40 dB per decade, the loop gain can be high at frequencies at which most disturbances are expected. The frequencies at which the controller must have a high loop gain are the frequencies of the harmonic distortions

of 30 Hz to 60 Hz. At these low fundamental frequencies, the woofer needs a large excursion in order to generate the required acoustic power. When the excursion of the diaphragm is large, the non-linear behaviour of the woofer is a big contributor to the overall acoustic power. The loop gain is designed such that it is over 10 dB between 60 Hz and 240 Hz, which captures both the second and third harmonics distortion of all frequencies in between 30 Hz and 60 Hz.

Figure 4-2 shows the bode plot of the transfer function of the controller. The controller is designed by multiplication of a series of transfer functions.

1. Two zeros at 44 Hz and two poles at 50 Hz. This creates an antiresonance at 44 Hz, adding phase in the low frequency band to increase the low frequency phase margin.
2. A compensation for the diaphragm break-up from 600 Hz to 800 Hz. This is a lead-lag compensator consisting of two poles and two zeros.
3. A notch filter for a resonance at 7.100 Hz, two poles and two zeros at 7.100 Hz
4. Two zeros at 60 Hz and two poles at 200 Hz, increasing the magnitude from 60 Hz to 200 Hz
5. Two poles at 90 Hz, leading to a descending slope of the magnitude
6. A zero at 300 Hz and a pole at 1.000 Hz in order to reduce the phase, so that the high frequency margin is larger

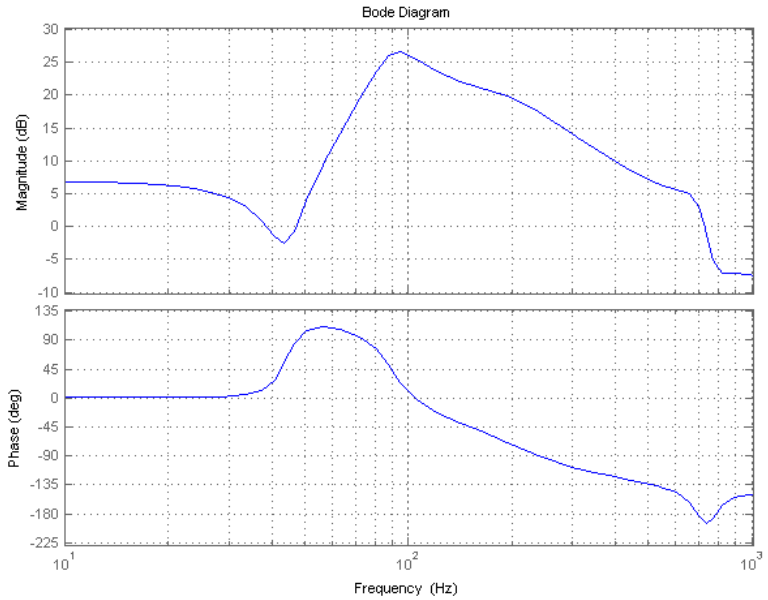

Figure 4-2: Bode plot of controller block transfer function

Multiplying the control block transfer function by the linear model of the system, leads to the open loop characteristics. This open loop is plotted in a Bode plot in Figure 4-3.

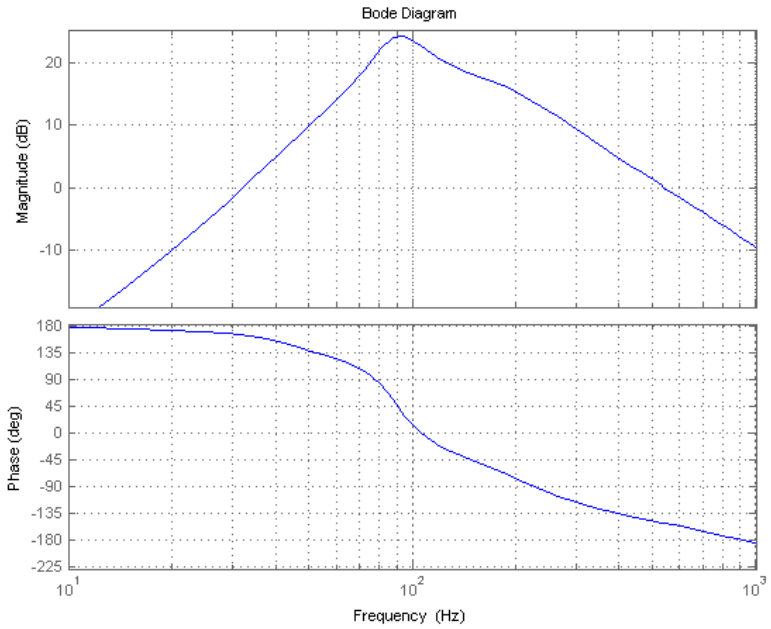

Figure 4-3: Bode plot of open loop transfer function

Figure 4-4 shows the stability margins of the open loop. For the crossover frequency of 30 Hz, the phase gain, φ_{lf}, is 20 degrees and the gain margin, g_{lf}, is 3 dB. The gain margin is smaller than the open loop model suggests. The low frequency magnitude slope of the model is not a perfect match to the real system. The gain margin therefore is smaller, because the magnitude below 30 Hz is larger than the magnitude of the linear model. For the crossover frequency of 500 Hz, the phase gain, φ_{hf}, is 25 degrees and the gain margin, g_{hf}, is 8 dB.

The open loop transfer function magnitude is over 10 dB, between 50 Hz and 270 Hz. The maximum loop gain is 23 dB at 95 Hz.

The objective of designing a controller that has an open loop gain that is over 10 dB is accomplished, while the stability margins are reasonable. The objective to have loop gain at the diaphragm break-up is not accomplished due to high frequency diaphragm break-up and model uncertainties. In order to guarantee stability, the crossover frequency is reduced to 500 Hz. For the initial experiments, this controller is implemented.

4-4 Closing the loop

The closed loop transfer function is the transfer from the reference value, r, to the system output, y, as shown in Figure 4-1 and Equation (4-3).

$$CL_{yr}(s) = \frac{P(s) \cdot C(s)}{1 + P(s) \cdot C(s)} \tag{4-3}$$

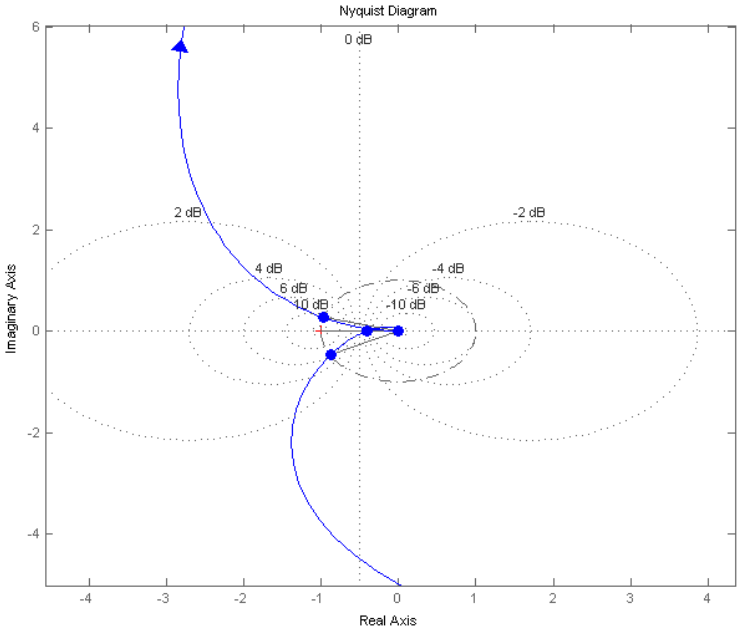

Figure 4-4: Nyquist plot of open loop transfer function

Designing the characteristics of the closed loop transfer function as in Equation 4-2 is the goal of the open loop shaping. Designing in the open loop is a tool in order to achieve the desired closed loop characteristics.

The performance of the closed loop transfer function can be described by analysing the sensitivity transfer function, $S(s)$. This transfer function can be interpreted as the residual of a disturbance, d, on the output, y, when the feedback loop is closed.

$$S(s) = \frac{1}{1 + C(s) \cdot P(s)} \tag{4-4}$$

The lower the value at a certain frequency, the higher the suppression of that disturbance. Figure 4-6 shows that the disturbances with a frequency content between 50 Hz and 270 Hz are suppressed by a minimum of 10 dB. Between 75 Hz and 130 Hz, the suppression is over 20 dB, a factor 10. One of the objectives is to implement a controller that reduces the THD to below 1%. When a 40 Hz tone is played at loud volume and the second and third harmonics are 80 Hz and 120 Hz, according to the Bode plot shown in Figure 4-6, these distortions are suppressed by a factor ten. If the controller is not implemented and the THD is 10%, it is calculated that with the implementation of the controller, the THD is reduced to 1%.

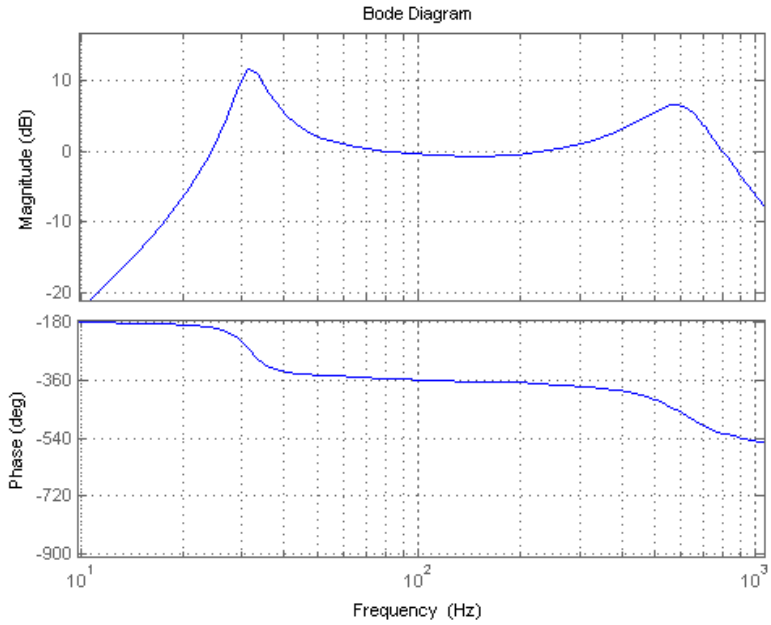

Figure 4-5: Bode plot of the closed loop transfer function

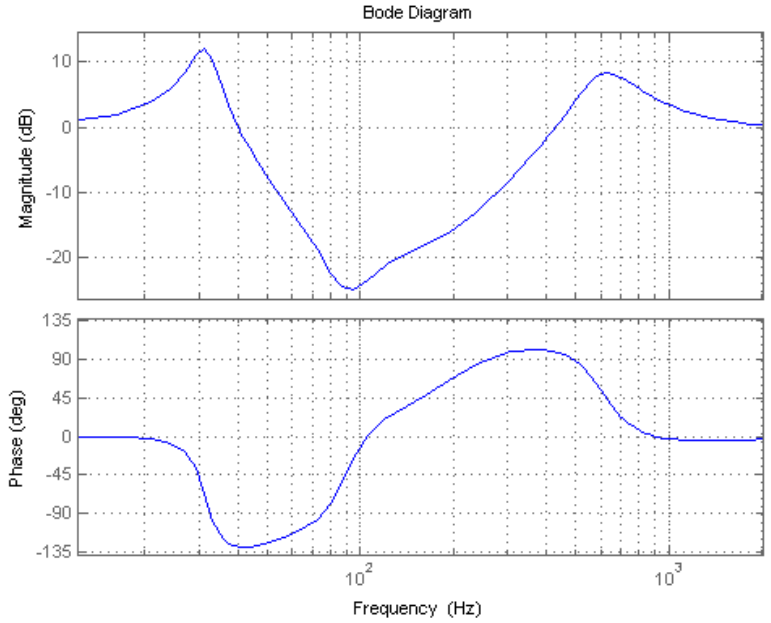

Figure 4-6: Bode plot of the sensitivity transfer function

Chapter 5

Controller implementation

The sensitivity transfer function from Chapter 4 is only a simulated controller performance. In order to test the actual performance, the controller is implemented and tested on the actual set-up.

5-1 Digital implementation, dSpace environment

In order to implement the controller in the set-up, the Laplace notation of the controller block, $C(s)$, is rewritten in a discrete time state-space notation and implemented in a dSpace DS1103 PPC controller board, as described in Appendix A-20. This controller board can be programmed within the environment of Matlab and Simulink. The real-time module of Matlab compiles the model of Simulink into a DSP format and can upload the compiled code to the DSP of the dSpace DS1103.

5-1-1 Why use a DSP

Using a DSP with the flexibility of the dSpace DS1103 brings advantages over building a prototype with analogue electronics. Altering a controller implementation, adding signal magnitude limitations or adding non-linear implementations of controllers is easier in the digital domain than in the analogue domain.

5-1-2 Drawbacks of using a digital implementation

Using a DSP for feedback systems introduces new problems over analogue circuits.

1. An analogue-to-digital (ADC) conversion is required in order to provide the DSP with digital information. These ADC have a limited bit-depth and a time delay due to filtering expressed by latency.

2. A digital-to-analogue (DAC) conversion is required in order to transform the DSP outcome to a analogue signal. These DAC have a limited bit-depth and a time delay due to filtering expressed by latency.

3. DSP's have a limited computational power that limits the amount of calculations a DSP can perform per sample.

For this research, the dSpace DS1103 DSP is used since the limitations of the digital implementation do not outweigh the advantage of having the flexibility of tuning the controller.

5-2 Sample-rate selection

The latency of the dSpace board is programmable and for this purpose small enough to introduce only a small amount of added phase in the control bandwidth. The sample-rate is set to 100 kHz. The measured latency is verified to be 1/100.000th of a second. For a 100 kHz sine wave, this period is as large as a full cycle, or a phase of 360 degrees. In order to verify that the added phase due to sampling is sufficiently small, the added phase at 1 kHz is calculated. The phase added by introducing the delay is 3,6 degrees at 1 kHz. This amount is acceptable for this application. If a DSP is used that has a latency of 1/10.000th of a second, the added phase at 1 kHz would be 36 degrees, an additional phase to be taken into account when designing the open loop dynamics.

5-3 Measuring the disturbance rejection

The figures in chapter 4-4 are obtained from the linear model of the system and the designed controller. In order to verify the actual performance of the controller, the controller is implemented in the real set-up. Figure 5-1 shows the result from a measurement at which a disturbance is introduced on the accelerometer by adding a signal on the amplifier input. When closing the loop, the disturbance is reduced or increased depending on the frequency of the disturbance. The remaining fraction of the disturbance is a match to the calculated sensitivity function, shown in Figure 4-6. At 40 Hz and around 450 Hz, the disturbance introduced is not suppressed and is identical on the output. Within 40 Hz and 450 Hz, the remainder of the disturbance is lowest at 90 Hz at just under 8%. This value is very close to the predicted -23 dB, which in fraction results in a 7,1% remainder. The slope from 90 Hz to the 0 dB suppression frequency at 40 Hz and 450 Hz are identical.

A second test is performed to verify the predicted suppression of disturbances from the woofer motion. A sine wave is used as a reference signal. The magnitude of the 40 Hz sine is such that the output at the accelerometer is 700 mV RMS at 40 Hz. A fast fourier transform is used in order to measure the power at frequencies from 1 Hz to 5.000 Hz.

Figure 5-2 shows the frequency content measured from the accelerometer sensor. The fundamental frequency of 40 Hz is clearly visible and the second and third harmonics at 80 Hz and 120 Hz are -18 dB respectively -17 dB. The fourth and fifth harmonics at 160 Hz and 200 Hz are -40 dB respectively -35 dB. It is expected that when implementing the controller, these harmonic distortions are reduced by the corresponding magnitude of the sensitivity function.

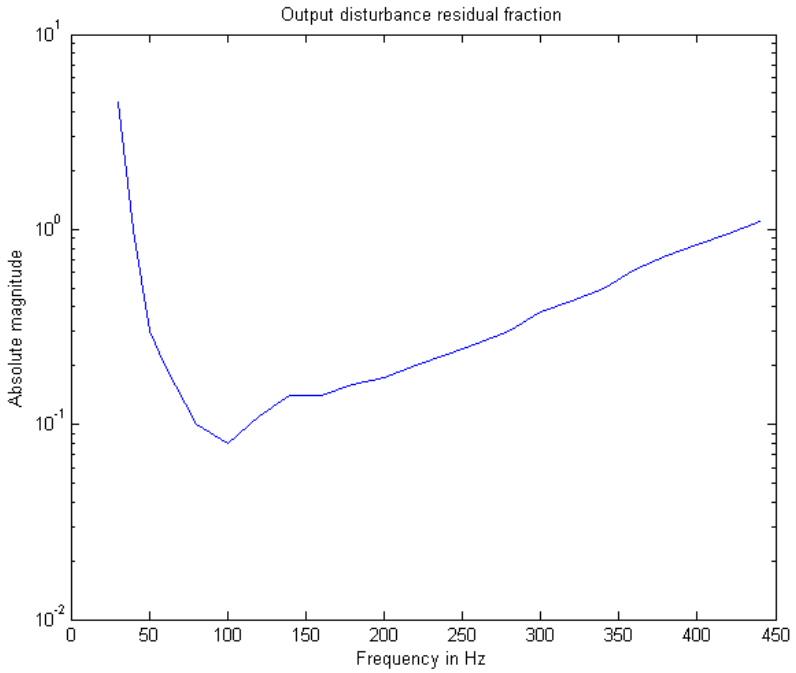

Figure 5-1: Measured fraction on output when introducing a disturbance

The 80 Hz and 120 Hz content is introduced by the signal generator, amplifier, woofer, accelerometer and the ADC of the computer set-up. The contribution of the harmonic distortion by the woofer is the dominant source of harmonic distortion, as described in Appendix A-8.

Figure 5-3 shows the result from the measurement, with the implementation of the feedback controller. The second and third harmonics are no longer in de -20 dB scale but reduced to -40 dB. This suppression of -20 dB is the exact value that was calculated for that bandwidth. The fourth and fifth harmonic distortions are suppressed by the calculated magnitude too and are reduced to -55 dB and -50 dB, 15 dB lower than the original value.

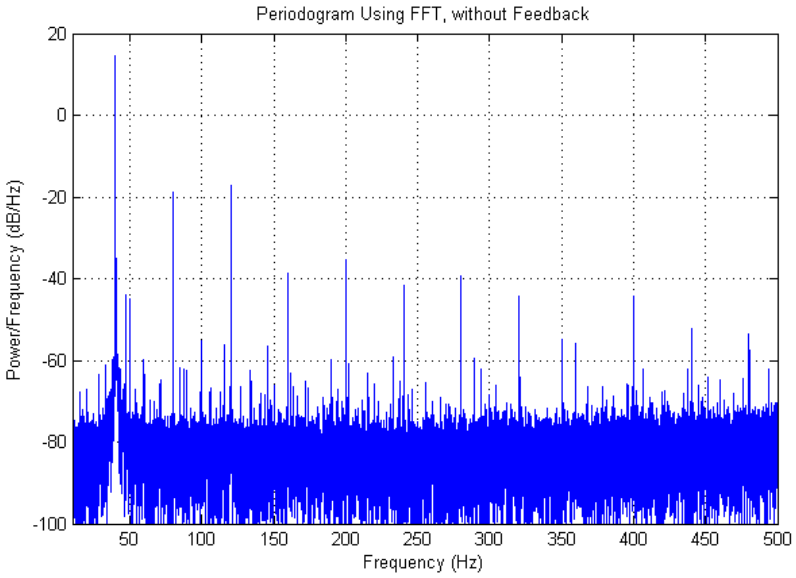

Figure 5-2: Fast fourier transform of 40 Hz fundamental frequency without feedback controller

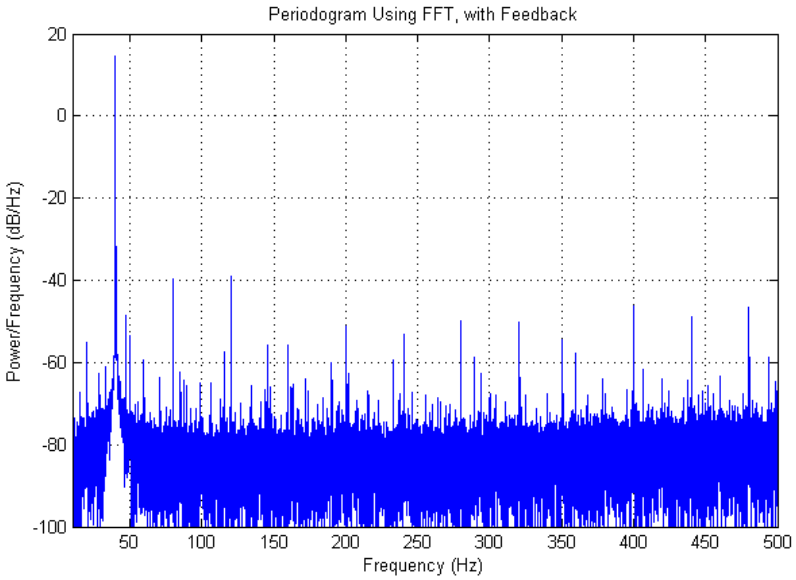

Figure 5-3: Fast fourier transform of 40 Hz fundamental frequency with feedback controller

Chapter 6

Acoustic measurements

The accelerometer sensor confirms the increase in performance of the motion of the diaphragm by the application of feedback. The difference between Figure 5-3 and Figure 5-2, as described in Section 5-3, indicates the enhanced performance of the motion of the accelerometer attached to the voice-coil. In order to measure the acoustic increase of performance of the woofer, measurements are performed with a microphone.

6-1 Initial measurements

In order to get an initial impression of the acoustic performance with and without the implementation of the controller, a measurement is performed. The actuated frequency is 40 Hz. The microphone used is a Panasonic WM-61A, described in detail in Appendix A-15, that is equipped with a gain stage and modification in order to be capable of higher sound pressure levels.

The first measurement is performed without feedback. This is the reference performance of the woofer without any corrections performed by the feedback loop. Figure 6-1 shows the fundamental frequency captured by the microphone at 40 Hz and the content of the harmonic distortions. Due to the suppression of disturbances measured in Chapter 5, the harmonic distortion should be reduced by 20 dB between 60 Hz to 200 Hz. Figure 6-2 shows the measurement, with the feedback controller implemented. The peak of the fundamental frequency is identical to the peak in Figure 6-1. The harmonics at 80 Hz and 120 Hz are, in contrast to the expectations, not reduced by 20 dB, but by 7 dB and 10 dB, noted in Table 6-1.

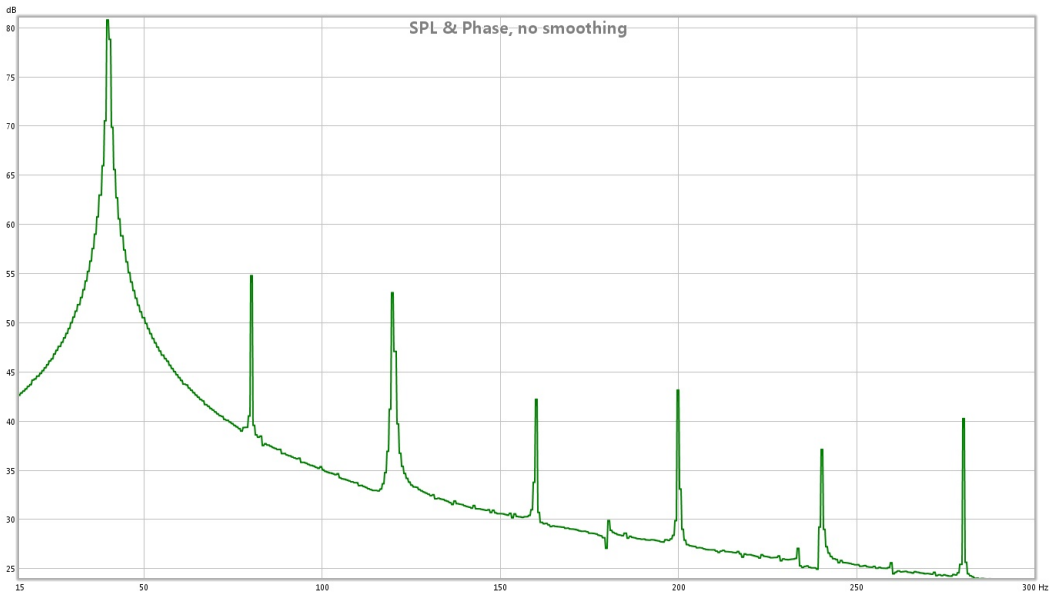

Figure 6-1: Acoustic measurement without feedback corrections

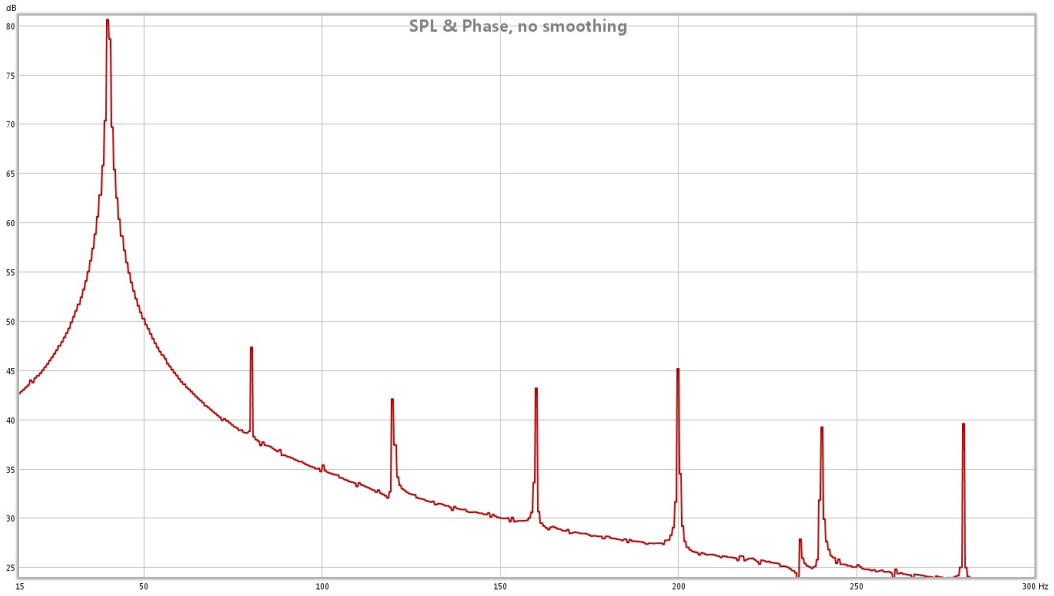

Figure 6-2: Acoustic measurement with feedback corrections

Table 6-1: Microphone measurement at 40 Hz

Frequency	No feedback	Feedback	Difference
40 Hz	81 dB	81 dB	0 dB
80 Hz	54 dB	47 dB	-7 dB
120 Hz	52 dB	42 dB	-10 dB

6-2 Interpretation of initial measurements

In contrast to the disturbance suppression measured on the accelerometer, the acoustic suppression of distortion is of a smaller magnitude. The increased performance of the measured sensor output is not a representation of the increase in acoustic performance. This observation leads to the theory that the motion and distortion measured by the accelerometer is not fully representative of the acoustic distortion of the set-up.

From Section 3-2, it is known that the surround of the woofer diaphragm is of large influence on the acoustic radiation. In order to find the source of the distortion, an acoustic measurement is performed locally on several locations of the woofer diaphragm. These measurements indicate that the surround of the woofer contributes to the distortion. Since the contribution of the propagated acoustic power of the surround is, by its larger diameter, as large as that of the centre of the woofer, the harmonic distortion is only reduced by a small amount. Since the surround cannot be directly controlled by the Lorentz actuator, it will still influence the acoustics.

Figure 6-3 and Figure 6-4 show the reference measurement, without applied feedback. The measured distortion at 80 Hz is 20 dB larger on the surround compared to the measurement on the centre of the woofer. Figure 6-5 and Figure 6-6 show that with the implementation of feedback, the surround is still radiating acoustic distortion. The combined acoustic radiation of both the centre and the surround lead to the observation of Chapter 6-1.

The problem is not caused by the concept of the feedback loop, but by the woofer evaluated in the research. The character that makes the woofer interesting as described in Chapter 2-4, is the fact that the surround of the diaphragm does not move identical to the centre of the diaphragm. It is believed that this character backfires when a feedback loop is applied that only enhances the performance on one specific point. Distortion introduced by the surround is still present, even though the motion of the centre of the diaphragm is controlled.

The results from the acoustic measurements on the Peerless woofer set-up are not satisfactory. The accelerometer sensor is indicating a suppression of harmonic distortion, but the microphone is not indicating equal suppression. The objective to suppress the THD below 1% therefore cannot be accomplished with the current controller and set-up.

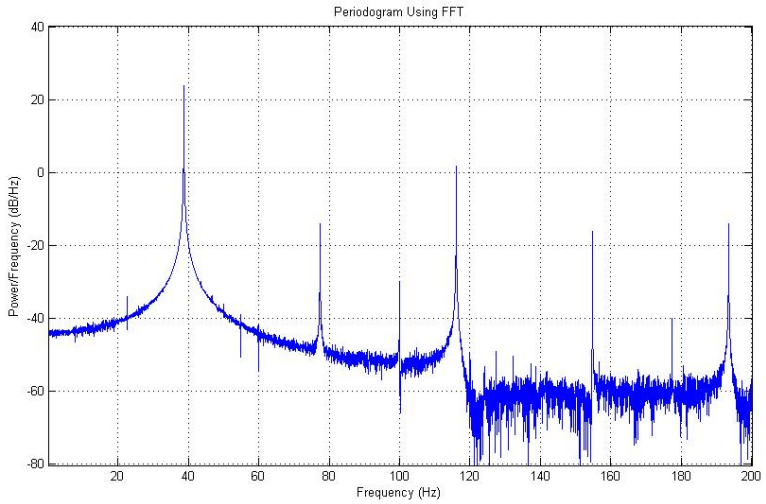

Figure 6-3: Acoustic measurement reference, microphone close to center of the woofer

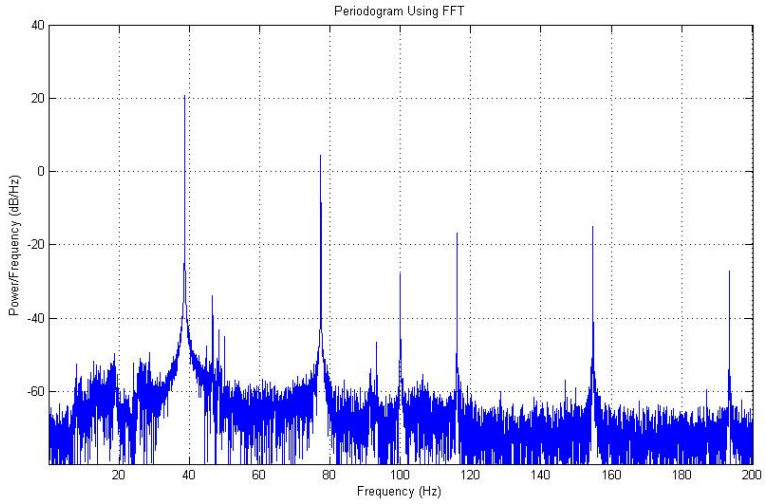

Figure 6-4: Acoustic measurement reference, microphone close to rubber surround of the woofer

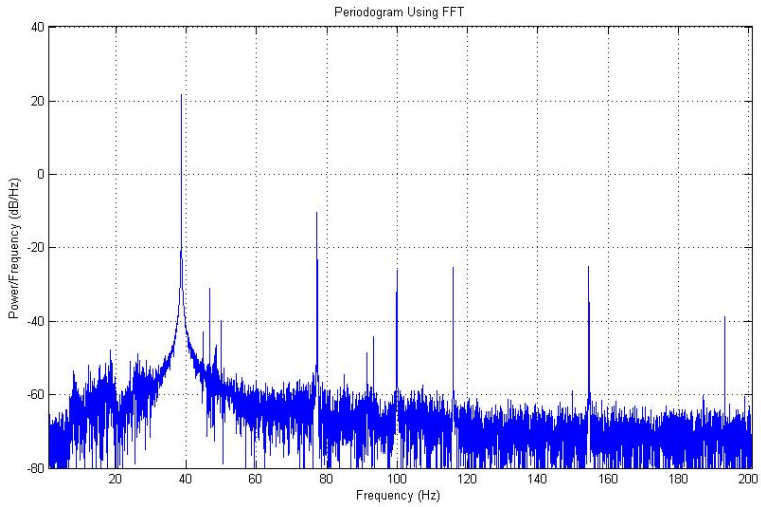

Figure 6-5: Acoustic measurement with feedback applied, microphone close to center of the woofer

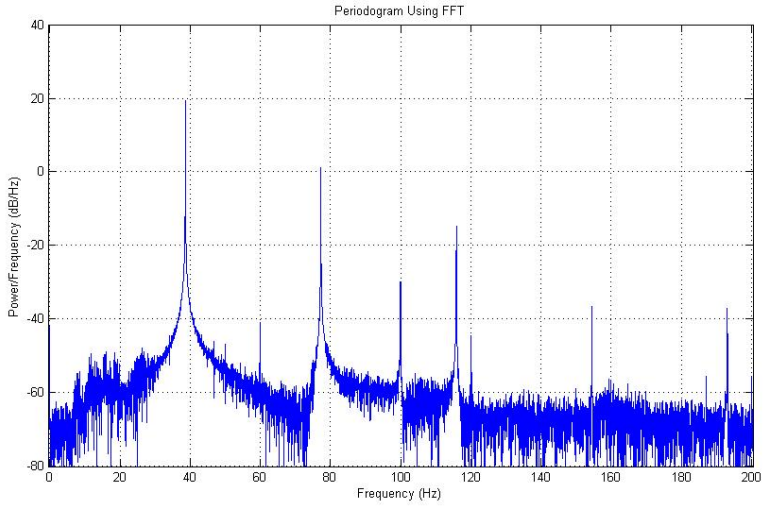

Figure 6-6: Acoustic measurement with feedback applied, microphone close to rubber surround of the woofer

Chapter 7

Enhancing the acoustic performance

In order to test the theory from Chapter 6-2, a different woofer is measured in a similar manner. The woofer of choice is a SEAS L26RO4Y, shown in Figure 7-1 and described in detail in Appendix A-12.

7-1 Woofer selection

The SEAS L26RO4Y has a stiff diaphragm due to the shape and materials used. The material of the diaphragm is aluminium. This is a stiffer material, compared to the coated paper diaphragm of the Peerless woofer. Secondly, the Peerless driver has a diaphragm shape that is relatively flat, compared to the deeper cone shape of the SEAS diaphragm.

These observations are backed up by the manufacturer, claiming that there are no signs of diaphragm edge resonances and distortion.

It is expected that the acoustic radiation of the SEAS woofer is less influenced by a-synchronised local movement of the diaphragm. If that is the case, applied feedback control leads to a larger improvement of acoustic performance, compared to the Peerless woofer.

7-2 Measurements of different locations of membrane

As is described in Chapter 6-2 for the Peerless woofer, the SEAS woofer is excited at 40 Hz with an excursion of 5 mm one-way. Since the SEAS woofer has a larger diameter, the SPL is higher compared to the measurements on the Peerless woofer.

Figure 7-2, Figure 7-3 and Figure 7-4 show that the distribution of distortion across the woofer diaphragm is within a 12 dB difference of the second harmonic distortion and 4 dB of the third harmonic distortion. The largest deviation from the distortion profile of the centre, is a 12 dB lower second harmonic distortion measured on the surround. The increase in performance of the motion of the centre of the diaphragm is expected to lead to a closer increase of acoustic performance.

Figure 7-1: SEAS L26RO4Y

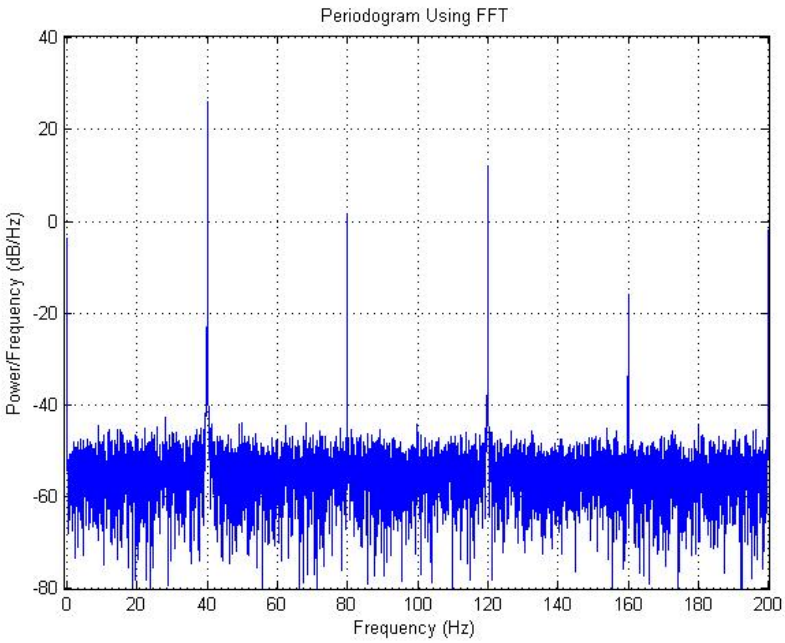

Figure 7-2: Acoustic measurement, SEAS woofer, close to the center of the woofer

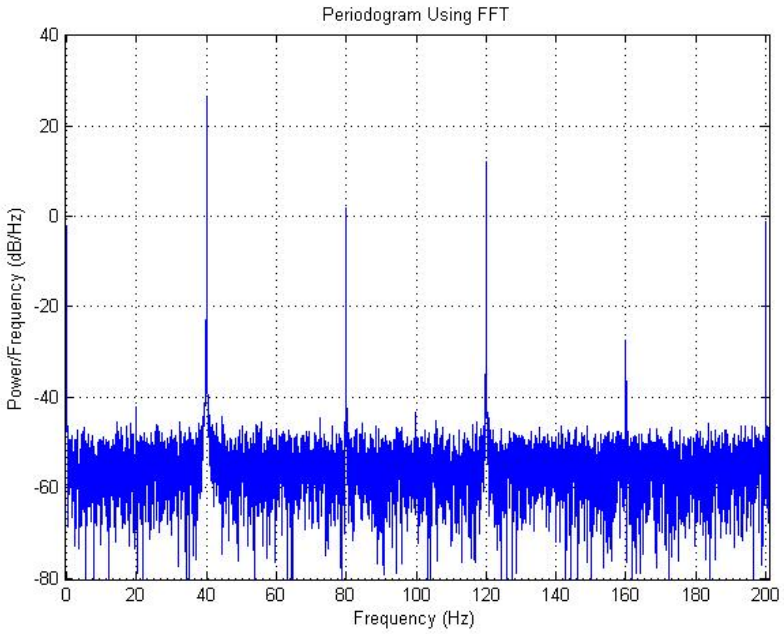

Figure 7-3: Acoustic measurement, SEAS woofer, between the centre and surround of the woofer

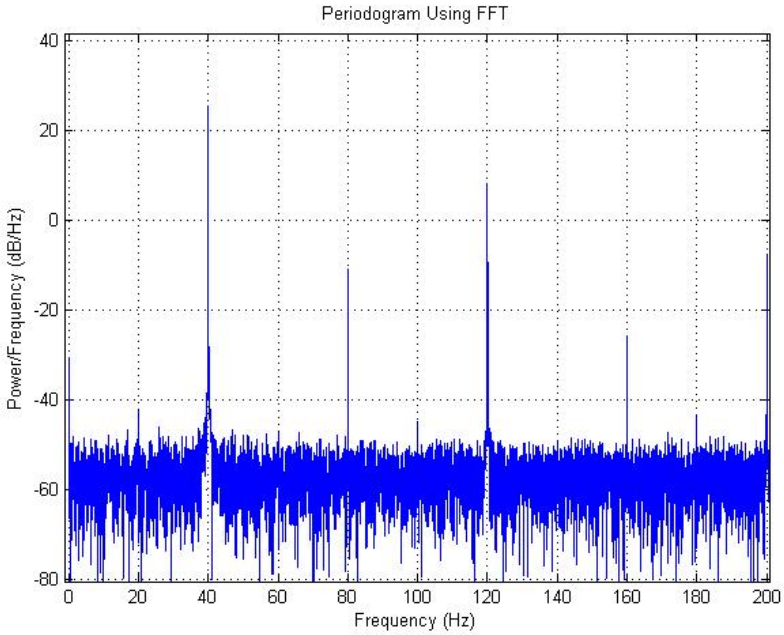

Figure 7-4: Acoustic measurement, SEAS woofer, close to the surround of the woofer

Chapter 8

Feedback setup of SEAS L26RO4Y

As described in Section 7-2, the expected increase of performance of the SEAS woofer is higher then the obtained increase in performance of the Peerless woofer, as is described in Section 6-1. It is therefore decided to implement a feedback controller on the SEAS woofer.

8-1 Changes in setup based on experience with Peerless woofer

The Peerless woofer set-up introduced problems that have not been dealt with due to the nature of a more troublesome issue of reduced increase of performance, as described in Chapter 6-2. These problems are related to the sensor data.

1. The noise level of the sensor output is high, due to the use of a wrong type of op-amp in the gain stage, shown in Figure 3-6
2. At low frequencies, the magnitude of the signal from the accelerometer is larger than the linear model of the system suggests.

8-1-1 Advanced sensor gain stage

Since the SEAS woofer is equipped with a new sensor and gain stage, the sensor gain stage is redesigned such that the noise level of the gain stage is lower, compared to the gain stage used earlier.

The gain stage consists of an instrumentation amplifier with a pair of output op-amps so that the output signal is a low noise balanced signal, as described in Appendix A-9

The new gain stage has a noise floor of 0.5mV RMS. The gain stage used before has a noise floor of 2mV RMS, with identical gain settings.

8-1-2 Low frequency magnitude error

As observed in Chapter 3, in the 1 Hz to 30 Hz frequency band, there is a mismatch between the measured sensor output magnitude and the modelled output value. This error results in a limited amount of open loop gain due to stability limitations at the low frequency unity gain crossover frequency. It is believed that this error is caused by stress leading to deformation of the sensor. The sensor is not only measuring the acceleration, but deformation by forces on the sensor too.

In order to test this theory, a similar mount to that shown in Figure 3-7 is used as a mount for the sensor. This reference measurement indicates a similar low frequency behaviour. Figure 8-1 shows the steep slope of the linear model of the system and the blue lines are the ETFEs of several measurements. At 10 Hz, there is an error in magnitude of 16 dB.

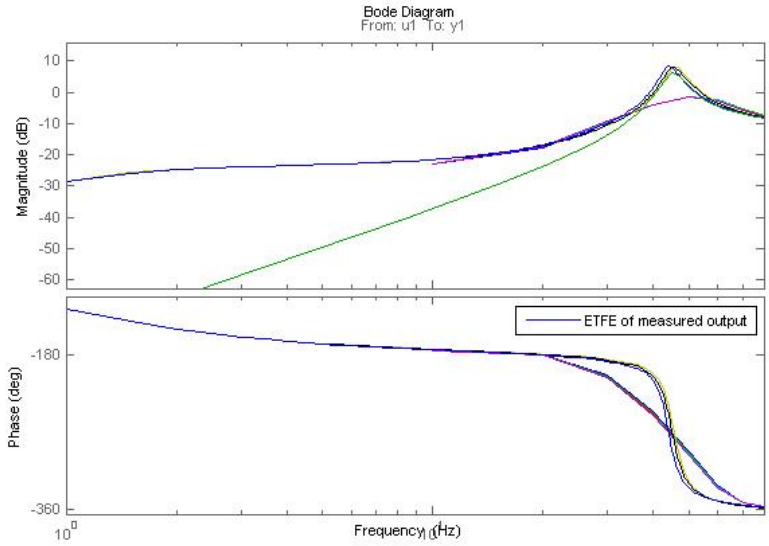

Figure 8-1: Low frequency sensor output estimated transfer function compared to model

In order to test that the linear model is accurate, the low frequency movement is measured by a triangular laser position sensor by Micro Epsilon. This sensor, the optoNCDT1401, as described in Appendix A-14, can track the movement of the diaphragm at low frequencies. The ETFE indicates a nearly flat response, shown in Figure 8-2. When translating the position measurement of the laser to the acceleration, that leads to the modelled low frequency magnitude.

It can be concluded that the sensor output from the accelerometer is not only of the acceleration, but from deformation of the sensor too. From the data sheet of the sensor in Appendix A-19, this observation is confirmed. The sensitivity due to deformation of the sensor is 0.3 g per $\mu\epsilon$. This deformation sensor output does not fit the model and leads to difficulties when designing a high gain, high damping feedback controller.

An alternative sensor mount is designed and implemented. This mount, as shown Figure 8-3, reduces the deformation of the accelerometer sensor. The table-like structure, on which the sensor is mounted, is connected to the voice coil carrier by a structure that is less stiff in the

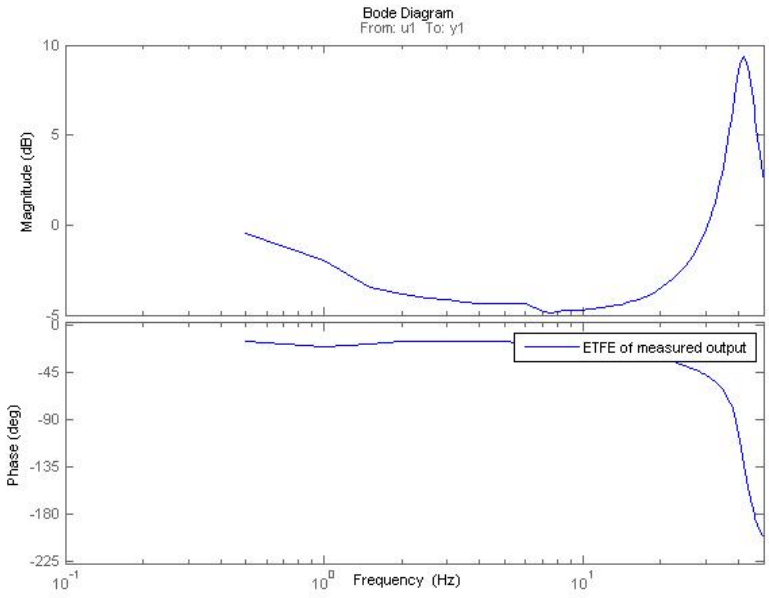

Figure 8-2: Low frequency laser measurement of position

lateral plane while keeping stiffness in the axis of the measured acceleration. This makes sure that the strain from the ring glued in the voice coil carrier, is transferred to the sensor table by a smaller amount. The holes in the structure ensure that the air flow is not restricted as well.

The physical implementation of the redesigned sensor mount, as shown in Figure 8-4, is constructed by a rapid prototyping 3D deposition printer, as described in Appendix A-18.

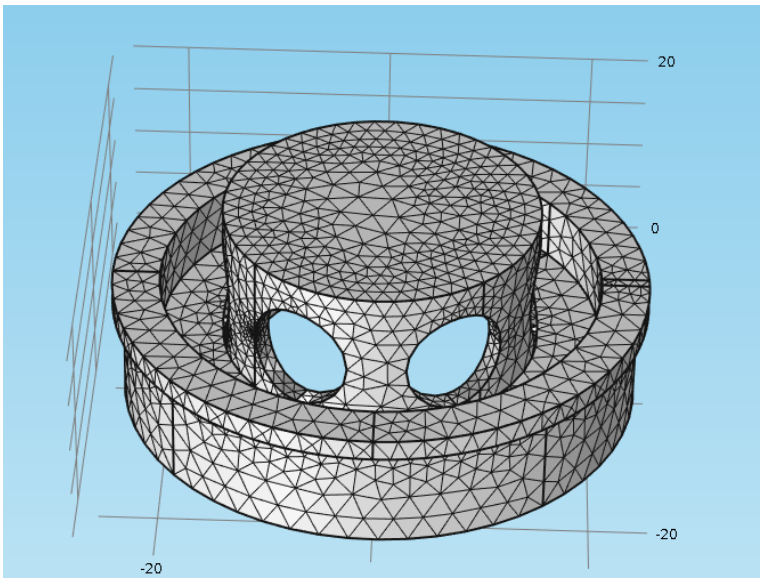

Figure 8-3: Model of new sensor mount

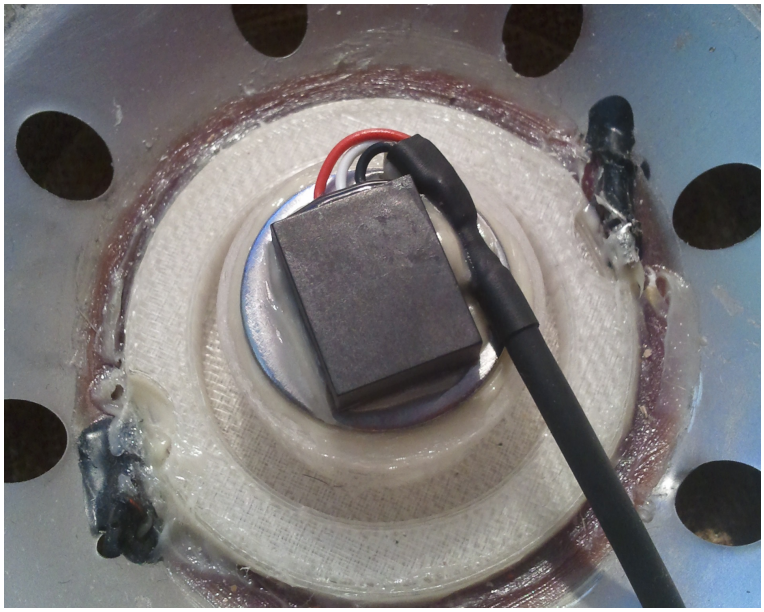

Figure 8-4: Physical implementation of new sensor mount

Chapter 9

System Identification of SEAS L26RO4Y

As described in Section 3-4, the dynamics of the open loop system are required in order to design a feedback controller. The steps performed in order to identify the dynamic behaviour of the Peerless woofer are repeated for the SEAS woofer.

Three measurements are performed that, when combined, lead to the modelled system frequency response shown in Figure 9-1.

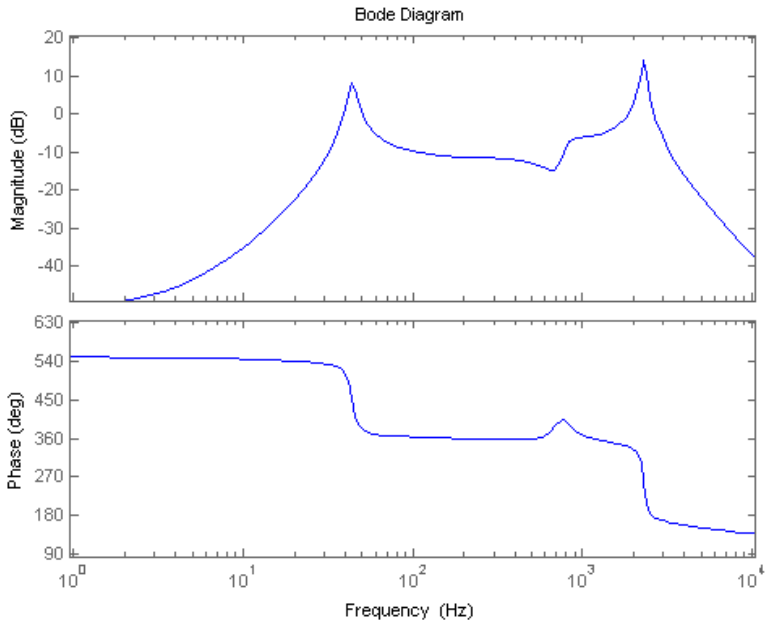

Figure 9-1: System model of the dynamics of the SEAS woofer

The ETFE from the identification dataset shows a series of characteristics that are related to a combination of mechanical phenomena and are implemented in the linear system model.

1. A high pass filter at 1 Hz, caused by the sensor
2. A high pass peaking filter at 45 Hz
3. A small magnitude change between 70 Hz and 500 Hz.
4. A coupling and decoupling behaviour in the magnitude plot from 600 Hz to 800 Hz.
5. A resonance in the magnitude plot around 7.000 Hz.

When identifying the model of the Peerless woofer in Chapter 3-4, these characteristics were observed too. The low frequency dynamics are a close match to the second order high pass filter observed before in Section 3-4. For the 500 Hz to 1.000 Hz regions, a coupling and decoupling behaviour is observed. This phenomenon is observed at a different frequency, but this coupling and decoupling seems to be present in many woofers in the 500 Hz to 1.000 Hz region. The impact of this diaphragm break-up on the measured acoustic radiation is different for every woofer.

In contrast to the observations in Section 8-1-2, the low frequency magnitude and phase are a closer match to the characteristics of a second order high-pass filter. The magnitude of the ETFE at 10 Hz is over 15 dB lower with the redesigned sensor mount. The implementation of the new sensor mount, as shown in Figure 8-4, solved the low frequency problem by reducing the deformation of the accelerometer.

Chapter 10

Performance of SEAS L26RO4Y

In order to test the theory that a different woofer is more suitable for the use of feedback, a controller is designed and implemented for the new woofer. The process of developing the controller is identical to the process used in Chapter 4 in terms of practical- and stability-considerations.

The controller is developed by combining a series of transfer functions.

1. First order low frequency high pass filter in order to reduce open loop DC gain.
2. A compensation for the diaphragm break up at 600 Hz to 800 Hz. This is a lead-lag compensator consisting of two poles and two zeros.
3. A notch filter for the resonance at 2.300 Hz, two poles and two zeros at 2.300 Hz
4. A pole at 2 Hz, in order to get additional phase
5. Two zeros at 45 Hz, to increase the loop gain between 45 and 200 Hz
6. Two poles at 200 Hz, in order to have a descending slope of magnitude

The Bode plot of the controller block in Figure 10-1 shows the transfer function of the controller. Figure 10-2 shows the open loop and its potential performance, of the SEAS set-up.

Between 25 Hz and 250 Hz, the open loop gain is a minimum of 10 dB. The frequency band between 40 Hz and 150 Hz, has a minimum gain of 20 dB.

In contrast to the Peerless woofer test frequency of 40 Hz used in Chapter 6, the SEAS woofer driver is capable of driving lower frequencies. This is possible due to the following differences to the set-up used initially.

1. The woofer diaphragm surface is larger by a factor 3.
2. The maximum excursion is larger by a factor 3,5.

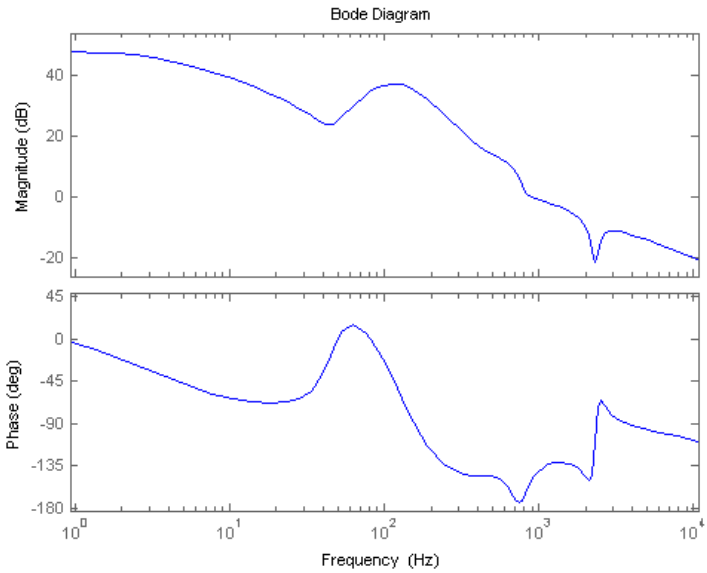

Figure 10-1: Controller transfer function for SEAS L26RO4Y

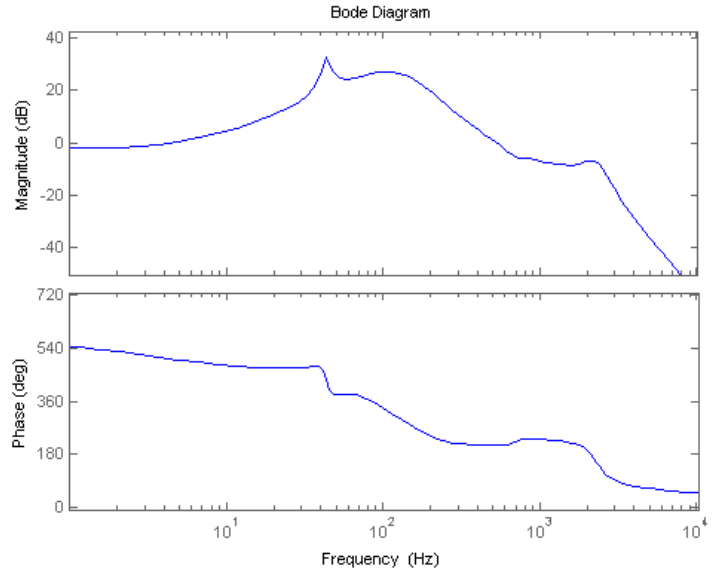

Figure 10-2: Open loop transfer function of new controller in combination with SEAS L26RO4Y

Due to the differences mentioned above, the test frequencies used are 20 Hz, 25 Hz and 30 Hz. At these frequencies, the measured harmonic distortion is high due to the large excursion and corresponding non-linear behaviour. It can therefore be demonstrated that in that bandwidth, the highest amount of performance gain can be obtained.

10-1 Measurements on the accelerometer

The accelerometer output is the signal used for feedback and should therefore be a close match to the predicted performance.

The FFT is a representation of the magnitude of a specific frequency in a measured signal. This FFT is used in order to evaluate the magnitude of distortions in the signal measured. The measurement time is 20 seconds for all measurements.

Measured magnitudes of -70 dB and under are less reliable since these values are very close to the noise level of both the DAQ and dSpace interface. Therefore, values close to the noise floor of either the DAQ or dSpace interface are not included in the table.

The measurements are used to verify the predicted increase in performance on the accelerometer. By comparing a reference measurement to a measurement with the implementation of the controller, the difference between the two measurements can be evaluated.

The magnitude of the excursion is chosen such, that both the dSpace voltage output range and additional electronics are just below clipping voltage. In practice, this means the signal send to the current amplifier is just under 15 V peak-to-peak. With the hardware used, this is the highest amount of excursion possible at the specific test frequency. Throughout the measurements of the accelerometer, the input voltage range of the DAQ, described in Appendix A-17, is equally set. Since the maximum magnitude of the specific frequency is different for every measurement, the magnitude of the fundamental frequency is different for different frequencies.

Under test circumstances, when comparing the performance with feedback to the performance without feedback, the conditions are identical in terms of maximum excursion of the woofer diaphragm. The accelerometer output value in both conditions is matched in peak-value.

10-1-1 20 Hz test frequency

The first test frequency is 20 Hz. This frequency is considered to be the lowest in the audible frequency range.

Accelerometer data at 20 Hz

The diaphragm travel is 5 mm both ways, 10 mm in total.

Table 10-1: Accelerometer measurement at 20 Hz

Frequency	No feedback	Feedback	Difference
20 Hz	0 dB	0 dB	0 dB
40 Hz	-18 dB	-40 dB	-22 dB
60 Hz	-23 dB	-43 dB	-20 dB
80 Hz	-48 dB	-	-
100 Hz	-50 dB	-	-

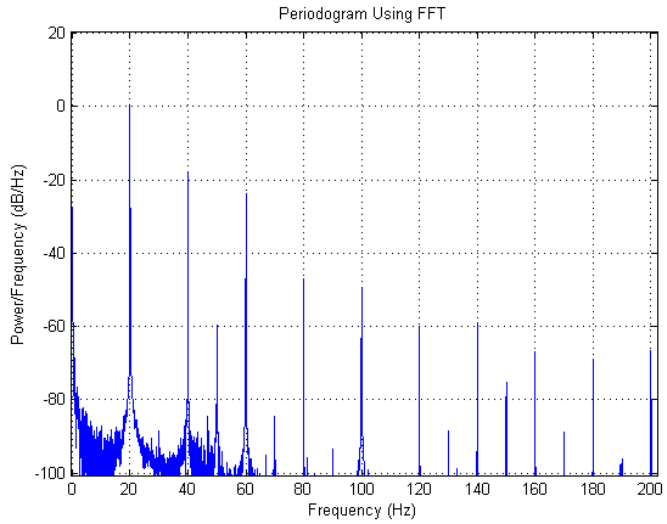

Figure 10-3: FFT of 20 Hz fundamental frequency without feedback, accelerometer data

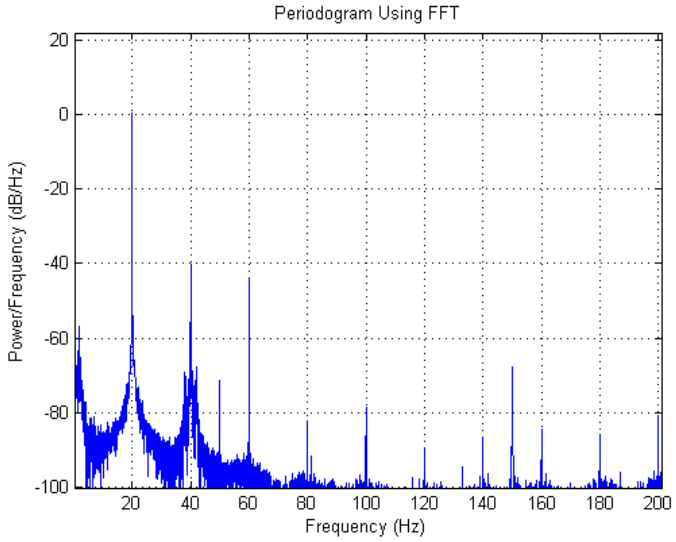

Figure 10-4: FFT of 20 Hz fundamental frequency with feedback, accelerometer data

10-1-2 25 Hz test frequency

This frequency is produced by the lowest pedal notes of a pipe organ.

Accelerometer data at 25 Hz

The diaphragm travel is 4.5 mm both ways, so 9 mm in total.

Table 10-2: Accelerometer measurement at 25 Hz

Frequency	No feedback	Feedback	Difference
25 Hz	4 dB	4 dB	0 dB
50 Hz	-22 dB	-44 dB	-22 dB
75 Hz	-28 dB	-50 dB	-22 dB
100 Hz	-	-	-
125 Hz	-50 dB	-	-

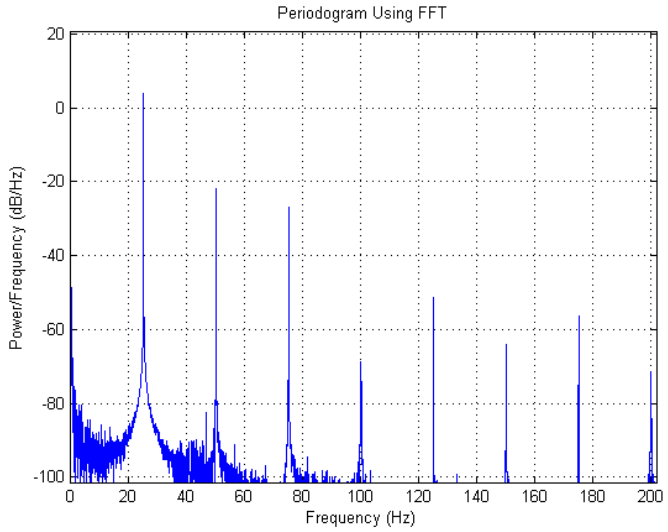

Figure 10-5: FFT of 25 Hz fundamental frequency without feedback, accelerometer data

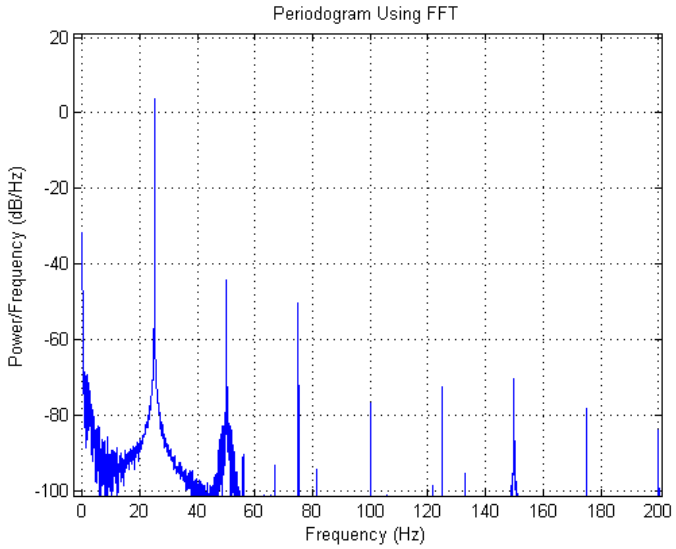

Figure 10-6: FFT of 25 Hz fundamental frequency with feedback, accelerometer data

10-1-3 30 Hz test frequency

30 Hz is the lowest frequency a five string double bass can produce with the B-string.

Accelerometer data at 30 Hz

The diaphragm travel is 6 mm both ways, so 12 mm in total.

Table 10-3: Accelerometer measurement at 30 Hz

Frequency	No feedback	Feedback	Difference
30 Hz	10 dB	10 dB	0 dB
60 Hz	-30 dB	-50 dB	-20 dB
90 Hz	-24 dB	-48 dB	-24 dB
120 Hz	-54 dB	-	-
150 Hz	-48 dB	-66 dB	-18 dB

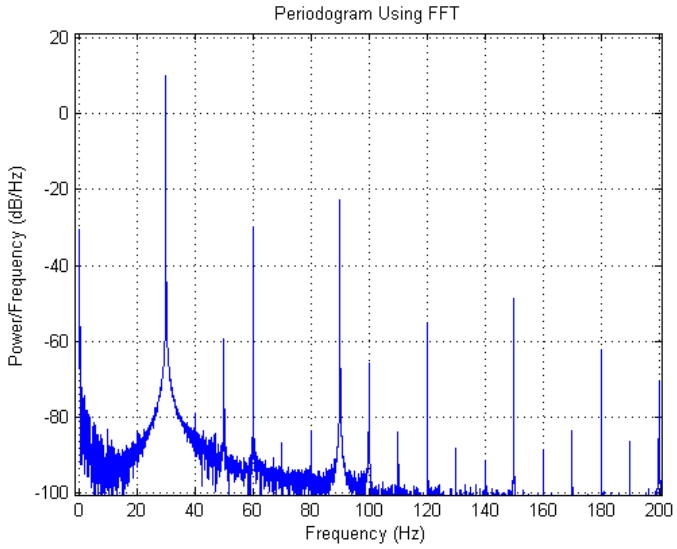

Figure 10-7: FFT of 30 Hz fundamental frequency without feedback, accelerometer data

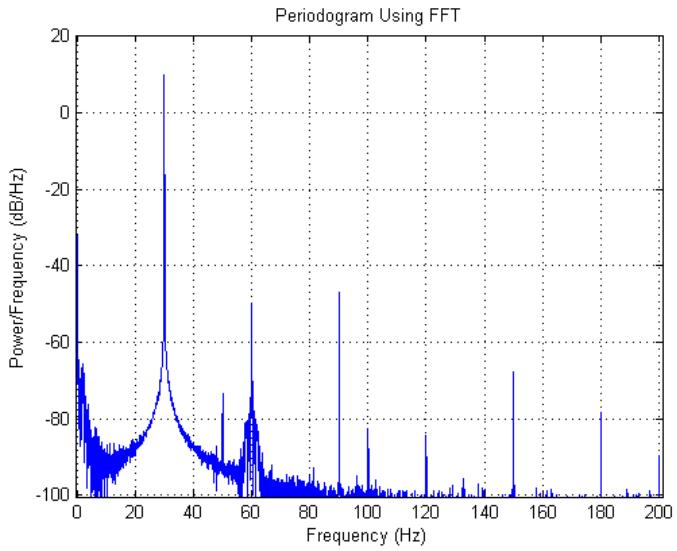

Figure 10-8: FFT of 30 Hz fundamental frequency with feedback, accelerometer data

10-2 Measurements on the microphone

The microphone output is the signal that is used in order to evaluate the acoustic differences in performance. The microphone is positioned close to the diaphragm in order to ensure that the radiated pressure waves of the loudspeaker cone are dominant over reflections of the room. The distance of the microphone to the diaphragm during all tests is 10 cm.

The FFT is a representation of the magnitude of a specific frequency in a measured signal. This FFT is used in order to evaluate the magnitude of distortions in the signal measured. The measurement time is 20 seconds for all measurements.

Measured magnitudes of -60 dB and under are less reliable since these values are very close to the noise level of the microphone and DAQ. Therefore, values close to the noise floor of either the DAQ or microphone are not included in the tables.

Depending on the magnitude of the signals measured, the input voltage-range of the DAQ is changed. This change in input voltage range, in combination with the change in maximum magnitude, as described in Section 10-1, leads to a variation in measured magnitude peaks.

Under test circumstances, when comparing the performance with feedback to the performance without feedback, the conditions are identical in terms of excursion of the woofer diaphragm. The accelerometer output value in both conditions is matched in peak-to-peak value.

The THD of the system is commonly referred to as the sum of the magnitudes of the harmonic distortions divided by the magnitude of the fundamental frequency, as described in 10-1.

$$THD = \frac{V_2 + V_3 + V_4 ... V_n}{V_1} \cdot 100 \tag{10-1}$$

10-2-1 Microphone data at 20 Hz

The measurements have a fundamental frequency of 20 Hz. Without feedback, the first harmonic distortion is at -12 dB under the fundamental frequency. The third harmonic distortion is -18 dB and the fourth is -40 dB under the fundamental frequency. The frequency content at 100 Hz is neglected due to the fact that at this frequency, the contribution of the power supply of the microphone is more dominant than the actual measured acoustic radiation, as described in Appendix A-6.

The THD of the reference measurement without feedback is 38.7%. With feedback, the THD is reduced to 3.4%.

Table 10-4: Microphone measurement at 20 Hz

Frequency	No feedback	Feedback	Difference
20 Hz	10 dB	10 dB	0 dB
40 Hz	-2 dB	-24 dB	-22 dB
60 Hz	-8 dB	-28 dB	-20 dB
80 Hz	-30 dB	-	-
100 Hz	-28 dB	-28 dB	0 dB

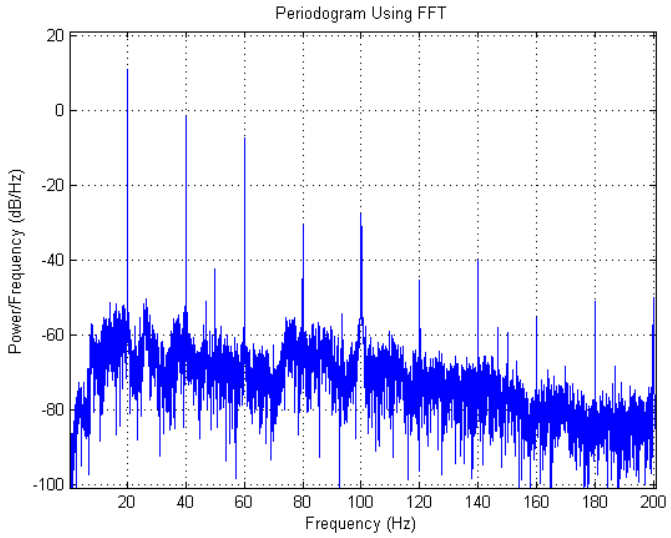

Figure 10-9: FFT of 20 Hz fundamental frequency without feedback, microphone data

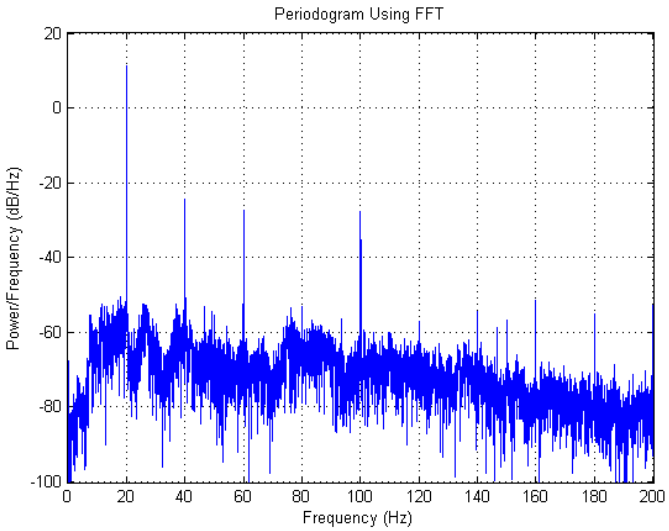

Figure 10-10: FFT of 20 Hz fundamental frequency with feedback, microphone data

10-2-2 Microphone data at 25 Hz

The measurements have a fundamental frequency of 25 Hz. Without feedback, the first harmonic distortion is at -22 dB under the fundamental frequency. The third harmonic distortion is -28 dB and the fifth is -52 dB under the fundamental frequency. The frequency content at 100 Hz is neglected due to the fact that at this frequency, the contribution of the power supply of the microphone is more dominant than the actual measured acoustic radiation, as described in Appendix A-6.

The THD of the reference measurement without feedback is 12.2%. With feedback, the THD is reduced to 1.7%.

Table 10-5: Microphone measurement at 25 Hz

Frequency	No feedback	Feedback	Difference
25 Hz	18 dB	18 dB	0 dB
50 Hz	-4 dB	-20 dB	-16 dB
75 Hz	-10 dB	–30 dB	-20 dB
100 Hz	-32 dB	-28 dB	+4 dB
125 Hz	-34 dB	-44 dB	-10 dB

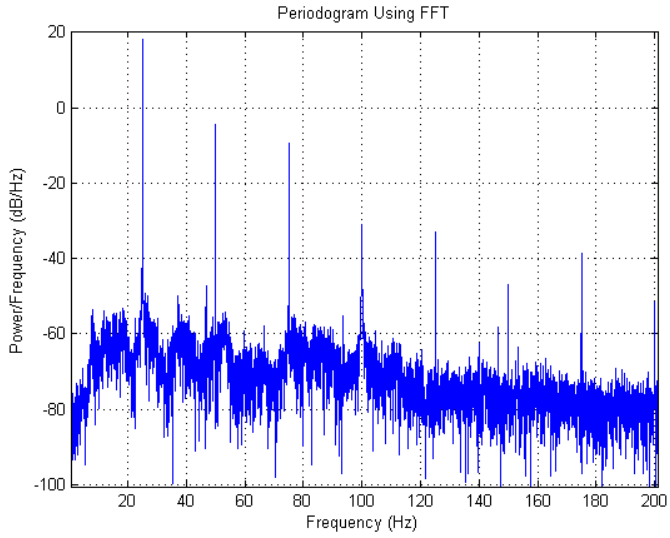

Figure 10-11: FFT of 25 Hz fundamental frequency without feedback, microphone data

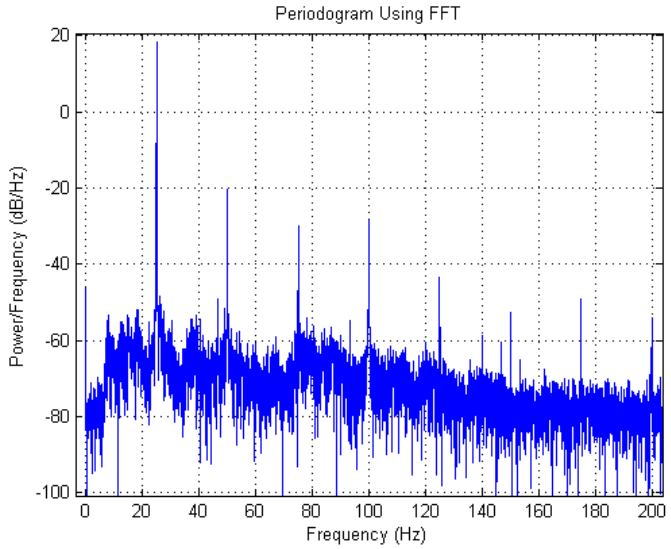

Figure 10-12: FFT of 25 Hz fundamental frequency with feedback, microphone data

10-2-3 Microphone data at 30 Hz

The measurements have a fundamental frequency of 30 Hz. Without feedback, the first harmonic distortion is at -32 dB under the fundamental frequency. The third harmonic distortion is -30 dB, the fourth is -56 dB and the fifth is -54 dB under the fundamental frequency.

The THD of the reference measurement without feedback is 6.0%. With feedback, the THD is reduced to 2.1%.

Table 10-6: Microphone measurement at 30 Hz

Frequency	No feedback	Feedback	Difference
30 Hz	4 dB	4 dB	0 dB
60 Hz	-28 dB	-32 dB	-4 dB
90 Hz	-26 dB	–46 dB	-20 dB
120 Hz	-52	-56 dB	-4 dB
150 Hz	-50	-54 dB	-4 dB

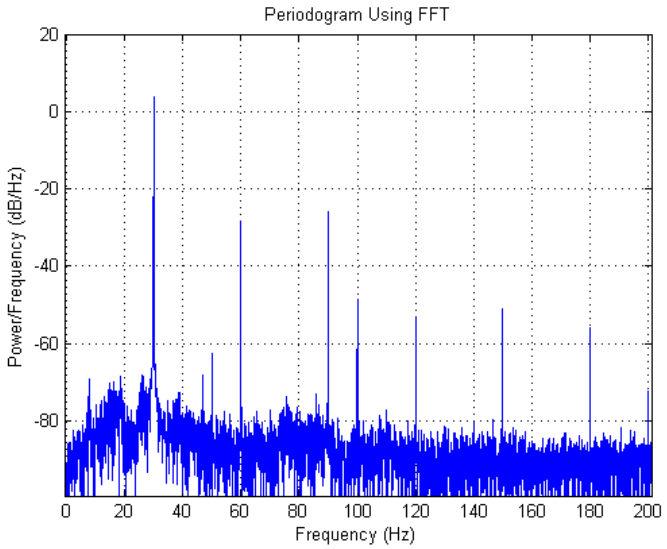

Figure 10-13: FFT of 30 Hz fundamental frequency without feedback, microphone data

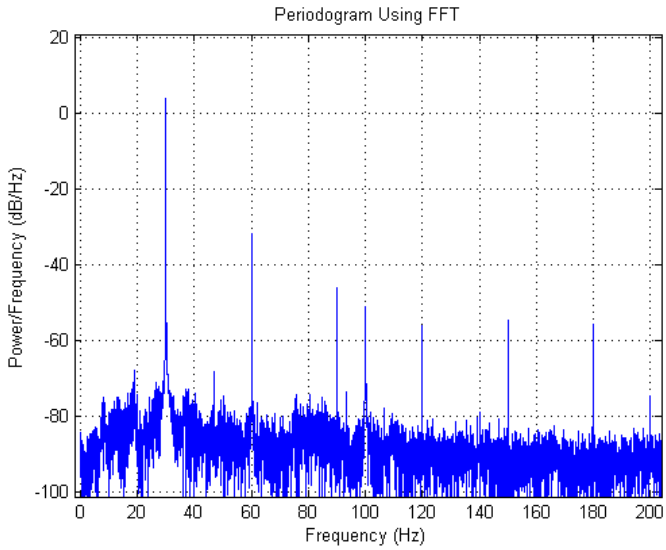

Figure 10-14: FFT of 30 Hz fundamental frequency with feedback, microphone data

10-3 Evaluating the measurements

As described in Chapter 5-3, the reduction of harmonic distortion on the accelerometer sensor is a match to the predicted reduction in harmonics. Depending on the magnitude of the distortion and the frequency, the most dominant second- and third-order harmonic distortion magnitudes are reduced by approximately 20 dB, a factor ten. In practice, when the measurements of the sensor output are compared, the reduction of harmonic distortion is indeed 20 dB, a factor ten.

In contract to Chapter 6, the performance measured by the microphone with the new set-up is improved significantly. The reduction of harmonic distortion measured by the microphone is reduced up to 22 dB, but in other measurements reduced less. When analysing all measurements performed by the microphone, the average gain in performance is a factor seven.

One of the objectives of this research is to suppress the THD to a level below 1%. When evaluating the increase in performance measured by the microphone, this objective is not accomplished. The reduction in THD, up to a factor 11, is just not enough to suppress the THD below 1%, but still significantly better than normal subwoofer systems.

Chapter 11

Reflection and recommendations

Looking back on the the research, I am pleased with the final results and with the knowledge gained on this topic. The final measurements, as described in Chapter 10, show that the concept of MFB is one with potential when analysed properly.

The objectives set are not reached. Depending on the excursion of the woofer, the THD is not reduced below 1% under testconditions. The improvement in terms of THD are up to a factor 11, but even with that suppression, the THD can reach 4% at a 20 Hz high level reference signal. Tuning the controller can make the controller suppress the harmonic distortion by a higher magnitude, but at the cost of low frequency stability. The second objective was to control the diaphragm break-up. The controller however, was limited in control bandwidth due to stability issues. The analysis of the diaphragm break-up remains a interesting subject, but with the accelerometer sensor used, it was not possible to measure and control both the centre and the surround of the diaphragm.

The process of building a test set-up from scratch is a real challenge. One can in advance only imagine the obstacles that need to be overcome in order to get to a satisfactory result. Noisy sensors, faulty readings or unforeseen mechanical issues all contributed to evaluation of each and every aspect of the concept. Encountering all these difficulties and fixing them, has increased the know-how on the topic of MFB.

For further research, it is advised to further evaluate the effect of strain of a piezo based sensor on the sensor output. This effect can be explained, but in practice needs to be dealt with in order to design high performance (sub)woofer set-ups.

For further research, it is advised to evaluate the possibility of measuring the movement of several locations on the diaphragm. Possibly, with more advanced controllers, the diaphragm break-up can be reduced in acoustic influence.

For further research it is advised to re-evaluate the concept of a woofer for feedback. Commercially available woofers are designed to be be used in conventional loudspeakers, not for feedback purposes. For instance, if the Lorentz actuator is attached to the diaphragm on a location where the first diaphragm break-up is not monitored, the break-up does no longer influence the measured system dynamics that limit potential loop gain.

Appendix A

Appendix

A-1 System identification signal

```
%Create signal parameters
Fs = 100000;
t_end = 20;
t= 0:1/Fs:t_end;
fo=30;  f1=6000;
u_scale = 0.15;

%Create Sweep
u=chirp(t,fo,t_end-0.1,f1,'logarithmic');
u = u*u_scale;

%Remember, the last value output will remain output, even after stop(AO)
%command. Therefore, force the last couple values of the test signal to
    0.
u(length(u)) = 0;

%Puts info from DAQ in separate variable
daq=daqhwinfo;

%Define Adapter ID as AO, Analog Out and same for AI
AO=analogoutput(daq.InstalledAdaptors{1},'Dev1'); %nidaq
AI=analoginput(daq.InstalledAdaptors{1},'Dev1'); %nidaq

%Set the sampletime matching the in and outpu of the signal
set(AO,'SampleRate',Fs);
set(AI,'SampleRate',Fs);
AI.inputtype='SingleEnded';

%Determine which channels are selectted
AOcurrent = addchannel(AO,1,'Current');
```

```
AIcurrent = addchannel(AI,[1  2],'Current');

set(AI,'SamplesPerTrigger',Fs*t_end);

%Define what signal is used for output
putdata(AO,u');

%Start the output signal
display('Starting measurement')
display('Starting output')
start(AI);
start(AO);

%Let it run for t_end seconds
wait(AO,Fs*t_end+1)

%Force stop the measurement
stop(AI);
stop(AO);

display('Stopped signal output and measurement')

%Get the data from the measurement and put it in a data-vector
y = getdata(AI);
```

A-2 Reshaping the measured time domain data

```
%Remove LF drift
ydetrend = detrend(y);

%Resample signal so only actuated dynamics are shown
r_scale = 10;
yresample = resample(ydetrend,1,r_scale);

%Put data in ID Data object
iddat = iddata(yresample(:,1),yresample(:,2),r_scale/Fs)

%Define ETFE and plot VS model
s1 = etfe(iddat,1000,1000)
h1 = bodeplot(s1,PLANT5,{25*2*pi,5000*2*pi});
setoptions(h1,'FreqUnits','Hz');
```

A-3 Testing FFT code

```
clear all
clc

%Testing FFT functionality

Fs=200;
t_end = 20;
```

```
t = 1/Fs:1/Fs:t_end;

signal1 = 10*sin(t*2*pi*50);
signal2 = 10*cos(t*2*pi*10);

y = (signal1+signal2)';

%Plot FFT
N = length(y);
xdft = fft(y);
xdft = xdft(1:N/2+1);
psdx = (1/(Fs*N)).*abs(xdft).^2;
psdx(2:end-1) = 2*psdx(2:end-1);
freq = 0:Fs/length(y):Fs/2;
plot(freq,10*log10(psdx)); grid on;
title('Periodogram Using FFT');
xlabel('Frequency (Hz)'); ylabel('Power/Frequency (dB/Hz)');
```

A-4 Designing a model to the ETFE

```
%Define plant
s = tf([1 0],[1]);

%Introduce fase by sampling at 100kHz
DELAY = ss(exp(-1e-5*s))*10^(-8/20);

%Resonance peak subwoofer at 44Hz
PLANT1 = DELAY *s^2/(s^2+(44*2*pi)/5*s + (44*2*pi)^2);

% Damping on system, showing presencence from 1 000 Hz
pole = 6000/(s+6000)

%600 to 800 Hz coupling and decoupling of suspension
PLANT2 = PLANT1 * (s^2+4450/5*s+4450^2)/(s^2+4900/6*s + 4900^2)*pole

%HF resonance
PLANT3 = PLANT2* (s^2+30000/7*s+30000^2)/(s^2+23000/5*s + 23000^2)

PLANT4 = PLANT3 * 36000^2/(s^2+36000*s/14+36000^2)...
    *(s^2+1315*2*pi*s/50+(1315*2*pi)^2)/(s^2+1310*2*pi*s/50+(1310*2*pi)
       ^2)

%Details
PLANT5 = PLANT4 * (s^2+28000*s/1+28000^2)/(s^2+28000*s/2+28000^2)

%Plant defined
```

A-5 Microphone performance test

In order to verify that the measurements from the Panasonic microphone capsule used, A-15, are correct, a reference measurement is performed with a Beyerdynamic MM1 microphone,

A-22. The Beyerdynamic MM1 is designed for the purpose of measuring the performance of loudspeaker systems. This microphone too, has an unknown distortion profile, but due to the reputation of the microphone, it is used as a reference.

The comparison consists of measuring a acoustic signal with both microphones close together. The microphone output is passed through the dedicated pre-amplifiers and the analogue output is measured with the DAQ, A-17. The test frequencies are 20 Hz, 30 Hz and 40 Hz. Since the microphone is used for measuring harmonic distortion, that performance is evaluated.

The sensitivity and gain stages of the microphones are not identical during the tests. Therefore, a change in measured magnitude is expected. The deviation from that offset is the measurement error.

A-5-1 20 Hz comparison

The measured magnitude of the signal is within +/- 2 dB of a 4 dB gain difference.

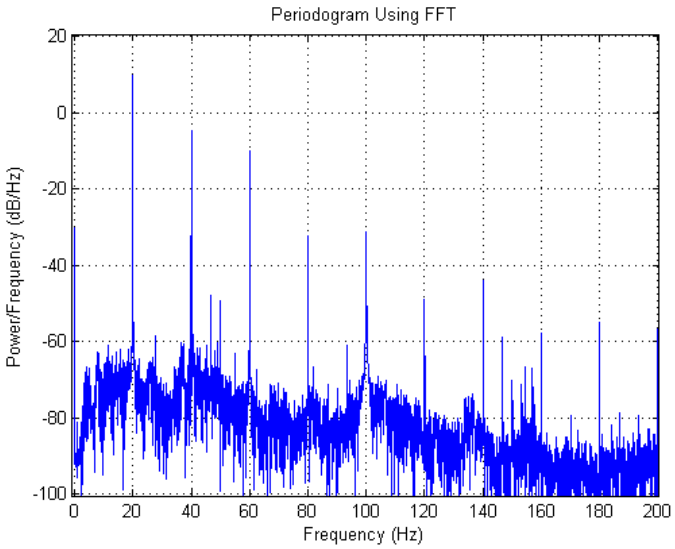

Figure A-1: FFT of 20 Hz fundamental frequency, Beyerdynamic

Frequency	Beyerdynamic MM1	Panasonic WM-61A	Difference
20 Hz	10 dB	14 dB	4 dB
40 Hz	-4 dB	1 dB	5 dB
60 Hz	-10 dB	-4 dB	6 dB
80 Hz	-32	-27 dB	5 dB
100 Hz	-31	-28 dB	3 dB

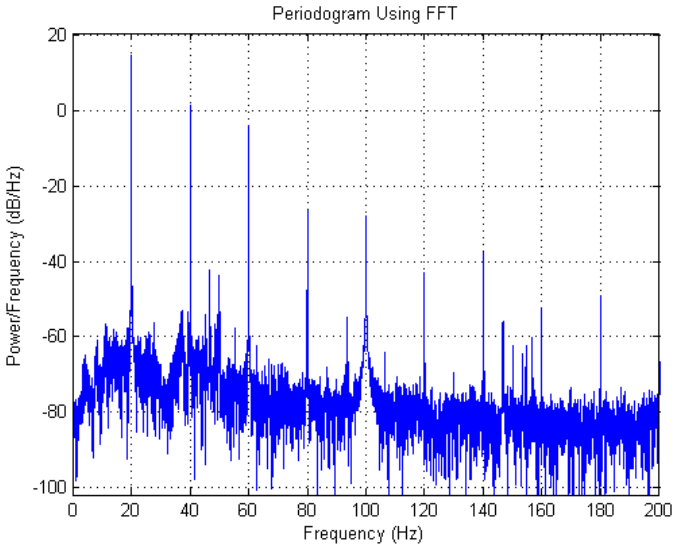

Figure A-2: FFT of 30 Hz fundamental frequency without feedback, microphone data

A-5-2 30 Hz comparison

The measured magnitude of the signal is within +/- 2 dB of a 9 dB gain difference.

Frequency	Beyerdynamic MM1	Panasonic WM-61A	Difference
30 Hz	11 dB	20 dB	9 dB
60 Hz	-25 dB	-14 dB	11 dB
90 Hz	-25 dB	-16 dB	9 dB
120 Hz	-59	-52 dB	7 dB
150 Hz	-45	-35 dB	10 dB

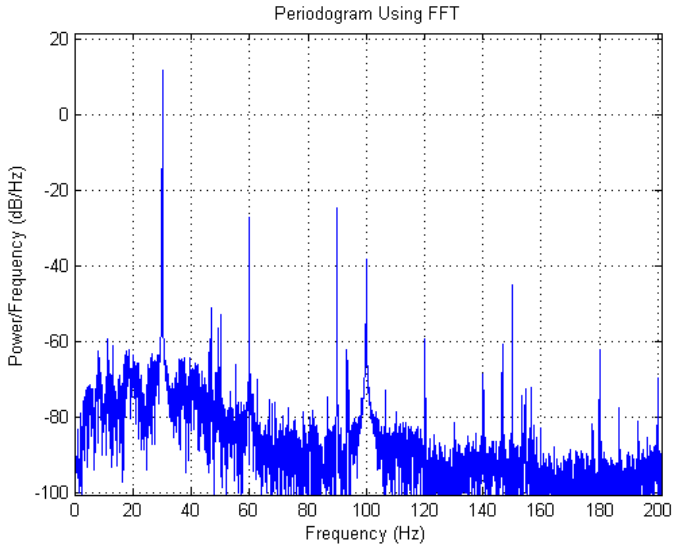

Figure A-3: FFT of 30 Hz fundamental frequency, Beyerdynamic MM-1

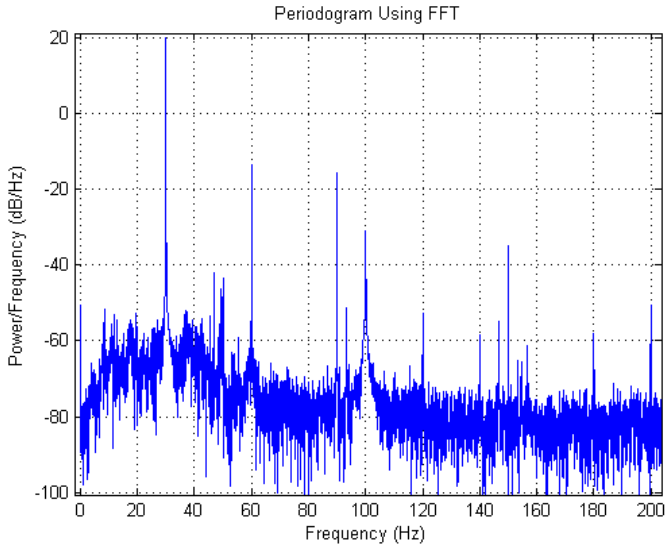

Figure A-4: FFT of 30 Hz fundamental frequency without feedback, Panasonic WM-61A

A-5-3 40 Hz comparison

The measured magnitude of the signal is within +/- 3 dB of a 9 dB gain difference. Only one measurement is outside this range. Since all other measurements are within a +/-3 dB difference, the 80 Hz measurement is ignored.

Frequency	Beyerdynamic MM1	Panasonic WM-61A	Difference
40 Hz	11 dB	20 dB	9 dB
80 Hz	-42 dB	-22 dB	20 dB
120 Hz	-36 dB	-27 dB	9 dB
160 Hz	-64	-51 dB	8 dB
200 Hz	-49	–43 dB	6 dB

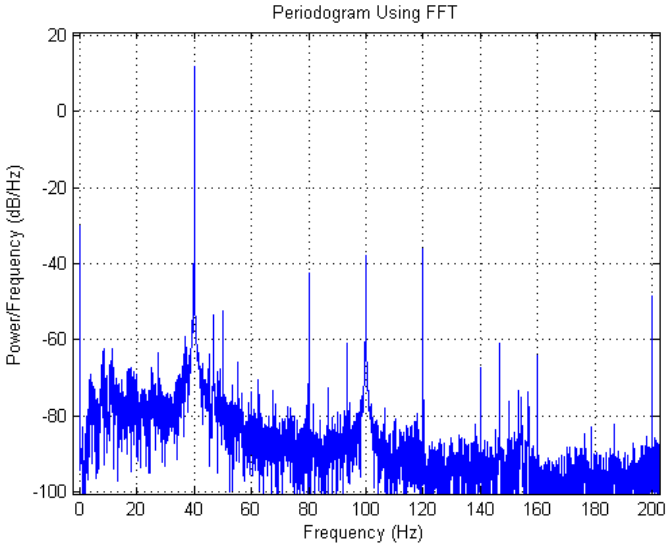

Figure A-5: FFT of 40 Hz fundamental frequency, Beyerdynamic MM1

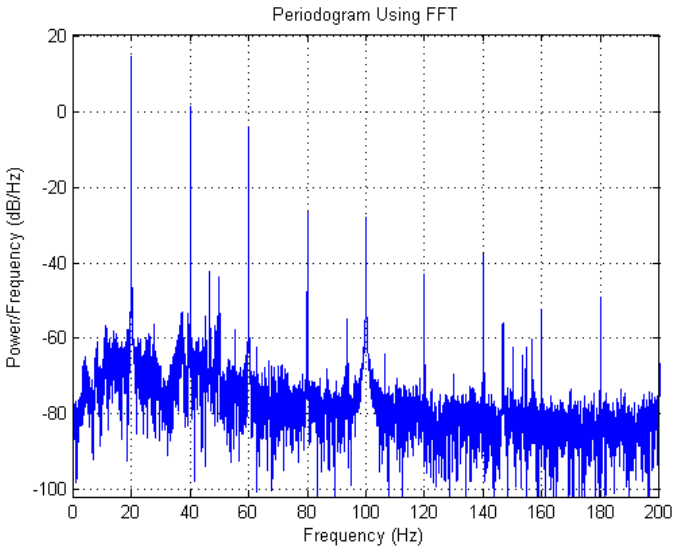

Figure A-6: FFT of 40 Hz fundamental frequency without feedback, Panasonic WM-61A

A-5-4 Conclusion

The Panasonic WM-61A, used in the report, deviates in terms of sensitivity from the Beyerdynamic MM1, but is within acceptable magnitudes of error.

A-6 Power supply influence on microphone measurement

Evaluating the power spectral density figures of the microphone data used throughout the report, lead to the conclusion that for 100 Hz, the improvement obtained by the feedback loop is lower than expected. It is believed that due to the simplistic microphone power supply and gain stage, the mains frequency is present in the analysed time domain data captured.

The test is performed with the exact same Matlab code as the other microphone measurements. A relatively quiet room is used. Depending on the amount of gain used in the gain stage, the 100 Hz content is around -35 dB compared to the reference. When the 20 dB gain stage is not used, which during some measurements was required, the 100 Hz content is lowered by the predicted amount of -20 dB to -55 dB.

This indicates that for measuring harmonic distortions of 100 Hz, the setup is not reliable since the influence from the power supply is contributing to the actual harmonic acoustic distortion.

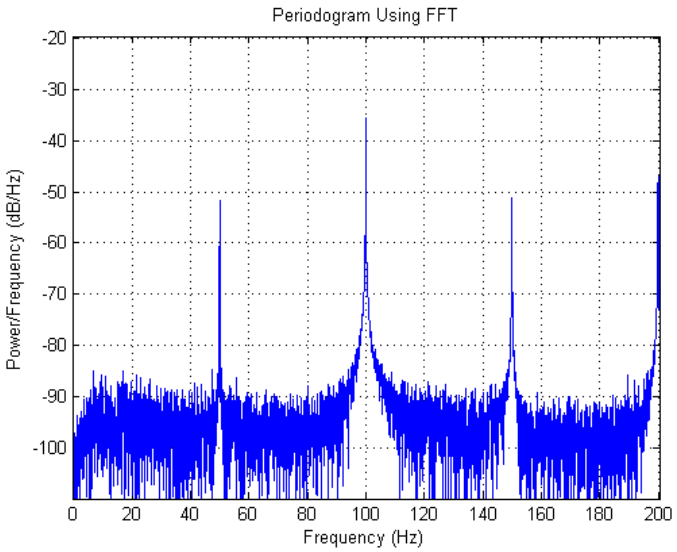

Figure A-7: FFT of microphone data in quiet room, Panasonic WM-61A

A-7 3D printer filament Young's modulus experiment

The 3D printer used, A-18, uses a PLA filament to build the model. This material has some unknown material properties. Due to the use of this material in the sensor mount, shown in

Figure 8-4, it is desired to know the Young's modulus in order to evaluate the stiffness of the structure.

A 100% filled beam 3D print is used for the experiment. The beam measures 150 mm long and has two sides of 10mm. The beam is clamped in a vise and a load is applied. By measuring the deflection of the beam, the Young's modulus is calculated.

This experiment indicates a Young's modulus of around 1,5 GPa. When the sensor mount is designed, this value is used in order to model the dynamic behaviour of the mount.

A-8 THD of components other than the loudspeaker

When evaluating the performance of the woofer, it is required to know whether the distortion measured is introduced by the amplfier, signal generator or woofer. In order to evaluate the performance in THD of the amplifier and signal generator, two tests have been performed.

The signal generator is tested by making a 40 Hz sine wave and directly recording it with the National Instruments DAQ, A-17. Figure A-8 shows that the second harmonic distortion is -80 dB under the fundamental frequency. This is equivalent to 0.01% THD. This is a factor 100 under the target total THD with the implementation of the woofer. The THD contribution of the signal generator to the THD in test conditions with the woofer, can therefore be neglected.

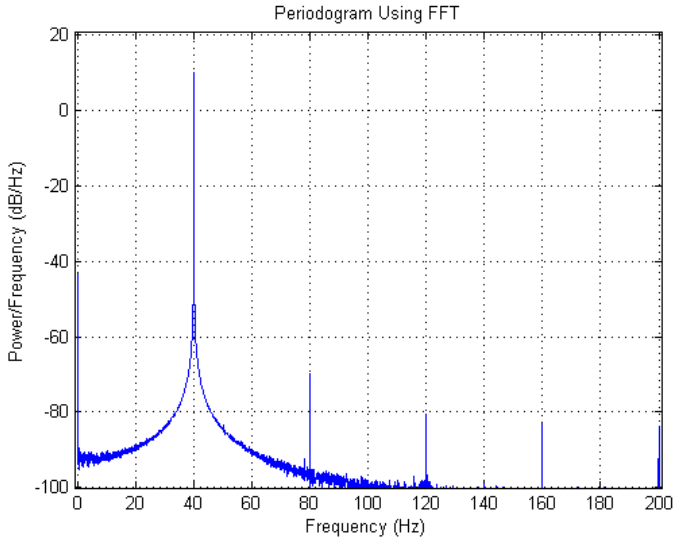

Figure A-8: FFT of signal generator with a fundamental frequency of 40 Hz, second harmonic distortion 80 dB under fundamental frequency

The amplifier THD is tested by using it to drive current through a power resistor. The input signal is the signal generation from which the performance in terms of THD is known. The second harmonic distortion is -76 dB under the fundamental frequency of 40 Hz. This leads to a THD of 0.016%. Again, this is a factor 63 lower than the target THD with the implementation of the woofer. The THD contribution in terms of THD introduced by the amplifier and signal generator can be neglected.

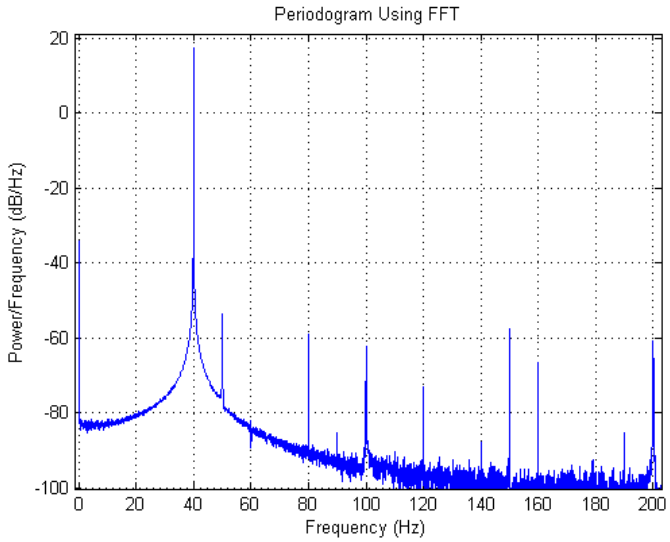

Figure A-9: FFT of signal generator and amplifier, with a fundamental frequency of 40 Hz, second harmonic distortion 76 dB under fundamental frequency

A-9 Sensor Gain stage

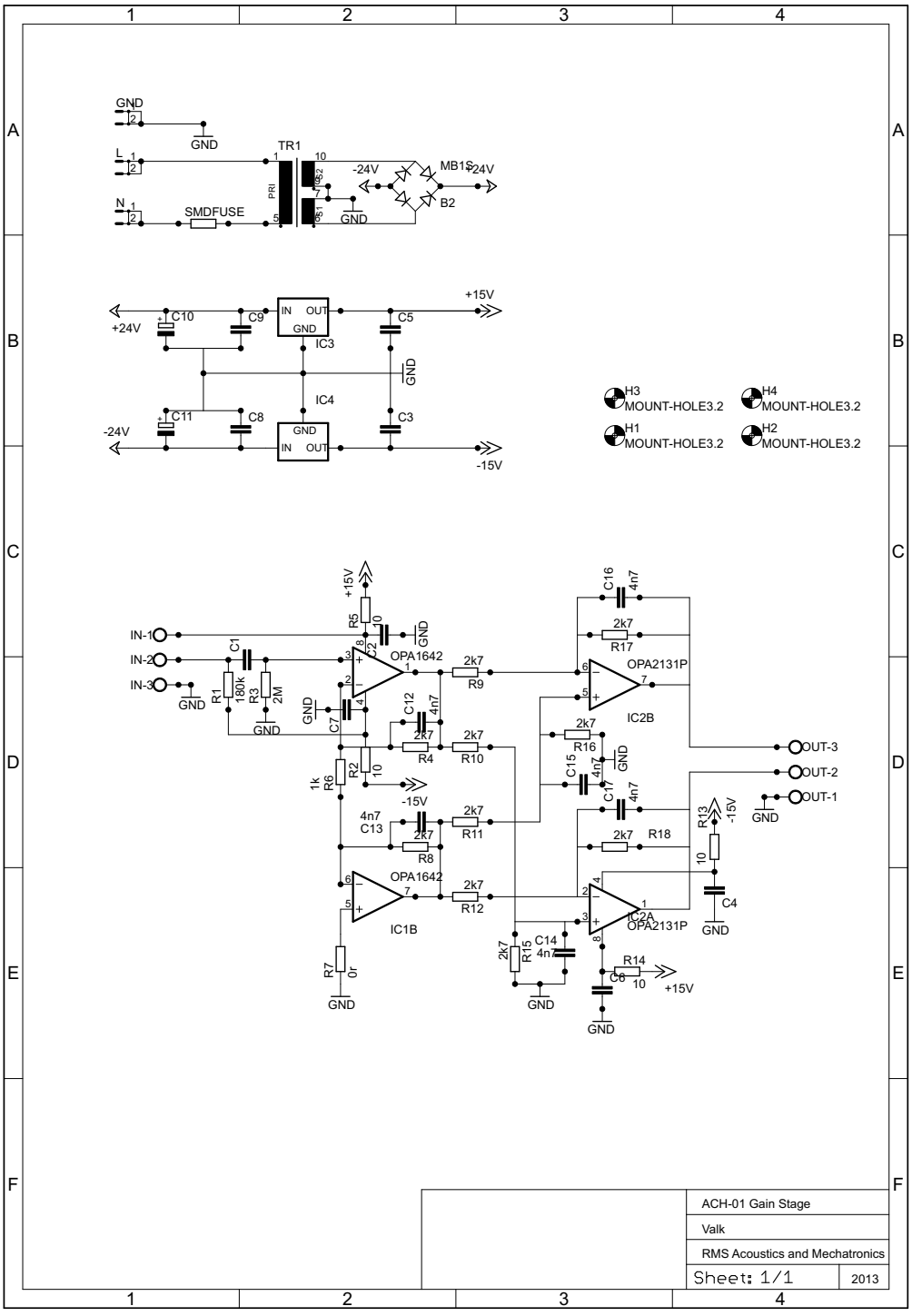

20-9-2013 7:39:30 D:\DropBox\Afstuderen MFB\Eagle\Gain Stage\gainstage_smd.sch (Sheet: 1/1)

A-10 Micro-Epsilon, LD1630

31

Model	LD 1610-0.5	LD 1610-2	LD 1610-4	LD 1610-10	LD 1610-20	LD 1610-50	LD 1610-100	LD 1610-200
Measuring range	0.5mm	2mm	4mm	10mm	20mm	50mm	100mm	200mm
Start of measuring range	23.75mm	23mm	22mm	40mm	55mm	115mm	170mm	240mm
Linearity	1µm	4µm	8µm	20µm	40µm	100µm	200µm	400µm
	≤0.2 % FSO							
Resolution (dynamic*)	0.3µm	1.3µm	2.6µm	6.5µm	13.0µm	32.5µm	65µm	200µm
Resolution (static**)	0.02µm	0.1µm	0.2µm	0.5µm	1µm	2.5µm	6µm	20µm
Spot diameter	0.1mm	0.2mm	0.3mm	0.6mm	0.9mm	1.5mm	1.5mm	2mm
Frequency response	10kHz (-3dB)							
Light source	laser, wavelength 670 nm, red							
Laser safety class	class 2							
Vibration	10 g ... 1 kHz (sensor, 20 g option)							
Operation temperature	0° ... +50°C							
Storage temperature	-20° ... +70°C							

* Measurement on white target with 10kHz ** Measurement on white target with 20Hz

Model	LD 1630-0.5	LD 1630-2	LD 1630-4	LD 1630-10	LD 1630-20	LD 1630-50
Measuring range	0.5mm	2mm	4mm	10mm	20mm	50mm
Start of measuring range	23.75mm	23mm	22mm	40mm	55mm	115mm
Linearity	1.5µm	6µm	12µm	30µm	60µm	150µm
	≤±0.3 % FSO					
Resolution (dynamic*)	0.8µm	3.5µm	7µm	17.5µm	35µm	50µm
Resolution (static**)	0.05µm	0.2µm	0.4µm	1µm	2µm	7.5µm
Spot diameter	0.1mm	0.2mm	0.3mm	0.6mm	0.9mm	1.5mm
Frequency response	100kHz (-3dB)					
Light source	laser, wavelength 670nm, red					
Laser safety class	class 2					
Vibration	5g ... 1kHz (sensor, 20g option)					
Operation temperature	0° ... +40°C					
Storage temperature	-30° ... +75°C					

* Measurement on white target with 100kHz ** Measurement on white target with 230Hz

Controller		
Digital ouput	Ethernet	TCP /IP factory default IP 192.168.122.245 (frequency response 1 - 30kHz)
Analogue output	displacement	±10V (option 0 ... 10V / 0 ... 5V); 4 ... 20mA
	impedance	appr. 0 Ohm (10mA max.)
	tilt	with 30° object inclination (axis A): appr. 0.5% (white target)
	cut off frequency	DC ... 10kHz / 100kHz
	temperature drift	0.02 % °C FSO
	intensitiy	0V ... 10V
Switching outputs	MIN	+24V when distance < MIN, LED yellow
	OK	+24V when distance > MIN and < MAX, LED green
	MAX	+24V when distance > MAX, LED orange
	Error	+24 V, LED red
Switching hysteresis		appr. 0.5 % FSO
Ambient light		20,000 LUX
Life time		50,000h laser diode
Isolation voltage		200V DC, 0V
Humidity		up to 90% RH
Protection class		sensor: IP 64, controller: IP 40
Power supply		+24V DC / 200mA (10 ... 30V)
Connector		25 pin Sub D male connector
Cable length (standard)		2m

A-11 Peerless, SLS-P830946

TYMPHANY

Transducer Specification Sheet

Model Number: SLS-P830946
Product Line: Peerless Silver

Revision: Rev 1_1
Date: 31-Aug-09

Peerless

Product Description:

The SLS line combines high quality performance with an affordable design. This 6.5 inch 4 ohm member of the SLS family features a rigid steel basket, a paper cone, and a ferrite magnet motor with aluminium shorting ring for improved distortion performance.

Mechanical 2D Drawing:

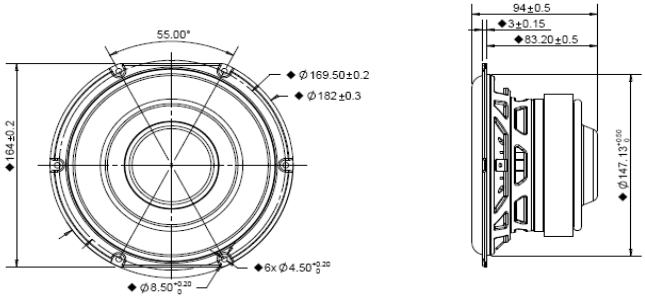

Specifications:

DC Resistance	R_{evc}	Ω	2.7	5.0%	Energy Bandwidth Product	EBP	$(1/Q_{es})\cdot f_s$	110
Minimum Impedance	Z_{min}	Ω	3.6	7.5%	Moving Mass	M_{ms}	g	30.5
Voice Coil Inductance	L_e	mH	0.65		Suspension Compliance	C_{ms}	um/N	467
Resonant Frequency	f_s	Hz	42	15.0%	Effective Cone Diameter	D	cm	12.54
Mechanical Q Factor	Q_{ms}	-	4.92		Effective Piston Area	S_D	cm^2	123.5
Electrical Q Factor	Q_{es}	-	0.38		Equivalent Volume	V_{as}	L	11.196
Total Q Factor	Q_{ts}	-	0.35		Motor Force Factor	BL	T·m	7.60
Ratio f_s / Q_{ts}	F	f_s / Q_{ts}	119		Motor Efficiency Factor	β	$(T\cdot m^3)/\Omega$	21.18
Half Space Sensitivity @ 2.83V	dB@2.83V/1m	dB	86.7	+/-1.0 [1]	Voice Coil Former Material	VC_{fm}	-	GSV
Sensitivity @ 1W/1m	1W/1m	dB	82.0	+/-1.0 [1]	Voice Coil Inner Diameter	VC_d	mm	38.44
					Gap Height	Gh	mm	8.00
Rated Noise Power (IEC 2685 18.1)	P	W	75		Maximum Linear Excursion	X_{max}	mm	8.20
Test Spectrum Bandwidth	20Hz - 1kHz		12 dB/Oct		Ferrofluid Type	FF		N/A
					Transducer Size	-	inch	6.5
1 - Piston Band Sensitivity Tolerance					Transducer Mass	-	kg	2.4

Frequency and Impedance Response:

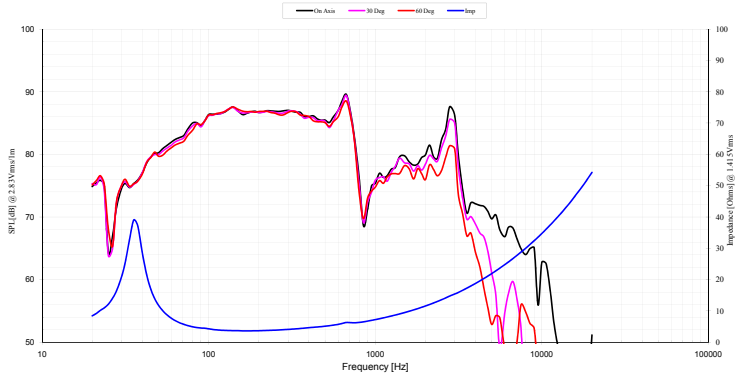

F088-0713A

Tymphany HK Ltd
Address : Room 1307-8 Dominion Centre, 43-59 Queen's Rd East, Wanchai, Hong Kong
E-mail: sales@tymphany.com

A-12 SEAS, L26RO4Y

DESIGN by seas

L26RO4Y
D1004

Extremely stiff and rigid aluminium cone gives tremendous bass precision. The cone and the long throw low loss rubber surround show no sign of the familiar cone edge resonance and distortion associated with soft cones.

Lead-out wires symetrically stitched to the spider to avoid resonances. Total suspension designed to assure stability for extreme excursions.

4-layer, extremely long, high temperature voice coil wound on an glassfiber voice coil former gives a high power handling capacity.

Cu-cap around the pole pieces reduce non linear and modulation distortion and increase overload margin.

Extra large magnet system provides high efficiency and low Q.

Extremely stiff and stable injection moulded metal basket keeps the critical components in perfect alignment. Large windows in the basket both above and below the spider reduce sound reflection, air flow noise and cavity resonance to a minimum.

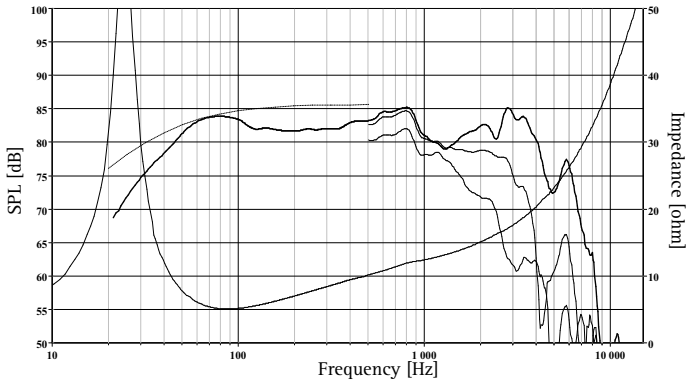

The frequency responses above show measured free field sound pressure in 0, 30, and 60 degrees angle using a 28L closed box. Input 2.83 Vrms, microphone distance 0.5m, normalized to SPL 1m.The dotted line is a calculated response in infinite baffle based on the parameters given for this specific driver. The impedance is measured in free air without baffle using a 2V sine signal.

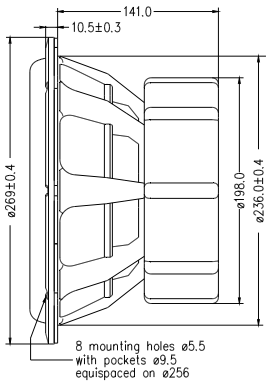

Nominal Impedance	4 Ohms	Voice Coil Resistance	3.3 Ohms
Recommended Frequency Range	20 - 1000 Hz	Voice Coil Inductance	3.85 mH
Short Term Power Handling *	500 W	Force Factor	18 N/A
Long Term Power Handling *	250 W	Free Air Resonance	24 Hz
Characteristic Sensitivity (2,83V, 1m)	85.5 dB	Moving Mass	173 g
Voice Coil Diameter	56 mm	Air Load Mass In IEC Baffle	4.0 g
Voice Coil Height	38 mm	Suspension Compliance	0.26 mm/N
Air Gap Height	10 mm	Suspension Mechanical Resistance	5.4 Ns/m
Linear Coil Travel (p-p)	28 mm	Effective Piston Area	363 cm²
Maximum Coil Travel (p-p)	56 mm	VAS	46 Litres
Magnetic Gap Flux Density	1.1 T	QMS	4.90
Magnet Weight	2.34 kg	QES	0.28
Total Weight	10 kg	QTS	0.27

Jun 2011-1

*IEC 268-5

SEAS reserves the right to change technical data

RoHS compliant product

www.seas.no

A-13 Kepco BOP-36-6M

RETURN TO INDEX

BOP MODEL TABLE

MODEL(1) (5)	d-c OUTPUT RANGE E_O max.	I_O max.	CLOSED LOOP GAIN VOLTAGE CHANNEL G_V (V/V)	CURRENT CHANNEL G_I (A/V)	OUTPUT IMPEDANCE VOLTAGE MODE SERIES R	SERIES L(2)	CURRENT MODE SHUNT R	SHUNT C(3)
100 WATT								
BOP 20-5M	± 20V	± 5A	2.0	0.5	80µΩ	20µH	40kΩ	0.05µF
BOP 50-2M	± 50V	± 2A	5.0	0.2	0.5mΩ	100µH	50kΩ	0.05µF
BOP 100-1M	± 100V	± 1A	10.0	0.1	2.0mΩ	200µH	100kΩ	0.05µF
200 WATT								
BOP 20-10M	± 20V	± 10A	2.0	1.0	40µΩ	50µH	20kΩ	0.1µF
BOP 36-6M	± 36V	± 6A	3.6	0.6	120µΩ	50µH	36kΩ	0.1µF
BOP 50-4M	± 50V	± 4A	5.0	0.4	0.25mΩ	100µH	50kΩ	0.05µF
BOP 72-3M	± 72V	± 3A	7.2	0.3	0.48mΩ	200µH	72kΩ	0.05µF
BOP 100-2M	± 100V	± 2A	10.0	0.2	1.0mΩ	200µH	100kΩ	0.05µF
BOP 200-1M(4)	± 200V	± 1A	20.0	0.1	4.0mΩ	1.2mH	200kΩ	0.03µF
400 WATT								
BOP 20-20M	± 20V	± 20A	2.0	2.0	20µΩ	50µH	20kΩ	0.2µF
BOP 36-12M	± 36V	± 12A	3.6	1.2	60µΩ	50µH	36kΩ	0.2µF
BOP 50-8M	± 50V	± 8A	5.0	0.8	125µΩ	100µH	50kΩ	0.15µF
BOP 72-6M	± 72V	± 6A	7.2	0.6	240µΩ	200µH	72kΩ	0.1µF
BOP 100-4M	± 100V	± 4A	10.0	0.4	500µΩ	200µH	100kΩ	0.1µF

(1) For factory installed digital interfaces add appropriate suffix. See page 55.
(2) For determining dynamic impedance in voltage mode.
(3) For determining dynamic impedance in current mode.
(4) Same size as 400W models.
(5) To specify digital display, substitute the suffix letter "D" for the suffix letter "M."

FEATURES

- Source and sink 100% of their current rating. See Figure 1.
- Separate control circuits for voltage and current with automatic crossover to current and voltage limits.
- All controls and flag signals accessible through a 50-terminal user-port at the rear.
- Zeroable preamplifier available for scaling and summing external signals.
- Optional digital displays. Specify by substituting the suffix "D" in place of the "M."

BOP accept plug-in cards for remote digital control

- BIT 4882 provides 12-bit IEEE 488.2 talk-listen control with SCPI support.
- BIT 4886 provides 16-bit IEEE 488.2 talk-listen control with SCPI support.
- BIT TMA-27 connect BOP to Kepco's single-address multiple instrument serial bus for long range (>300m) control from IEEE 488.2, RS 232 or VXI-based hosts.
- BIT 488B or BIT 488D offer listen-only GPIB support in binary or Hex format.

Cards may be factory installed. See page 55 for appropriate suffix designations.

VXI plug&play member

AN ISO 9001 COMPANY
KEPCO®
THE POWER SUPPLIER™
SINCE 1946

KEPCO, INC. • 131-38 Sanford Avenue • Flushing, NY 11352 USA • Tel: (718) 461-7000 • Fax: (718) 767-1102
Email: hq@kepcopower.com • www.kepcopower.com/bop.htm

51

A-14 Micro-Epsilon optoNCDT 1401

Technical data

MICRO-EPSILON

Model	ILD 1401-5	ILD 1401-10	ILD 1401-20	ILD 1401-50	ILD 1401-100	ILD 1401-200
Measuring range	5 mm (.20 ")	10 mm (.39 ")	20 mm (.79 ")	50 mm (1.97 ")	100 mm (3.94 ")	200 mm (7.87 ")
Start of measuring range	20 mm (.79 ")	20 mm (.79 ")	30 mm (1.18 ")	45 mm (1.77 ")	50 mm (1.97 ")	60 mm(2.36 ")
Mid of measuring range	22.5 mm (.89 ")	25 mm (.98 ")	40 mm (1.57 ")	70 mm (2.76 ")	100 mm (3.94 ")	160 mm (6.30 ")
End of measuring range	25 mm (.98 ")	30 mm (1.18 ")	50 mm (1.97 ")	95 mm (3.74 ")	150 mm (5.91 ")	260 mm (10.24 ")
Linearity	10 µm	20 µm	40 µm	100 µm	200 µm	400 µm
	≤± **0.2 %**					
Resolution	static 0.01 % FSO *					
	0,6 µm	1 µm	2 µm	5 µm	20 µm	40 µm
	dyn. at 1 kHz 0.05 % FSO					
	3 µm	5 µm	10 µm	25 µm	100 µm	200 µm
Measuring rate	1 kHz					
Light source	semiconductor laser 1 mW, 670 nm (red)					
Laser safety class	class 2 IEC 60825-1 : 2001-11					
Spot diameter SMR	110 µm	110 µm	210 µm	800 µm	1000 µm	2100 µm
Spot diameter Midrange	450 µm	830 µm	335 µm	110 µm	130 µm	2100 µm
Spot diameter EMR	830 µm	1600 µm	830 µm	730 µm	760 µm	2100 µm
Protection class	IP 67					
Vibration	15 g / 10 Hz ... 1 kHz					
Weight	appr. 100 g (without cable)					
Operating temperature	0 ... 55 °C (32 ... 130 °F)					
Storage temperature	-20 ... 70 °C (-4 ... 158 °F)					
Output analog	4 ... 20 mA (1 ... 5 V with cable PC 1401-3/U)					
Output digital	RS232					
Supply voltage	11 ... 30 VDC, typ. 24 VDC / 50 mA					
Electronics	integral signal processor					
Electromagnetic compatibility (EMC)	EN 50081-1 EN 50082-2					

FSO = Full scale output SMR = Start of Measuring Range EMR = End of Measuring Range

*) Note: with averaging factor 64

All specifications apply for a diffusely reflecting matt white ceramic target

IEC - Standard

optoNCDT 1401 uses a semiconductor laser with a wavelength of 670 nm (visible/red). The maximum optical output power is 1 mW. The sensor is classified as laser class II. A warning sign is attached to the sensor housing.

A-15 Panasonic, WM-61A

Panasonic Microphone Cartridges

Omnidirectional Back Electret Condenser Microphone Cartridge

Series: **WM-61A**
WM-61 B (pin type)

■ **Features**
- Small microphones for general use
- Back electret type designed for high resistance to vibrations, high signal-to-noise ratio
- High sensitivity type
- Microphone with pins for flexible PCB (WM-61B type)

■ **Sensitivity**

Vs = 2.0V RL = 2.2kΩ	–35 ± 4dB

■ **Specifications**

Sensitivity	–35±4dB (0db = 1V/pa, 1kHz)
Impedance	Less than 2.2 kΩ
Directivity	Omnidirectional
Frequency	20–20,000 Hz
Max. operation voltage	10V
Standard operation voltage	2V
Current consumption	Max. 0.5 mA
Sensitivity reduction	Within –3 dB at 1.5V
S/N ratio	More than 62 dB

■ **Typical Frequency Response Curve**

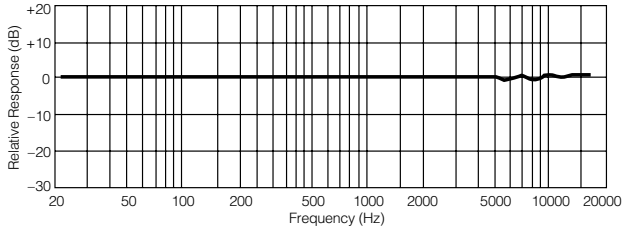

■ **Dimensions in mm** (not to scale)

WM-61A

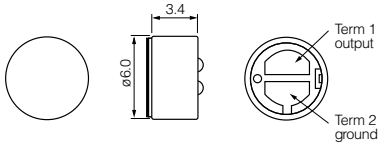

WM-61B

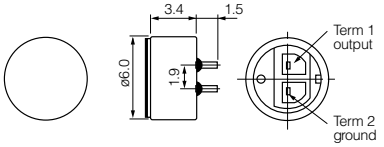

Design and specifications are subject to change without notice. Ask factory for technical specifications before purchase and/or use.
Whenever a doubt about safety arises from this product, please contact us immediately for technical consultation.

A-16 Polytec, PSV-400

Technical Data

Standard System Components	
Vibrometer system	■ OFV-5000 Vibrometer Controller, equipped with analog (PSV-400-B) and additional digital velocity decoder (M2-20: with analog displacement decoder) ■ PSV-I-400 Sensor Head, includes OFV-505 Vibrometer Sensor, precision scanner and color video camera with autofocus and 72X zoom, with transportation case ■ PSV-E-401 Junction Box with PSV-CL-10 main cable, 10 m
Computer	■ PSV-W-401 Data Management System ■ Industrial PC with Windows® XP or Visita 64, Gigabit Ethernet, data aquisition hardware ■ 24" Wide screen monitor, DVD writer, optical mouse and keyboard
Accessories	■ VIB-A-T02 Tripod with tip-tilt adapter ■ PSV-Z-051 Handset (optional for PSV-400-B)

Additional components depend upon PSV model and configuration

Optics			
Component	PSV-I-400 Sensor Head	PSV-A-420 Geometry Scan Unit (optional) with PSV-I-400	PSV-A-410 Close-up Unit (optional)
Dimensions [W x L x H]	190 mm x 376 mm x 163 mm (7.5 in x 14.8 in x 6.4 in)	238 mm x 376 mm x 163 mm (9.4 in x 14.8 in x 6.4 in)	124 mm x 90 mm x 75 mm (4.9 in x 3.5 in x 3.0 in)
Weight	7 kg (15.4 lbs)	7.4 kg (16.3 lbs)	0.35 kg (0.77 lbs)
Laser type	HeNe laser (633 nm)	Laser diode (620 … 690 nm)	–
Laser safety class	Class 2 (<1 mW visible output)	Class 2 (<1 mW output)	–
Working distance	With MR lens: 0.04 m…~100 m; with LR lens: 0.35 m…~100 m		> 152 mm
Sample size	From few mm² up to several m²		
Camera	Color video camera, CCD 1/4", 752x582 pixels, with Auto Focus and 72X Zoom (4X digital, 18X optical)		
Scanner	High precision scan unit (scanning range ±20° about X,Y); angular resolution <0.002°, angular stability <0.01°/hr		
Scan speed	Up to 30 points/s (typical)		

Data Acquisition/Data Processing					
Component		OFV-5000 Vibrometer Controller	PSV-E-401 Junction Box	PSV-E-408 Junction Box (optional for H-system)	PSV-W-401 Data Management System
Dimensions [W x L x H]	mm (in)	450 x 360 x 150 (17.7 x 14.1 x 5.9)	450 x 360 x 135 (17.7 x 14.1 x 5.3)	482 x 303 x 23 (19.0 x 11.9 x 0.9)	450 x 550 x 190 (17.7 x 21.7 x 7.5)
Weight		10 kg (22.0 lbs)	9 kg (19.8 lbs)	1.5 kg (3.3 lbs)	18 kg (39.7 lbs)

General Specifications	
Power	100 VAC...240 VAC ±10 %, 50/60 Hz; overall max. 800 W
Environmental conditions	Operating temperature: +5 °C … +40 °C (41 °F … 104 °F); storage temperature –10 °C … +65 °C (14 °F … 149 °F); relative humidity: max. 80 %, non-condensing
Calibration	Every 24 months (shorter re-calibration intervals available upon request)

PSV-400 Decoder/Performance Specifications						
Model	Decoder	# of ranges	Ranges mm s^{-1}/V	Full scale (p) m/s	Decoder frequency range	Resolution[1] µm s^{-1} /√Hz
PSV-400-B	VD-04	3	10 ... 1000	0.1 ... 10	0.5 Hz ... 250 kHz	0.1 ... 5
PSV-400-H4	VD-08	8	0.2 ... 50	0.002 ... 0.5	DC ... 25 kHz	< 0.01 ... 0.2
	VD-09	8	5 ... 1000	0.05 ... 10	DC ... 2.5 MHz	0.01 ... 4
PSV-400-H4-S	VD-03-S	3	20 … 2000	0.2 … 20	0.5 Hz ... 1.5 MHz	0.1 ... 5
	VD-07-S	6	2 … 100	0.02 … 1	DC ... 350 kHz	<0.05 ... 0.2
PSV-400-M2	VD-07	6	1 ... 50	0.01 ... 0.5	DC ... 350 kHz	<0.02 ... 0.2
PSV-400-M4	VD-09	8	5 ... 1000	0.05 ... 10	DC ... 2.5 MHz	0.01 ... 4
PSV-400-M4-S	VD-09-S VD-07-S	14	10 ... 2000	0.1 ... 20	DC ... 2.5 MHz	0.04 ... 8
PSV-400-M2-20 additionally	VD-05[2]	2	100/500	nom. 0.5/2.5	0.5 Hz ... 10 MHz	<3
	DD-300[2]	1	50 nm/V	75 nm[3]	30 kHz ... 24 MHz	<0.02 pm /√Hz[4]
Optional[5]	DD-900	16	0.05 ... 5000 µm/V	1 µm ... 100 mm[6]	DC ... 2.5 MHz	<0.015 ... 1500 nm[7]

A-17 National Instruments USB-6211

NI USB-621*x* Specifications

Specifications listed below are typical at 25 °C unless otherwise noted.

Analog Input

Number of channels
- USB-6210/6211/6215 ..... 8 differential or 16 single ended
- USB-6218 ..... 16 differential or 32 single ended

ADC resolution ..... 16 bits

DNL ..... No missing codes guaranteed

INL ..... Refer to the *AI Absolute Accuracy Table*

Sampling rate
- Maximum ..... 250 KS/s (aggregate)
- Minimum ..... 0 S/s
- Timing accuracy ..... 50 ppm of sample rate
- Timing resolution ..... 50 ns

Input coupling ..... DC

Input range ..... ±10 V, ±5 V, ±1 V, ±0.2 V

Maximum working voltage for analog inputs (signal + common mode) ..... ±10.4 V of AI GND

CMRR (DC to 60 Hz) ..... 100 dB

Input impedance
- Device on
  - AI+ to AI GND ..... >10 GΩ in parallel with 100 pF
  - AI– to AI GND ..... >10 GΩ in parallel with 100 pF
- Device off
  - AI+ to AI GND ..... 1200 Ω
  - AI– to AI GND ..... 1200 Ω

Input bias current ..... ±100 pA

Crosstalk (at 100 kHz)
- Adjacent channels ..... –75 dB
- Non-adjacent channels ..... –90 dB

Small signal bandwidth (–3 dB) ..... 450 kHz

Input FIFO size ..... 4,095 samples

Scan list memory ..... 4,095 entries

Data transfers ..... USB Signal Stream, programmed I/O

Overvoltage protection (AI <0..31>, AI SENSE)
- Device on ..... ±30 V for up to two AI pins
- Device off ..... ±20 V for up to two AI pins

Input current during overvoltage condition ..... ±20 mA max/AI pin

Settling Time for Multichannel Measurements

Accuracy, full scale step, all ranges
- ±90 ppm of step (±6 LSB) ..... 4 µs convert interval
- ±30 ppm of step (±2 LSB) ..... 5 µs convert interval
- ±15 ppm of step (±1 LSB) ..... 7 µs convert interval

A-18 Makerbot Replicator 2, 3D printer

MAKERBOT® REPLICATOR™ CUSTOMER LIST

3D Imaging
Activision
Alaska Manufacturing Extension Partnership
Amherst County Public Schools
Bainbridge Island School District
Bartlett School of Architecture
Biola University
Bloomington Public Library
Boston College
Boston University
Bowling Green State University
Brooklyn College
Brown University
BUR Bikes
CBS Network West Coast
Chang Bioscience, Inc
City University of Hong Kong
Coinstar
Columbus School for Girls
Corcoran Gallery of Art/College of Art & Design
Cornell University
Deloitte Innovation
Duke University
Edelman
Electronic Arts
Finnish Institute of Occupational Health
GE Power Conversion
Georgia Institute of Technology
Gonzaga University
Google
Gulfstream Aerospace Corporation
Hardin Marine
Harkins Custom Knives
Intel Corporation
JELD-WEN
Kennedy-Matsumoto Design
Kent State University
Kitchen Concepts LLC
Libero Jewelers
Mars Space Flight Facility
MIT
NASA
NASA Glenn Research Center
NASA Marshall Space Flight Center
NASA Goddard Space Flight Center
National Federation of the Blind
Neurosciences Research Foundation
New York Hall of Science
Northrop Grumman
The New York Times Company
Proctor & Gamble
Pixil Inc.
PPG Industries
Purdue University
Qualcomm Inc.
Rochester Institute of Technology
San Francisco Art Institute
Sandia National Labs
Seattle Academy of Arts and Science
SIU - School of Architecture
Sony Electronics
Southwest Energy
Stanford University
Texas A&M University
The Eli Whitney Museum
The New York Public Library
The University of Chicago
UC Berkeley
US Army
US Cutter
United Nations International School
Valley Fine Foods
Woodbury University School of Architecture
Yale University

SPECIFICATIONS

PRINTING

Print Technology:	Fused Filament Fabrication
Build Volume:	11.2 L x 6.0 W x 6.1 H in [28.5 x 15.3 x 15.5 cm]
Layer Resolution Settings:	High 100 microns [0.0039 in] Medium 270 microns [0.0106 in] Low 340 microns [0.0133 in]
Positioning Precision:	XY: 11 microns [0.0004 in]; Z: 2.5 microns [0.0001 in]
Filament Diameter:	1.75 mm [0.069 in]
Nozzle Diameter:	0.4 mm [0.015 in]

SOFTWARE

Software Bundle:	MakerBot MakerWare™ Bundle 1.0
File Types:	.stl, .obj, .thing
Supports:	Windows (XP/7), Linux (Ubuntu 10.04+), Mac OS X (10.7/10.8)

PHYSICAL DIMENSIONS

Without Spool:	19.1 x 12.8 x 14.7 in [49 x 32 x 38 cm]
With Spool:	19.1 x 16.5 x 14.7 in [49 x 42 x 38 cm]
Shipping Box:	23 x 21.5 x 17 in [59 x 55 x 43 cm]
Weight:	25.4 lbs [11.5 kg]
Shipping Weight:	32.0 lbs [14.5 kg]

TEMPERATURE

Ambient Operating Temperature:	15º – 32º C [60º – 90º F]
Storage Temperature:	0º – 32º C [32º – 90º F]

ELECTRICAL

AC Input:	100 – 240 V, ~2 amps, 50 – 60 Hz
Power Requirements:	24 V DC @ 6.25 amps
Connectivity:	USB, SD card [included]

MECHANICAL

Chassis:	Powder-coated steel
Body:	PVC Panels
Build Platform:	Acrylic
XYZ Bearings:	Wear-resistant, oil-infused bronze
Stepper Motors:	1.8º step angle with 1/16 micro-stepping

To purchase, visit **MakerBot.com/Replicator2** or call +1.347.334.6800 | 7

A-19 Measurement Specialities, ACH-01

MEASUREMENT SPECIALTIES

Accelerometer ACH-01

Application Specification
114-1089
30 DEC 00 Rev F

1.0 INTRODUCTION

This specification covers the application requirements of Measurement Specialties Accelerometer ACH-01. The ACH-01 is an inexpensive, general purpose accelerometer with outstanding performance characteristics. The use of piezoelectric polymer film in the ACH-01 provides many cost/performance advantages that allow it to be used in a wide range of applications where the use of traditional accelerometer technology is impractical. It is specifically designed for high volume applications which require the permanent installation of an accelerometer, such as machine health monitoring, modal analysis, automotive sensors, appliances, and feedback control systems.

Features of the accelerometer include:

- Wide Frequency Response
- Excellent Phase Response
- Wide Dynamic Range
- Low Cost
- Ultra-Low Power
- Very High Resonant Frequency
- Low Transverse Sensitivity
- Wide Temperature Range
- Small Temperature Dependence
- 3V to 40V Supply
- Impedance Buffered Output
- Excellent Linearity

Note: All dimensions in inches and are reference.

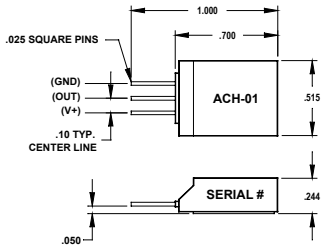

ACH-01-02 with Pins

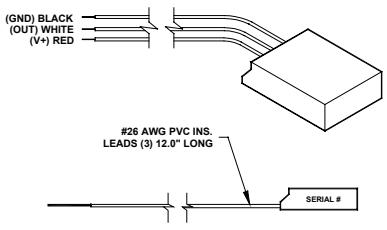

ACH-01-04 with Wires

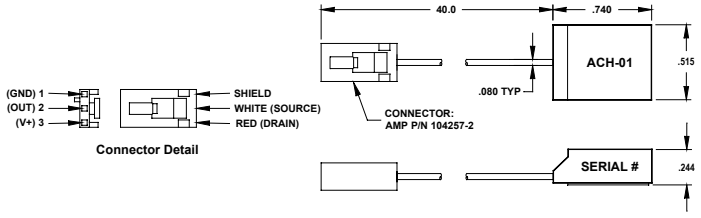

Connector Detail

ACH-01-03 with Shielded Cable

INFORMATIONAL NOTES AND DISCLAIMER

For drawings, technical data or samples, call 610-650-1500
Specifications subject to change. Consult MSI for latest specifications.

PN: 1004568-8 LOC ER

MEASUREMENT SPECIALTIES

Accelerometer ACH-01

114-1089

2.6 Specifications

Performance (T=25°C)	Symbol	Min	Typ	Max	Units
Sensitivity	M_o	7	9	11	mV/g
Lower Frequency Limit (1)	f_l	--	2	5	Hz
Upper Frequency Limit (1)	f_u	10	20	--	kHz
Equivalent Noise Floor 10Hz 100Hz 1kHz		 -- -- --	 130 20 6	 -- -- --	$\mu g/\sqrt{Hz}$
Dynamic Range	--	±150	--	--	g
Linearity	--	--	0.1	1.0	%
Transverse Sensitivity	M_t	--	2.0	5	%
Resonant Frequency	f_o	--	35	--	kHz
Phase Deviation (±5° Limit) (6)	θ	10	--	10,000	Hz
Supply Voltage	V+	3	--	40	Volts
Quiescent Supply Current	I_Q		10		μA
JFET Pinch Off Voltage	V_{gss}	-0.6	-0.8	-1.8	V
JFET Saturation Current	I_{dss}	30		90	μA
Output Impedance (6)	--	--	20	--	kΩ
Environmental Characteristics					
Operating Temperature (2)	T_o	-40	--	85	°C
Storage Temperature	T_s	-40	--	85	°C
Maximum Shock Level	A_m	1000	--	--	g
Base Strain Sensitivity (3)	--	--	0.3	--	g/με
Transient Temp Sensitivity (4)	--	--	0.35	--	g/°C
Physical Characteristics					
Weight (5) Cable	W	--	8	--	grams

(1) ±3 dB limit
(2) ±2 dB from nominal M_o at 1kHz
(3) @ 250με in base plane
(4) @ 3Hz LLF
(5) Includes 40" cable and connector
(6) Typical Value

A-20 dSpace, DS1103

Technical Details

Parameter		Specification
Processor	PowerPC Type	■ PPC 750GX
	CPU clock	■ 1 GHz
	Cache	■ 32 KB level 1 (L1) instruction cache ■ 32 KB level 1 (L1) data cache ■ 1 MB level 2 (L2)
	Bus frequency	■ 133 MHz
	Temperature sensor	■ Reads actual temperature at the PPC
Memory	Local memory	■ 32 MB application SDRAM as program memory, cached
	Global memory	■ 96 MB communication SDRAM for data storage and data exchange with host
Timer	2 general-purpose timers	■ One 32-bit down counter ■ Reload by software ■ 15-ns resolution
		■ One 32-bit up counter with compare register ■ Reload by software ■ 30-ns resolution
	1 sampling rate timer (decrementer)	■ 32-bit down counter ■ Reload by software ■ 30-ns resolution
	1 time base counter	■ 64-bit up counter ■ 30-ns resolution
Interrupt controller		■ 3 timer interrupts ■ 7 incremental encoder index line interrupts ■ 1 UART (universal asynchronous receiver and transmitter) interrupt ■ 1 CAN interrupt ■ 1 slave DSP interrupt ■ 2 slave DSP PWM interrupts ■ 1 host interrupt ■ 4 external interrupts (user interrupts)
A/D converter	Channels	■ 16 multiplexed channels equipped with 4 sample & hold A/D converters (4 channels belong to one A/D converter. 4 consecutive samplings are necessary to sample all channels belonging to one A/D converter.) ■ 4 parallel channels each equipped with one sample & hold A/D converter ■ Note: 8 A/D converter channels (4 multiplexed and 4 parallel) can be sampled simultaneously.
	Resolution	■ 16-bit
	Input voltage range	■ ±10 V
	Overvoltage protection	■ ±15 V
	Conversion time	■ Multiplexed channels: 1 µs[1)] ■ Parallel channels: 800 ns[1)]
	Offset error	■ ±5 mV
	Gain error	■ ±0.25%
	Offset drift	■ 40 µV/K
	Gain drift	■ 50 ppm/K
	Signal-to-noise ratio	■ >83 dB
D/A converter	Channels	■ 8 channels
	Resolution	■ 16-bit
	Output range	■ ±10 V
	Settling time	■ 5 µs (14-bit)
	Offset error	■ ±1 mV
	Gain error	■ ±0.5%
	Offset drift	■ 30 µV/K
	Gain drift	■ 25 ppm/K

[1)] *Speed and timing specifications describe the capabilities of the hardware components and circuits of our products. Depending on the software complexity, the attainable overall performance figures can deviate significantly from the hardware specifications.*

dSPACE GmbH • Rathenaustraße 26 • 33102 Paderborn • Germany • info@dspace.de • www.dspace.com

Parameter		Specification
D/A converter	Signal-to-noise ratio	■ >83 dB
	I_{max}	■ ±5 mA
	$C_{I_{max}}$	■ 10 nF
Digital I/O	Channels	■ 32-bit parallel I/O ■ Organized in four 8-bit groups ■ Each 8-bit group can be set to input or output (programmable by software)
	Voltage range	■ TTL input/output levels
	$I_{out, max}$	■ ±10 mA
Digital incremental encoder interface	Channels	■ 6 independent channels ■ Single-ended (TTL) or differential (RS422) input (software programmable for each channel)
	Position counters	■ 24-bit resolution ■ Max. 1.65 MHz input frequency, i.e.,fourfold pulse count up to 6.6 MHz ■ Counter reset or reload via software
	Encoder supply voltage	■ 5 V/1.5 A ■ Shared with analog incremental encoder interface
Analog incremental encoder interface	Channels	■ 1 channel ■ Sinusoidal signals: 1 Vpp differential or 11 µApp differential (software programmable)
	Position counters	■ < 5° resolution ■ 32-bit loadable position counter ■ Max. 0.6 MHz input frequency, i.e., fourfold pulse count up to 2.4 MHz
	A/D converter performance	■ 6-bit resolution ■ 10 MSPS
	Encoder supply voltage	■ 5 V/1.5 A ■ Shared with digital incremental encoder interface
CAN interface	Configuration	■ 1 channel based on SAB 80C164 microcontroller ■ ISO DIS 11898-2 CAN high-speed standard
	Baud rate	■ Max. 1 Mbit/s
Serial interface	Configuration	■ TL6C550C single UART with FIFO ■ PLL-driven UART for accurate baud rate selection ■ RS232/RS422 compatibility
	Baud rate	■ Up to 115.2 kBd (RS232) ■ Up to 1 MBd (RS422)
Slave DSP	Type	■ Texas Instruments TMS320F240 DSP
	Clock rate	■ 20 MHz
	Memory	■ 64 Kx16 external code memory ■ 28 Kx16 external data memory ■ 4 Kx16 dual-port memory for communication ■ 32 KB flash memory
	I/O channels[1)]	■ 16 A/D converter inputs ■ 10 PWM outputs ■ 4 capture inputs ■ 2 serial ports
	Input voltage range	■ TTL input/output level ■ A/D converter inputs: 0 … 5 V
	Output current	■ Max. ±13 mA
Host interface		■ Plug & Play support ■ Requires a full-size 16-bit ISA slot
Physical characteristics	Physical size	■ 340 x 125 x 45 mm (13.4 x 4.9 x 1.77 in)
	Ambient temperature	■ 0 … 50 °C (32 … 122 °F)
	Cooling	■ Passive cooling
	Power supply	■ +5 V ±5%, 4 A ■ +12 V ±5%, 0.75A ■ -12 V ±5%, 0.25A

1) *The exact number of I/O channels depends on your configuration and is described in the user documentation.*

A-21 Drawing sensor mount, Sensorcarrier1

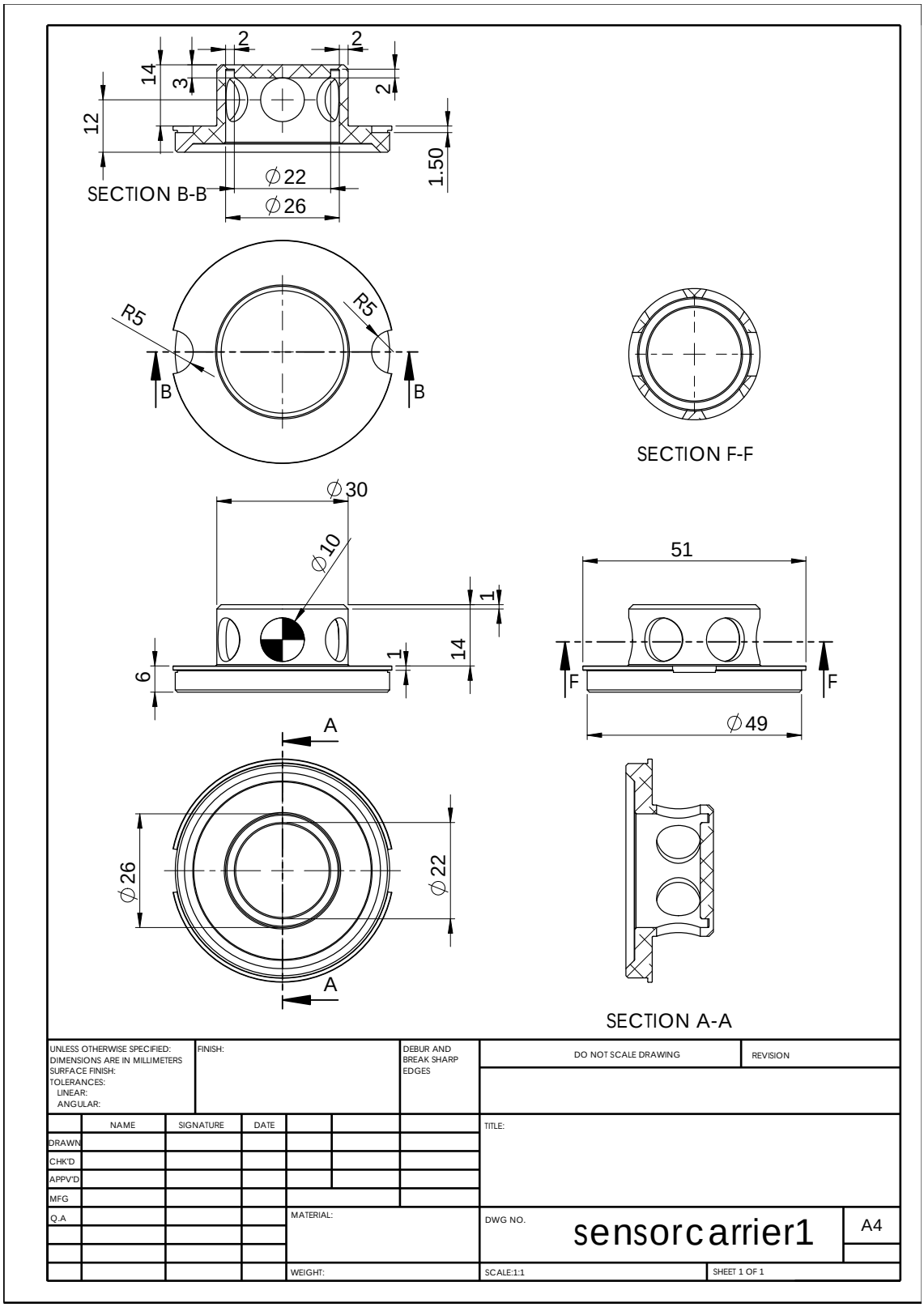

A-22 Beyerdynamic MM1 reference microphone

beyerdynamic

MM 1

Measurement Microphone

Order # 449.350

FEATURES

- Linear frequency response
- Omnidirectional polar pattern
- Calibrated open circuit voltage
- Narrow tubular construction

APPLICATIONS

The MM 1 is a measurement microphone which has been designed specifically for measuring sound reinforcement and PA-systems. It is designed to work with spectrum analysers for measuring frequency response and sound pressure levels of loud speaker systems. The MM 1 is the ideal microphone for the measurement of audio signals in the research, development, for reverberation testings and other applications.
The narrow tubular construction ensures that the microphone has negligable influence on the sound field so that an increase in sound pressure is avoided with high frequencies. A natural reproduction is achieved due to the linear frequency response.

OPTIONAL ACCESSORIES

GST 400	Microphone stand, 3/8", height 0.90 - 1.65 m, with G 400 boom	Order # 421.294
GST 500	Microphone stand, 3/8", height 0.85 - 1.60 m, with telescopic G 500 boom	Order # 406.252
ST 400	Microphone stand, 3/8", height 0.90 - 1.65 mm	Order # 421.286
ST 500	Microphone stand, 3/8", height 0.85 - 1.60 mm	Order # 406.643
WS 10	Windscreen, charcoal grey	Order # 403.008

Germany
Theresienstr. 8
D-74072 Heilbronn
Tel. +49 (0)71 31 / 6 17-0
Fax +49 (0)71 31 / 617-224
E-mail: info@beyerdynamic.de
Internet: www.beyerdynamic.de

United States
56 Central Ave.
Farmingdale, NY 11735
Tel. +1 (631) 293-3200
Fax +1 (631) 293-3288
E-mail: salesUSA@beyerdynamic.com
Internet: www.beyerdynamic.com

Great Britain
17 Albert Drive
Burgess Hill RH15 9TN
Tel. +44 (0)1444 / 258 258
Fax +44 (0)1444 / 258 444
E-mail: sales@beyerdynamic.co.uk
Internet: www.beyerdynamic.co.uk

TECHNICAL SPECIFICATIONS

Transducer type	Condenser (back electret)
Operating principle	Pressure
Frequency response	20 - 20,000 Hz (50 - 16,000 Hz ± 1.5 dB)
Polar pattern	Omnidirectional, diffuse field calibrated
Open circuit voltage at 1 kHz	15 mV/Pa (≙ -36.5 dBV) ± 1 dB
Nominal impedance	330 Ω
Nominal load impedance	≥ 2.2 kΩ
Max. SPL at f = 1 kHz, k = 1%, R_L = 2.2 kΩ	128 dB_{SPL}
S/N ratio rel. to 1 Pa	> 57 dB
A-weighted equivalent SPL	approx. 28 dB(A)
Power supply	12 - 48 V phantom supply
Current consumption	approx. 3.4 mA
Output	transformer balanced
Connection	3-pin XLR male
Dimensions	Length: 133 mm Shaft diameter: 19/9 mm Head diameter: 9 mm
Weight (w/out cable)	88 g

FREQUENCY RESPONSE & POLAR PATTERN

This polar pattern and frequency response curve (measuring tolerance ± 1.5 dB) correspond to a typical production sample for this microphone.

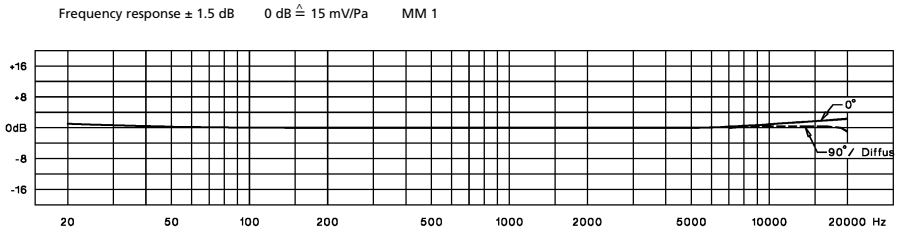

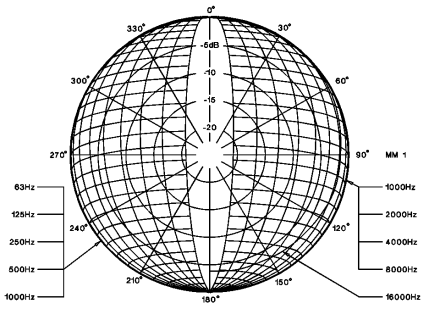

WIRING DIAGRAM

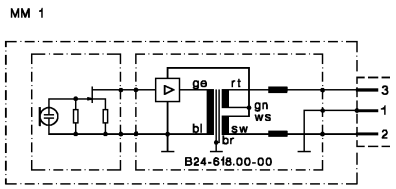

beyerdynamic)))) MM 1

Photos are non-contractual. Contents subject to change without notice. Printed in Germany.

A-23 Philips NatLab improved MFB

PHILIPS

Feed forward loop.

The linear distortion of the system has been eliminated in the operating range of the loudspeaker (40-500Hz) (We have extended the flat part of the spectrum towards lower frequencies, electronic bass boost). At the same time the excursion of the diaphragm at low frequencies has been increased considerably and this increases the non-linear distortion at those frequencies. This non-linear distortion can be reduced by applying a feedback from the accelerometer to the input (fig 4-12). However the closed loop system will be unstable due to the phase shifts at low ($f < 20$ Hz) and high ($f > 900$ Hz) frequencies as has been discussed earlier (chapter 3 and fig 4-11).

The closed loop system can be made stable in those frequency regions by adding a signal to the accelerometer signal which has a greater amplitude than the latter and the phase of which behaves properly at those frequencies. This signal must be blocked in the operating frequency region of the loudspeaker. The feedback of the sum signal yields a stable total system at all frequencies.

The high frequency feed forward loop can be realized with a first order network. However by applying a second order network with a sufficient high Q-factor, we can increase the distance (in dB) between the two signals in the operating region of the loudspeaker. In that case the effective feedback level has been increased (fig 4-15) and thus the non-linear distortion reduction.

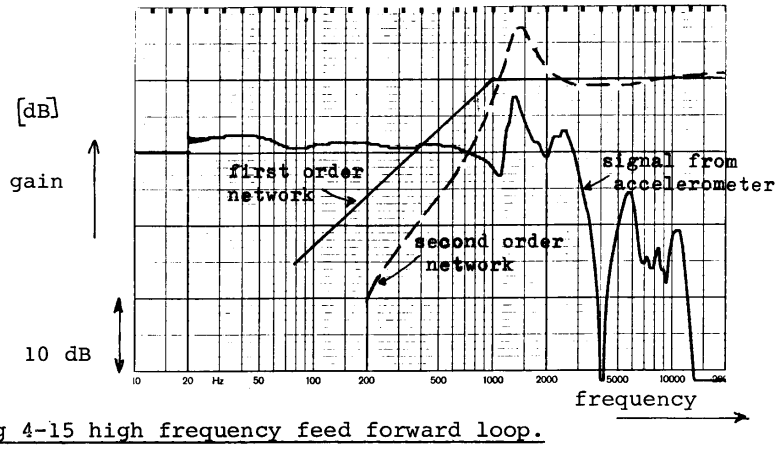

fig 4-15 high frequency feed forward loop.

The effective feedback level is the distance between the two signals ; the feed forward loop signal and the accelerometersignal as will be shown in appendix 1.

At the low frequency side we prepared the inverse network in order to be able to shift the feed forward loop to as low frequencies as possible.

The practical realization of the low and high frequency feed forward loops is shown in fig 4-16.

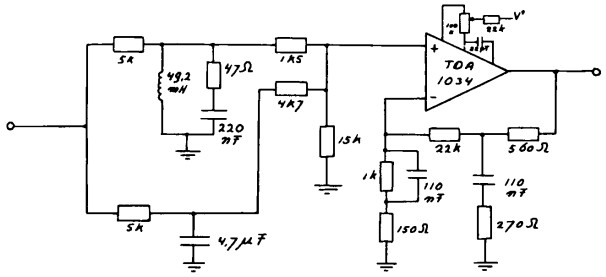

fig 4-16 feed forward loops (block 6 of fig 4-11).

the gain and phase versus frequency are shown in fig 4-17 ab.

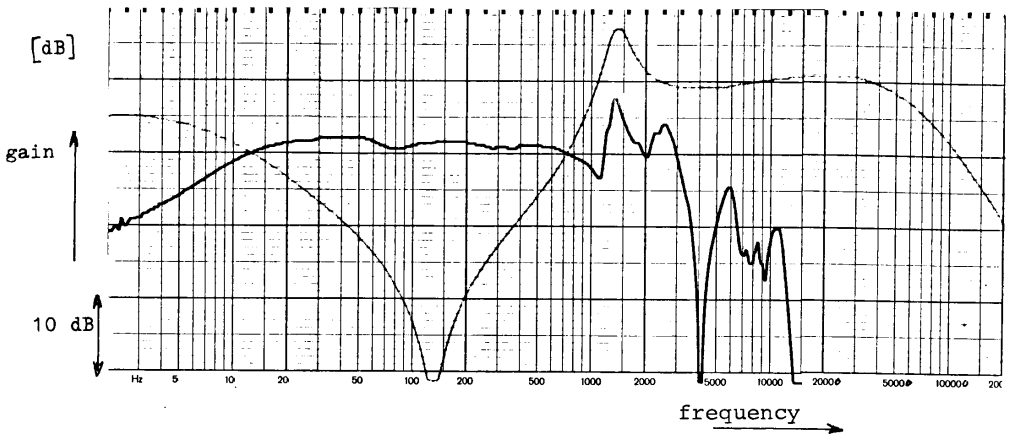

fig 4-17-a gain of feed forward loops.

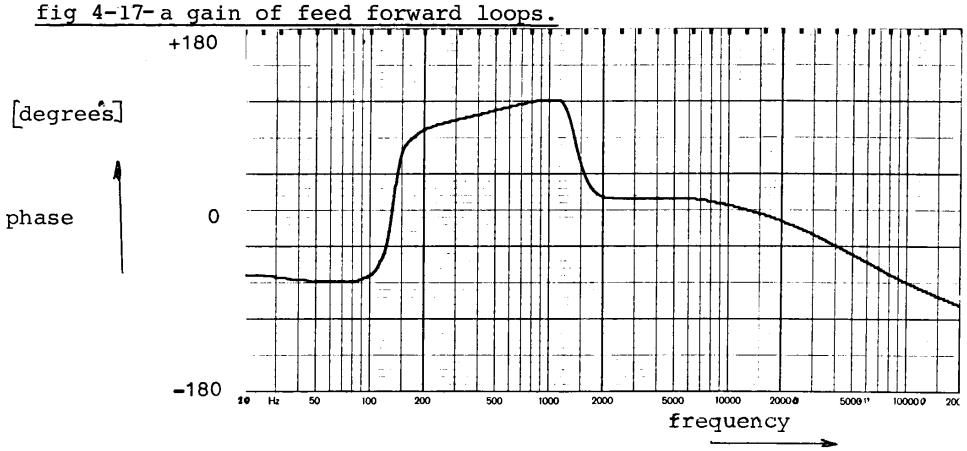

fig 4-17-b phase.

Due to the gain-frequency characteristic at high frequencies of the used operational amplifier (TDA 1034) another limitation of the feedback level occurs.

The gain in the feed forward loop above 12 kHz is about 53 dB. This gain level can be used until about 50 kHz (see open loop gain of the TDA 1034 in its specifications).

Above this frequency the gain slope equals the open loop gain slope of 6 dB/octave. At 200 kHz where the gain level has dropped-12 dB, a roll-off shape of -12 dB/octave starts due to the -6 dB slope of the feedback amplifier.

At this frequency the open loop gain must be below 0 dB to prevent instabilities in the closed loop system.

Thus the feedback level has a maximum of 12 dB. This maximum feedback level can be increased by realizing an additional roll-off in the feed forward loop starting at lower frequencies (1.8-18 kHz).

This roll-off network has been combined with the summation network as shown in fig 4-18.

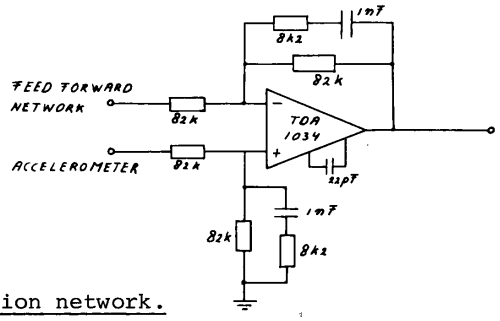

fig 4-18 summation network.

With this feed forward loop signal added to the accelerometersignal the closed loop system is stable for all frequencies.

Limitations of the m.f.b. system.

With the system described in the previous parts the sound pressure level is flat from 20-500 Hz. (Except an increase in sound pressure level above 250 Hz. This is compensated by a simple first order network as will be described at the end of this chapter).

The maximum output level however is limited by the low boundary of the flat frequency region. As can be seen in fig 2-9-c, the extension of the operating range of the loudspeaker (flat response region) towards lower frequencies dramatically increases the diaphragm excursion and the power requirement. So in practice this level, at a given lower frequency boundary, is limited by :

1. The maximum excursion of the loudspeaker diaphragm.
2. The power handling capacity of the loudspeaker.
3. The available power of the power amplifier. (The power requirement is naturally influenced by the sensitivity

of the loudspeaker).

4. The dynamic range of the system electronics (these should not influence the limitations).

If one demands a (higher) sound pressure level with a given loudspeaker and power amplifier (A loudspeakerbox must be able to produce a s.p.l. of 96 dB at 1 meter, see ref 9), then the lower frequency boundary is fixed to a higher frequency. In the system described in this report we used an 8" woofer (8067 MFB 4) and a power amplifier of 50 watts. In this system the limiting factor was the power amplifier and the lower frequency boundary had to be increased to 60 Hz. This was realized by preceding the m.f.b. system with a band pass filter (fig. 4-19, block 8) which limits the lowest frequency to 60 Hz. At the high frequency end it provides a proper cross over behaviour.

Overload protection.

In a standard loudspeaker system (without m.f.b.) the distortion due to an overload will increase gradually.

In a m.f.b. system however the feedback loop will clip (clipping loudspeaker or power amplifier) when an overload occurs. This can naturally not be corrected and the distortion will increase suddenly and dramatically due to the feedback gain.

This cannot be tolerated and therefore a limiter (fig 4-19 block 9) has to be added to the system.

This limiter is necessary in any m.f.b. system!

As a limiter which precedes the system however will limit the maximum available output level, we have to find another method.

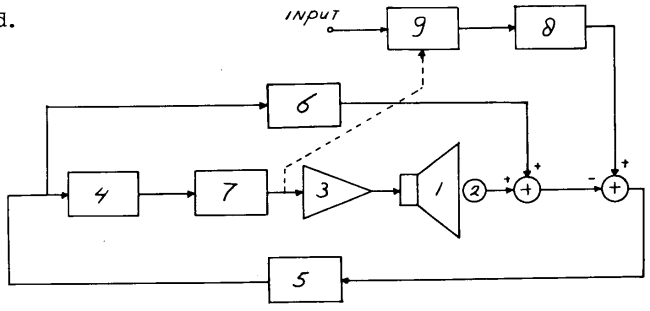

fig 4.19 blockdiagram of complete m.f.b. system.

The different blocks in fig. 4-19 are :

1. loudspeaker.
2. accelerometer.
3. power amplifier.
4. inverse network.
5. feedback amplifier.
6. feed forward loop.
7. notch filter.
8. bandpass filter.
9. limiter.

The speaker voltage versus frequency with constant input voltage has the behaviour as shown in fig 4-20 and the

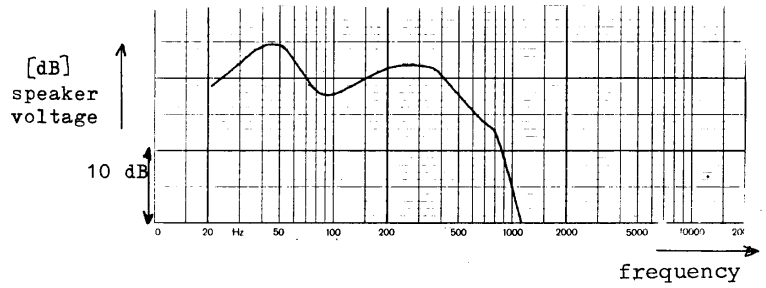

fig 4-20 speaker voltage versus frequency.

limiting level is determined by the highest level in the curve which is the peak at low frequencies. This was solved by using the speaker voltage to determine the limiting condition of the limiter.

Effectively we introduced a frequency dependence of the limiting level. The voltage of the speaker is filtered by a low pass filter to avoid a continously switching of the limiter. The limiter gradually switches on and off. Thus a slow (and cheap) limiter can be applied.

In our experiments a (fast) standard limiter (Signetics NE 570 N) has been used which should be replaced by a simpler (slow) circuit.

As a last point we have to compensate for the increase in sound pressure level relative to the acceleration of the voice coil above 250 Hz (See figs 4-7 a and 4-8). This can be done by preceding the loop with a first order low pass network. This correction network can be combined with the band pass filter.

Bibliography

[1] K. M. Al-Ali. *Loudspeakers: Modeling and Control*. PhD thesis, University of California at Berkeley, 1999.

[2] E. De Boer. Theory on motional feedback. *IRE Transactions on audio*, January-February:15–51, 1961.

[3] R. Breden. Roaring subwoofer. *Electronics world*, February:104–109, 1997.

[4] N. Quaegebeur A. Chaigne. Nonlinear vibrations of loudspeaker-like structures. *Journal of Sound and Vibration*, 309:178196, 2008.

[5] S. Chiu. A direct pwm loudspeaker feedback system. Master's thesis, Massachusetts Institute of Technology, 1996.

[6] Jr D. Davis E. Patronis. *Sound System Engineering*. Focal Press, 2006.

[7] D. de Greef J. Vandewege. Acceleration feedback loudspeaker. *Wireless world*, September:32–36, 1981.

[8] S. D. Dzisiewski-Smith. Positional loudspeaker feedback and control using dsp within a class d audio power amplifier system. Master's thesis, Imperial college London, 2007.

[9] P.A. Nelson S.J. Elliott. *Active Control of Sound*. Academic Press Inc., 1992.

[10] G. F. Franklin J. D. Powell A. Emami-Naeini. *Feedback control of dynamics systems*. Pearson Prentice Hall, 2006.

[11] B. Friedland. *Control System Design*. Dover Publications, 2005.

[12] M. Petyt P. N. Gélat. Vibration of loudspeaker cones using the dynamic stiffness method. *Applied Acoustics*, 53:313–332, 1998.

[13] S.M. Kuo R. K. Yenduri A. Gupta. Frequency domain delayless active sound quality control algorithm. *Journal of Sound and Vibration*, 318:714–724, 2008.

[14] P. G. L. Mills M. O. J. Hawksford. Transconductance power amplifier systems for current driver loudspeakers. *Audio Engineering Society*, 37, 10:809–822, 1989.

[15] L. Yali Y. Hongwu Z. Hui. Speaker identification based in emd. Technical report, College of Physics and Electronic Engineering, Northwest Normal University, China, 2009.

[16] Y. Jing. Robust vibration control based on identified models. *Journal of Sound and Vibration*, 269:3–17, 2004.

[17] M. J. Brennan S. M. Kim. Feedforward and feedback control of sound and vibration, a weiner filter approach. *Journal of Sound and Vibration*, 246:281–296, 2001.

[18] L. Kreitmeier. Fem simulation of loudspeakers and loudspeaker components. Technical report, Harman/becker automotive systems, Germany, 2002.

[19] A. G. A. Mathalif R. S. Langley. Active control of high-frequency vibration: Optimisation using the hybrid modelling method. *Journal of Sound and Vibration*, 331:2969–2983, 2012.

[20] S. J. Loutridis. Resonance identification on loudspeaker driver units: A comparison of techniques. *Applied Acoustics*, 66:1399–1426, 2005.

[21] R. Miller. Modal analysis of loudspeaker diaphragms. Master's thesis, Faculty of Rensselaer Polytechnic Institute, Connecticut, 2010.

[22] K. J. Aström R. M. Murray. *Feedback systems*. Princeton University Press, 2008.

[23] S. Cecchi E. Moretti F. Piazza. A new approach to bass enhancement based on prony's method. Technical report, Universita Politecnica della Marche, 2007.

[24] T. S. Hsu K. A. Poornima. Loudspeaker failure modes and error correction techniques. *Applied Acoustics*, 62:717–734, 2001.

[25] A. Draeger S. Engell H. Ranke. Model predictive control using neural networks. *IEEE Control*, October:61–66, 1995.

[26] R. Ravaud G. Lemarquand T. Roussel. Time-varying non linear modeling of electrodynamic loudspeakers. *Applied Acoustics*, 70:450–458, 2009.

[27] H. Schurer. Second order volterra inverses for compensation of loudspeaker nonlinearity. *Applications of Signal Processing to Audio and Acoustics*, 1:165–168, 1995.

[28] J. Shaw. Adaptive control for sound and vibration attenuation: a comparative study. *Journal of Sound and Vibration*, 235:671–684, 2000.

[29] Z. L. Zhang Q. T. Tao. Experimental study of non-linear vibrations in a loudspeaker cone. *Journal of Sound and Vibration*, 248:1–8, 2001.

[30] F. E. Toole. *Sound reproduction*. Elsevier, 2008.

[31] J. Suykens J. Vandewalle J. van Ginderdeuren. Feedback linearization of nonlinear distortion in electrodynamic loudspeakers. *Journal of the Audio Engineering Soviety*, 43:690–694, 1995.

[32] C. R. Fuller A. H. von Flotow. Active control of sound and vibration. *IEEE Control Systems*, December:9–19, 1995.

[33] A.J.M. Kaizer C.A.M. Wesche. An improved motional feedback loudspeaker system. Technical report, Philips NAT.LAB., 1978.

[34] J. Peifang L. Wei W. Schuaibing Y. Jun G. Woon-Seng. An alternative method to measure the on-axis difference-frequency sound in a parametric loudspeaker without using an acoustic filter. *Applied Acoustics*, 73:1244–1250, 2012.

[35] J. Wei G. Woon-Seng. Identification of a parametric loudspeaker system using an adaptive volterra filter. *Applied Acoustics*, 73:1251–1262, 2012.

[36] Z. Limin W. Lifu Q. Xiaojun. An intuitive approach for feedback active noise controller design. *Applied Acoustics*, 74:160–168, 2013.

[37] U Zölzer. *Digital Audio Signal Processing*. Wiley, 2008.